Quantenfluktuationen im Einzel-Elektronen-Transistor

Zur Erlangung des akademischen Grades eines
DOKTORS DER NATURWISSENSCHAFTEN
von der Fakultät für Physik der
Universität Karlsruhe (TH)

genehmigte

DISSERTATION

von

Dipl.-Phys. Jürgen König

aus Karlsruhe

Tag der mündlichen Prüfung:	11. Dezember 1998
Hauptreferent:	Prof. Dr. Gerd Schön
Korreferent:	Prof. Dr. Hermann Grabert

Quantum Fluctuations in the Single-Electron Transistor

Jürgen König

Universität Karlsruhe (TH), Germany

Acknowledgements

It is a great pleasure to me to sincerely thank Gerd Schön for his support in recent recent years. I have enjoyed working with him and his group very much. He has helped me in my work in every conceivable way. Among many other things he initiated the collaboration with colleagues and gave me the possibility to present my work at conferences.

I thank Hermann Grabert for refereeing this thesis and for helpful discussions.

Most parts of the thesis are the result of a productive cooperation with Herbert Schoeller. I owe sincere thanks to him.

I appreciate joint papers with Rosario Fazio, Yuval Gefen, Dmitrii Golubev, Teemu Pohjola, Martti Salomaa, Jörg Schmid, Herbert Schoeller, Gerd Schön, and Andrei Zaikin.

Furthermore, helpful discussions with Fabian Braun, Christoph Bruder, Jan von Delft, Daniel Esteve, Georg Göppert, Rolf Haug, Carlos Herrero, Philippe Joyez, Leo Kouwenhoven, Frank Kuczera, Jukka Pekola, Jens Siewert, Jürgen Weis, David Wharam, and Frank Wilhelm have contributed to this thesis.

I thank all colleagues at TFP and TKM for the pleasant working atmosphere, especially (in addition to those who were already mentioned above) Reinhard Baltin, Wolfgang Belzig, Philipp Brune, Andreas Poenicke, Alexander Shnirman, and Karl-Heinz Wagenblast.

The hospitality of Yuval Gefen during my stay at the Weizmann Institute of Science in Rehovot (Israel) is gratefully acknowledged.

I want to thank my wife Bärbel for her support and wonderful years together.

This work was supported by the SFB 195 of the DFG.

Contents

Deutsche Zusammenfassung

Ladung ist quantisiert. Elektronen tragen die Elementarladung $e \approx 1.602 \times 10^{-19}$C. Während dies eine fundamentale Entdeckung in der Physik darstellt, spielt die Diskretheit der Ladung in gängigen elektronischen Schaltkreisen keine Rolle. Selbst in der heute etablierten Computertechnologie mit Schaltkreisen auf der Skala von Mikrometern wird der Stromfluß von einer riesigen Zahl von Elektronen getragen.

In den letzten Jahren ist jedoch ein wesentlicher Fortschritt in der Fabrikation von Strukturen auf der Skala von Nanometern erzielt worden. Die ist nicht einfach nur ein weiterer Miniaturisierungsschritt, sondern eröffnet ein neues Feld von Anwendungen, die auf der Quantisierung der Ladung beruhen. Dazu muß die mit der Temperatur verknüpften Energieskala kleiner sein als die relevante Energieskala für Ladungseffekte, nämlich die Ladungsenergie für ein Elektron $E_C = e^2/2C$. Es ist möglich geworden, metallische Tunnelkontakte mit Kapazitäten im Bereich von $C = 10^{-15}$F kontrolliert herzustellen. Die zugehörige Temperaturskala E_C/k_B liegt in der Größenordnung von 1 K, was experimentell zugänglich ist. Ein alternativer Ansatz besteht in der Strukturierung von zweidimensionalen Elektronengasen, die an internen Grenzflächen geschichteter Halbleitermaterialien auftreten. Auf diese Weise sind Quantenpunkte hergestellt worden, in denen die Coulombenergie durch Kapazitäten im Bereich von $C = 10^{-15}$F und weniger charakterisiert werden kann. Molekulare Systeme mit noch niedrigeren Kapazitäten im Bereich von $C = 10^{-18}$F stellen die neueste Herausforderung für Experimentatoren dar.

Ein einfaches System, das Ladungseffekte zeigt, ist der Einzel-Elektronen-Transistor, in dem eine Insel mittels zweier Tunnelkontakte an zwei Zuleitungen gekoppelt ist. Der Strom durch den Transistor geschieht durch sequentiellen Elektronentransport, d.h. ein Elektron nach dem andern durchquert die Insel. Die Coulomb-Abstoßung verhindert, daß ein weiteres Elektron auf die Insel gelangt, bevor das erste dieselbe verlassen hat. Bei geeigneter angelegter Steuerspannung kann der Transport sogar vollständig blockiert sein (*Coulomb-Blockade*). Der Strom als Funktion der Steuerspannung zeigt eine Aufeinanderfolge von Maxima (*Coulomb-Oszillationen*). Da die Transporteigenschaften durch die Ladung von einzelnen Elektronen bestimmt wird, konnte man Anwendungen als Elektrometer und Strom- und Kapazitätsstandards mit enormer Genauigkeit realisieren. Auf der Basis von Ladungseffekten sind außerdem Niedrig-Temperatur-Thermometer und logische Schalt- und Speicherelemente möglich.

Eine Beschreibung von sequentiellem Tunneln mit Hilfe einer Mastergleichung reicht aus, solange die Kopplung der Insel an die Zuleitungen schwach und die Temperatur

sowie die Transportspannung nicht zu klein ist. Dann findet der Stromtransport in einer inkohärenten Abfolge von unkorrelierten Tunnelprozessen statt. Die zugehörigen Raten können mit Fermis Goldener Regel abgeleitet werden. Dieses Schema bildet die sog. *orthodoxe Theorie*.

Es gibt aber experimentelle und theoretische Hinweise, daß die Physik des Einzel-Elektronen-Transistors sehr viel reichhaltiger ist. Die orthodoxe Theorie berücksichtigt Ladungseffekte als Folge der Diskretheit der Ladung, vernachlässigt aber Quantenfluktuationen und Tunnelprozesse höherer Ordnung. Erstens ist der Transport im Coulomb-Blockade Bereich, in dem sequentielles Tunneln exponentiell unterdrückt ist, durch *Cotunneln* dominiert, einem Prozeß zweiter Ordnung, in dem ein Elektron über einen virtuellen Zustand der Insel durch den gesamten Transistor tunnelt. Zweitens haben Prozesse höherer Ordnung für stärkere Tunnelkopplungen oder tiefe Temperaturen und Transportspannungen sogar an der Resonanz (also obwohl sequentielles Tunneln stattfindet) signifikante Auswirkungen auf die Transportcharakteristik. Im allgemeinen müssen Prozesse beliebig hoher Ordnung (*Resonanztunneln*) berücksichtigt werden.

Ziel dieser Arbeit ist eine gemeinsame theoretische Beschreibung von sowohl Ladungseffekten als auch Quantenfluktuationen. Aus zweierlei Gründen ist dies eine wichtige Aufgabe. Erstens schmieren Quantenfluktuationen, ähnlich wie thermische Fluktuationen, ausgeprägte Strukturen in der Strom-Spannungs-Charakteristik aus. Dies reduziert die Genauigkeit der Bauteile. Theoretische Vorhersagen sind daher notwendig, um den Arbeitsbereich möglicher Anwendungen abzuschätzen. Quantenfluktuationen sind, zweitens, aus einem fundamentalerem Gesichtspunkt interessant. Der Einzel-Elektronen-Transistor kann je nach Realisierung in Quantenpunkten oder metallischen Inseln mit dem Einkanal- oder Vielkanal-Kondomodell in Verbindung gebracht werden. Diese Modelle beinhalten einen komplizierten Vielteilchen-Grundzustand, der qualitativ neues Verhalten aufzeigt (*Kondo-Physik*). Die Herstellungstechnologie erlaubt ein kontrolliertes Verändern der Systemparameter. Kondo-Verhalten kann daher in einem großen Parameterbereich experimentell untersucht werden. Vorhersagen bezgl. des Niedrigenergie-Verhaltens wurden in jüngsten Experimenten bestätigt. Theoretische und praktische Fragestellungen sind auf diese Weise miteinander kombiniert.

Diese Arbeit gliedert sich wie folgt. Kapitel 2 ist eine Einleitung zum allgemeinen Konzept der Ladungsenergie. Wir diskutieren Quantenpunkte und metallische Inseln als zwei Realisierungen des Einzel-Elektronen-Transistors in verschiedenen Grenzfällen, nämlich mit einem diskreten bzw. kontinuierlichen Levelspektrum auf der Insel. In Kapitel 3 wird eine allgemeine Real Zeit Transporttheorie entwickelt. Wir leiten eine diagrammatische Sprache ab, in der jedes Diagramm physikalisch als ein spezifischer Tunnelprozeß oder Renormierungsterm interpretiert werden kann. In Kapitel 4 wenden wir unsere Theorie auf Quantenpunkte an und diskutieren die Kondo-Physik darin. Diese zeigt sich in ausgeprägten Anomalien des Leitwertes bei verschwindender Transportspannung. Je nach Wahl der Parameter finden wir ein Maximum oder sagen ein Minimum voraus. Kapitel 5 ist Einzel-Elektronen-Transistoren mit metallischen Inseln gewidmet. In diesem Fall wurde die Kondo-Physik in der logarithmischen Temperaturabhängigkeit der Peakhöhe in den Coulomboszillationen experimentell nachgewiesen. Dies kann auf

Quantenfluktuationen zurückgeführt werden und wird quantitativ in zweiter Ordnung Störungstheorie (*Cotunneln an der Resonanz*) erklärt. Außerdem diskutieren wir die Renormierung der Ladungsenergielücke und der Tunnelkopplungsstärke im Rahmen der *Resonanztunnel-Approximation*. In Kapitel 6 entwickeln wir eine neue Renormierungsgruppen-Methode, die ein noch stärkeres Werkzeug zur Beschreibung von Quantenfluktuationen zu werden verspricht als die diagrammatische Sprache. Wir zeigen erste Resultate für die metallische Einzel-Elektron-Box bei Temperatur null. Schließlich diskutieren wir in Kapitel 7, wie Quantenfluktuationen die statistischen Eigenschaften der Levelverteilung beeinflussen. Im Gegensatz zu den vorhergehenden Teilen dieser Arbeit vernachlässigen wir hier Ladungseffekte. We präsentieren exakte Ergebnisse und finden ein neues asymptotisches Verhalten der Levelstatistik.

Chapter 1

Introduction

Charge is quantized. Electrons carry the elementary charge $e \approx 1.602 \times 10^{-19}$C. While this discovery is fundamental in physics, discreteness of charge does not play any role in usual electronic circuits. Even in the established computer technology, which handles circuits on the micrometer scale, current flow is carried by a huge number of electrons.

In the last few years, however, substantial progress has been achieved in the fabrication technology on the nanometer scale. This is not just a further step in miniaturization but opens the field to exploit charge quantization for new kinds of applications. In order to do so, the energy scale provided by temperature has to be lower than the relevant energy scale for charging effects, namely the charging energy for one electron $E_C = e^2/2C$. It has become possible to fabricate metallic junctions with capacitances in the range of $C = 10^{-15}$F in a controlled way. The corresponding temperature scale E_C/k_B is of the order of 1 K, which is experimentally accessible. An alternative approach is to structure a two-dimensional electron gas (2DEG) realized at an internal surface of a layered semiconductor material. In this way quantum dots have been fabricated in which the Coulomb energy can be characterized by capacitances in the range of $C = 10^{-15}$F or less. A recent challenge for experimentalists is provided by molecular systems with capacitances as low as $C = 10^{-18}$F. Under these circumstances, charging effects should become visible even at room temperature.

A simple system which shows charging effects is the *single-electron transistor* in which an island is coupled via two tunnel junctions to two leads. Current through the transistor is established by sequential transport of electrons, i.e., one electron after the other crosses the system. The Coulomb repulsion prevents a second electron to enter the island before the first one has left it. Depending on an applied gate voltage transport can even be blocked completely (*Coulomb blockade*). As a function of the gate voltage the current shows a series of peaks (*Coulomb oscillations*). Since transport properties are determined by the charge of single electrons applications as electrometers, current and capacitance standards with enormous accuracy have been realized. Furthermore, low-temperature thermometers, logical elements and memory devices based on charging effects are possible. The experimental and theoretical developments in *single electronics* are reviewed, for instance, in Refs. [1–6].

A master-equation description of sequential tunneling [1–11] is sufficient as long as the

coupling of the island to the leads is weak and the temperature and transport voltage are not too small. In this regime, transport occurs incoherently in sequences of uncorrelated tunnel processes. The corresponding tunnel rates can be derived from Golden rule arguments. This scheme establishes the so-called *orthodox theory*.

There is experimental and theoretical evidence [12–46], however, that in general, the physics of the single-electron transistor is much richer than described within the orthodox theory. The latter accounts for charging effects due to the discreteness of charge, but quantum fluctuations and higher-order tunnel processes are neglected. First, in the Coulomb blockade regime, in which sequential tunneling is exponentially suppressed, transport is dominated by *cotunneling* [47, 48], a coherent, second-order process, where an electron tunnels through the whole transistor via a virtual state of the island. Second, for larger tunnel coupling or low temperature and transport voltage, even at resonance, higher-order processes have significant effects on the transport characteristics [33,35], though sequential tunneling takes place. In general, processes of arbitrarily high order (*resonant tunneling*) have to be taken into account [25, 26, 30, 31, 39].

The aim of this thesis is to present a theoretical description which incorporates both charging effects *and* quantum fluctuations. This is an important task for the following reasons. First, quantum fluctuations wash out pronounced structures in the current-voltage characteristics similar as thermal fluctuations do. This reduces the accuracy of the devices. Theoretical predictions are therefore needed in order to estimate the working range of possible applications. Second, the study of quantum fluctuations is interesting from a more fundamental point of view. Depending on the realization in quantum dots or metallic islands, the single-electron transistor is related to the single-channel and multi-channel Kondo model, respectively. These models have a complicated many-particle ground state which gives rise to qualitative new behavior (*Kondo physics*). Since the fabrication technology allows for a controlled tuning of most parameters, an experimental study of Kondo behavior is possible over a wide range. Predictions concerning the low-energy behavior have been confirmed in recent experiments [49–53], thus combining questions of theoretical and practical relevance.

The outline of this thesis is as follows. Chapter 2 is an introduction to the general concept of the charging energy. We discuss quantum dots and metallic islands as two realizations of the single-electron transistor in different limits with a discrete and continuous level spectrum on the island, respectively. A general real-time transport theory is developed in Chapter 3. We derive a diagrammatic language in which each diagram can be interpreted physically as a specific tunnel process or renormalization term. In Chapter 4 we apply our theory to quantum dots and discuss the Kondo physics therein [39–44]. The latter leads to pronounced zero-bias anomalies in the conductance. Depending on the choice of parameters we find a zero-bias maximum or predict a zero-bias minimum. Chapter 5 is devoted to single-electron transistors with metallic islands [30–38]. The Kondo physics is seen experimentally [53] as a logarithmic temperature dependence of the peak height of the Coulomb oscillations. This can be traced back to quantum fluctuations and is quantitatively explained within second-order perturbation theory (*cotunneling at resonance*) [33, 35]. Furthermore, we discuss renormalization of the charging-energy gap and

the tunnel strength within the *resonant-tunneling approximation*. In Chapter 6 we develop a new renormalization-group method which promises to become an even more powerful tool to describe quantum fluctuations than the diagrammatic language. We present first results for the metallic single-electron box at zero temperature [45]. Finally, in Chapter 7, we discuss how quantum fluctuations influence the statistical properties of the level distribution of the dot. In contrast to the previous parts of the thesis neglect charging effects. We present exact results and find a new asymptotic behavior in the level statistics [46].

Chapter 2

Charging Energy and Charge Transport in Single-Electron Devices

Single-electron devices are mesoscopic structures in which the quantization of electric charge leads to Coulomb blockade phenomena due to small capacitances [1–6]. The simplest systems showing Coulomb blockade effects are the single-electron box and the single-electron transistor. In this chapter we discuss how the Coulomb blockade can be understood within the general concept of the charging energy. Depending on the realization of system, the transport characteristics of the transistor show specific features. We discuss the quantum dot and the metallic island as two limiting cases. While the qualitative behavior of the Coulomb effects is the same for all realizations, quantum fluctuations will affect transport properties in a very different way.

2.1 Single-Electron Devices

The single-electron transistor consists of a small island which is coupled by tunnel junctions to two leads (the equivalent electrotechnical circuit is shown in Fig. 2.1). An applied transport voltage $V = V_L - V_R$ drives a current through the system. The electrochemical potential of the island can be tuned by a capacitively coupled gate voltage V_G. For small systems and low temperatures and transport voltages the interaction of the island electrons will become important. In a simple transport cycle one electron enters the island via the left tunnel junction and then, before a second electron enters, an electron (the same or another one) leaves the island via the right tunnel junction. Thus, electrons are transferred one by one (see Fig. 2.2). This is called *sequential tunneling* or *single-electron tunneling* (SET). Whether this transport cycle is possible or not depends on the potential of the island which is controlled by the gate voltage (see Section 2.3).

At zero transport voltage, $V = 0$, the transistor becomes equivalent to the single-electron box (see Fig. 2.3). The two junctions of the transistor can be replaced by one junction with capacitance $C_J = C_L + C_R$ and tunnel resistance $R = [1/R_L + 1/R_R]^{-1}$. Therefore, we proceed with the description of the transistor. The physics of the box is

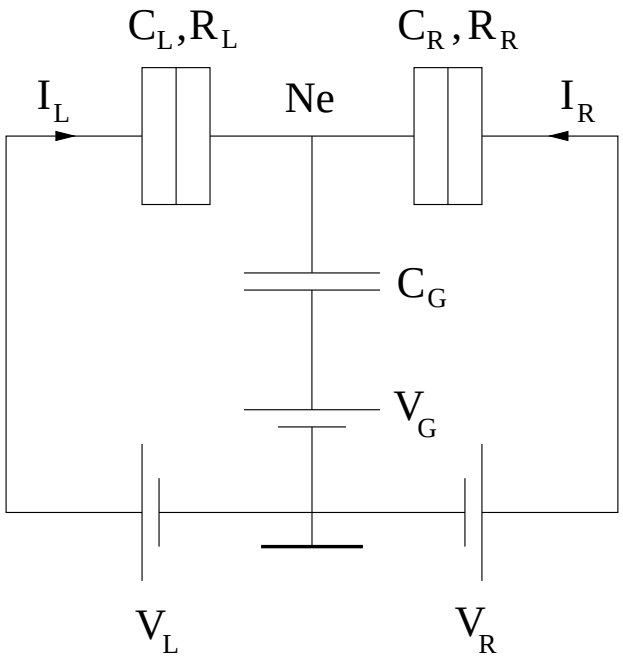

Figure 2.1: The single-electron transistor and the single-electron box.

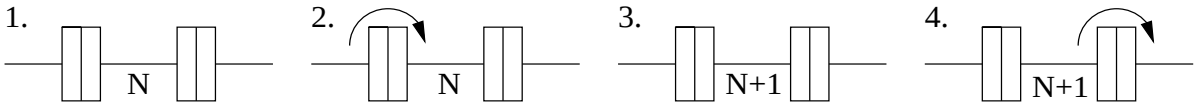

Figure 2.2: A transport cycle consists of two tunneling processes. Electrons are transferred through the transistor one by one (sequential tunneling).

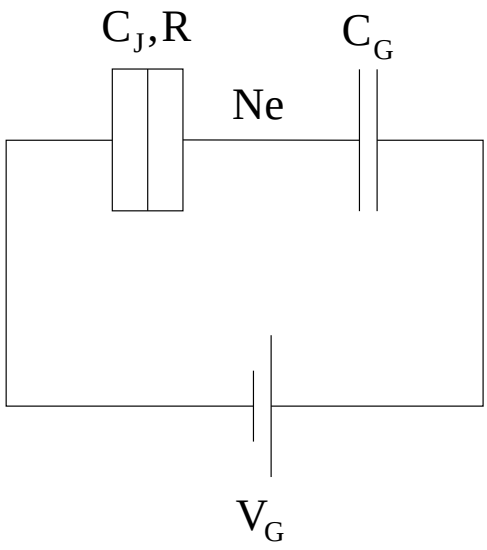

Figure 2.3: The single-electron box.

completely described by the equilibrium properties of the transistor.

2.2 Realizations: Quantum Dot and Metallic Island

Different techniques have been employed to build up single-electron transistors. The common feature is that a small island has to be isolated from leads by tunneling barriers.

In *lateral* quantum dots, a two-dimensional electron gas (2DEG) in a semiconductor heterostructure is patterned by metallic finger gates sitting atop the sample [6, 54–58]. By applying a negative potential to these finger gates the electron gas underneath is depleted. A schematic picture is given in Fig. 2.4. *Vertical* quantum dots (see Fig. 2.5) are layered structures with small diameter. The real edges of the sample confine the electrons. The diameter of the island is even smaller than that of the sample [59, 60]. Since the Fermi wavelength in semiconductors is comparable to the system size, quantization of the single-particle energies become visible.

Tunnel junctions between metallic leads and metallic islands (see Fig. 2.6) have been produced with the help of shadow evaporation techniques [3] . In these systems the single-particle spectrum on the island remains continuous.

In a more recent technique a small Al particle is placed on a quantum point contact [61–63] (see Fig. 2.7). Although the island is metallic the small system size implies a discrete spectrum of the electronic states on the islands. Therefore, this system shows the same behavior as quantum dots.

Even smaller single-electron transistors have been realized with nanocrystals as islands [64] or with atoms between a scanning-tunneling microscope (STM) tip and a substrate [65]. In the latter case Coulomb blockade has been observed at room temperature.

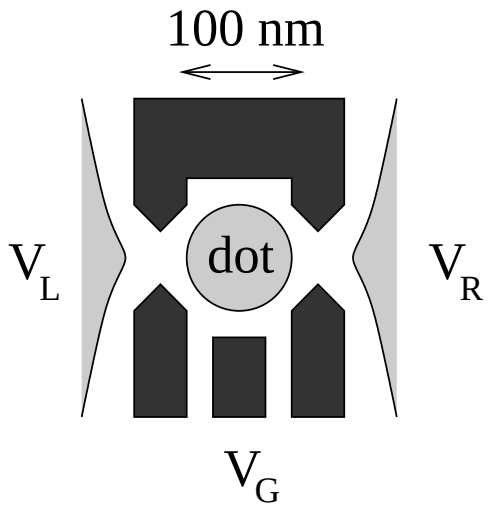

Figure 2.4: A lateral quantum dot. Metallic gates define the dot in the 2DEG underneath.

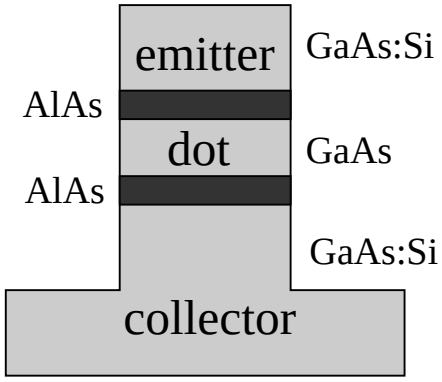

Figure 2.5: A vertical quantum dot. The thickness of the AlAs and GaAs-layers are typically several nm.

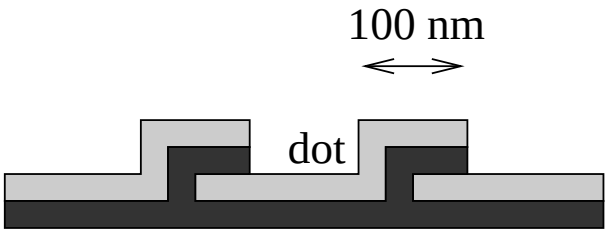

Figure 2.6: A single-electron transistor in Al with overlap junctions.

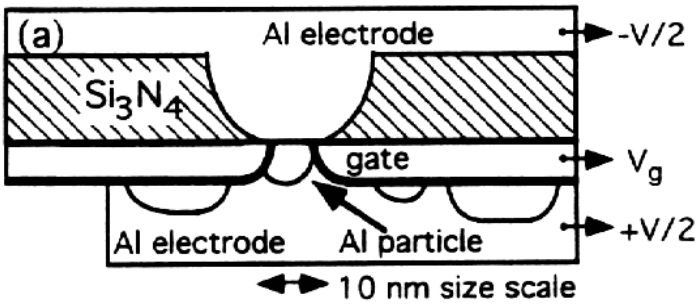

Figure 2.7: A nanoparticle single-electron transistor.

2.3 Charging Energy

The Coulomb interaction of the electrons on the island is accounted for by the classical electrostatic energy. This is possible since the tunnel junctions are very well characterized by capacitances C_L and C_R. This energy is called *charging energy* and is given by [1–5]

$$E_{ch}(N, n_x) = E_C(N - n_x)^2 \,. \tag{2.1}$$

Here, we have dropped a constant term $-E_C n_x^2$, which is independent of the number of excess charges N on the island. The external charge $en_x = C_L V_L + C_R V_R + C_G V_G$ can be tuned continuously by the gate voltage V_G. The total island capacitance $C = C_L + C_R + C_G$ (or $C = C_J + C_G$ for the box) defines the energy scale for the charging energy

$$E_C \equiv \frac{e^2}{2C} \,. \tag{2.2}$$

A set of parabolas $E_{ch}(n_x)$ for different values of N is shown in Fig. 2.8. On varying the gate voltage V_G the ground-state energy E_G follows the bottom line. At low temperature and transport voltage, i.e.,

$$E_C \gg \max\{k_B T, eV\} \,, \tag{2.3}$$

the number of island electrons N is fixed for n_x being away from half-integer values. Transport is suppressed (*Coulomb blockade*) since during a transport cycle N has to be increased or decreased. Current through the system can only flow near the intersection points of the parabolas (i.e., near half-integer values of n_x). The current I and the conductance $G = \partial I/\partial V$ show a periodic structure as a function of V_G (see Fig. 2.9), called *Coulomb oscillations*. The system is called *transistor* since by tuning the gate voltage V_G the current can be switched on and off.

The existence of Coulomb oscillations can be explained with the classical concept of charging energy. But in some cases quantization effects due to the smallness of the island are also important. Then, the total energy is the sum

$$E_N(n_x) = E_{ch}(N, n_x) + \sum_{l=1}^{N} \epsilon_l \,, \tag{2.4}$$

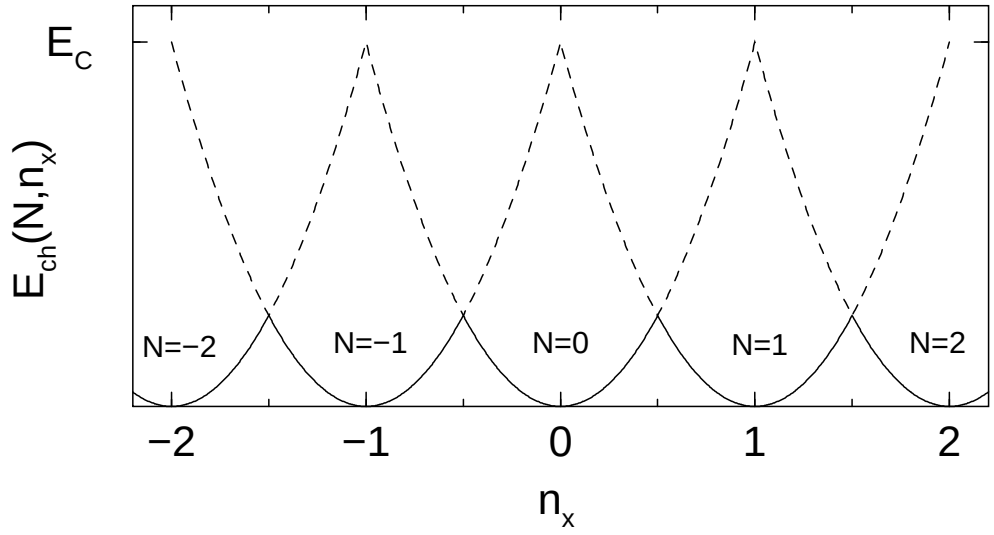

Figure 2.8: The charging energy E_{ch} as a function of n_x for different values of N. The ground-state energy follows the solid line.

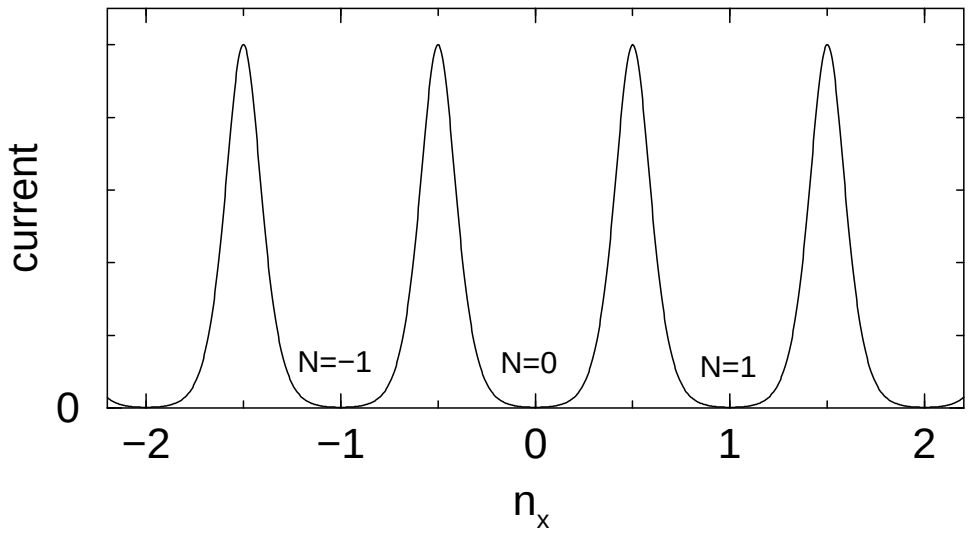

Figure 2.9: The *Coulomb oscillations* and *Coulomb blockade*: The current is maximal at the degeneracy points of adjacent charge states. In between the current is suppressed.

where ϵ_l are the single-particle energies with spacing $\Delta\epsilon$. This means that the conductance peaks determined by the condition $E_N(n_x) = E_{N+1}(n_x)$ are separated by $2E_C + \Delta\epsilon$. In the following, we consider the two limiting cases of
(i) a discrete spectrum with high level spacing ("$\Delta\epsilon = \infty$") and
(ii) a continuous spectrum ("$\Delta\epsilon = 0$").
The first case is an extreme quantum dot with only one level while the second one describes systems with metallic islands.

2.4 Hamiltonian

The single-electron transistor is modeled by the standard Hamiltonian $H = H_0 + H_T$, in which H_0 describes the decoupled system and H_T the tunneling between the leads and the island. The decoupled system consists of noninteracting electrons in the left and right lead and interacting electrons in the dot,

$$H_0 = H_L + H_R + H_D + H_{ch} \,. \tag{2.5}$$

For the interaction of the island electrons we use the capacitive model for Coulomb blockade, $H_{ch} = E_C(N - n_x)^2$. Electron tunneling occurs in the left and right junction, i.e.,

$$H_T = H_{T,L} + H_{T,R} \,. \tag{2.6}$$

We now specify the notation for the limits of a single-level quantum dot and the metallic island with many transverse channels.

2.4.1 Discrete Spectrum: Anderson Model

The extreme case of a quantum dot containing only one level is described by the Anderson model. The kinetic energy of the noninteracting electrons in the leads and the electrons in the dot is

$$H_r = \sum_{k\sigma} \epsilon_{k\sigma r} a^\dagger_{k\sigma r} a_{k\sigma r} \qquad \text{for} \qquad r = L, R \tag{2.7}$$

$$H_D = \sum_{\sigma} \epsilon_\sigma c^\dagger_\sigma c_\sigma \,, \tag{2.8}$$

respectively. The wave vectors k label the electron states for fixed reservoir index r and spin $\sigma = 1, \ldots, M$ where M is the spin degeneracy. The interaction term can be written in the form

$$H_{ch} = U \sum_{\sigma<\sigma'} n_\sigma n_{\sigma'} \,. \tag{2.9}$$

This is equivalent to the capacitive model of Eq. (2.1) for $U = 2E_C$ and shifting the level position in Eq. (2.8), $\epsilon_\sigma + 2E_C - eV_G C_G/C - a_c eV/2 \to \epsilon_\sigma$ with $V = V_L - V_R$. The

asymmetry factor $a_c = (C_L - C_R)/C$ accounts for a different capacitive coupling of the left and right lead. We see here that the effective level position in the Anderson model depends on the gate voltage V_G as well as, due to a_c, on the transport voltage V.

The tunneling part of the Hamiltonian couples the dot to the leads,

$$H_{T,r} = \sum_{k\sigma} \left(T^r_{k\sigma} a^\dagger_{k\sigma r} c_\sigma + h.c. \right) \qquad \text{for} \qquad r = L, R \,. \tag{2.10}$$

The spin σ is conserved during a tunnel process. We assume the tunnel matrix elements to be independent of the spin, $T^r_{k\sigma} = T^r_k$. The tunnel coupling leads to a finite lifetime τ of the dot states and, therefore, to an intrinsic level broadening $\Gamma = \hbar/\tau$. The latter is related to the classical tunnel rates $2\pi\gamma^\pm_r(\omega) = \Gamma_r(\omega) f^\pm_r(\omega)$ into (out of) the dot through barrier r, obtained from simple golden-rule arguments, by $\Gamma = \sum_r \Gamma_r$ and

$$\Gamma_r(\omega) = \frac{2\pi}{\hbar} \sum_k |T^r_k|^2 \, \delta(\omega - \epsilon_{kr}) \,. \tag{2.11}$$

Here and in the following, $f^+_r(\omega)$ is the Fermi distribution $[\exp(\beta(\omega - \mu_r)) + 1]^{-1}$ of reservoir r with electrochemical potential $\mu_r = -eV_r$, while $f^-_r(\omega) = 1 - f^+_r(\omega)$.

2.4.2 Continuous Spectrum: Metallic Island

Typical junctions in metallic transistors have an area of the order of $100\text{nm} \times 100\text{nm}$. This means that they contain a large number of transverse channels N_{ch}. From a comparison of Andreev reflection and single-electron tunneling in small normal-superconducting junctions one can conclude that for a typical system the number of channels is $N_{ch} \gtrsim 10^3$.

Furthermore, the single-particle spectrum of the electronic states on the island is dense, and the electron number of the island large. It is, therefore, justified to separate charge and fermionic degrees of freedom by introducing a phase operator φ, which is the canonical conjugate of the number of island electrons N, i.e., $[N, e^{i\varphi}] = e^{i\varphi}$, and to treat them independently of the field operators c and $c^\dagger$ for the electronic states on the island. The Hamiltonian then reads

$$H_r = \sum_{kn} \epsilon_{knr} a^\dagger_{knr} a_{knr} \qquad \text{for} \qquad r = L, R \tag{2.12}$$

$$H_D + H_{ch} = \sum_{qn} \epsilon_{qn} c^\dagger_{qn} c_{qn} + E_C \left(N - n_x \right)^2 \tag{2.13}$$

$$H_{T,r} = \sum_{kqn} \left(T^{rn}_{kq} a^\dagger_{knr} c_{qn} e^{-i\varphi} + h.c. \right) \qquad \text{for} \qquad r = L, R \,. \tag{2.14}$$

The wave vector q and n label the island states and the transverse channels which include the spin, respectively. The channel number is conserved during tunneling. The tunnel matrix elements $T^{rn}_{kq} = T^{rn}$ are considered independent of the states k and q. They are

related to the tunnel resistances R_r of the left and right junction

$$\frac{1}{R_r} = \frac{2\pi e^2}{\hbar} \sum_n N_r^n(0) N_I^n(0) |T^{rn}|^2, \tag{2.15}$$

where $N_I^n(0)$ and $N_r^n(0)$ are the densities of states of the island and the lead r, for channel n, respectively. The quantum resistance $R_K = h/e^2$ provides a natural scale for the tunnel resistance. We can, therefore, characterize each barrier by its transmission $\mathcal{T}_r = R_K/R_r$ or the dimensionless conductance

$$\alpha_0^r = \frac{R_K}{4\pi^2 R_r}\,. \tag{2.16}$$

As we shall see in Chapter 5 the small parameter for a systematic perturbation theory in the tunneling will be $\alpha_0 = \sum_r \alpha_0^r$. Therefore, it is convenient to include the factor $4\pi^2$ here. The classical rate for tunneling into (out of) the island is given by $2\pi\alpha_r^{\pm}(\omega)$ with

$$\alpha_r^{\pm}(\omega) = \alpha_0^r \int_{-\infty}^{\infty} dE\, f_r^{\pm}(E+\omega) f^{\mp}(E) = \pm\alpha_0^r \frac{\omega - \mu_r}{\exp[\pm\beta(\omega-\mu_r)] - 1}\,. \tag{2.17}$$

The energy difference of adjacent charge states N and $N+1$ reads

$$\Delta_N = E_{ch}(N+1) - E_{ch}(N) = E_C\left[1 + 2(N - n_x)\right]\,. \tag{2.18}$$

2.5 Quantum Fluctuations and Higher-Order Processes

For high tunnel barriers transport is dominated by incoherent, sequential tunneling processes, and a description within the *orthodox theory* which treats tunneling in lowest-order perturbation theory (golden rule), is sufficient. In Figs. 2.10a and 2.11a we show sequential-tunneling processes in an energy plot. In general, however, higher-order tunneling processes have to be taken into account.

First, in the Coulomb blockade regime, sequential tunneling is exponentially suppressed. *Cotunneling*, a second-order process where electrons tunnel via a virtual state of the island, provides the leading contribution [47, 48] (see Figs. 2.10b and 2.11b).

Second, at resonance, even though sequential tunneling occurs, higher-order processes have a significant effect on the gate-voltage dependent linear and nonlinear conductance [33, 35].

In general, there are coherent processes with an arbitrary number of tunnel events (*resonant tunneling*) at both junctions (see Figs. 2.10c and 2.11c) contributing to the conductance [25, 26, 30, 31, 39].

Higher-order processes in the metallic case are *inelastic* since different electronic island states are involved with overwhelming probability, i.e., particle-hole excitations remain after the process. For a dot containing only one level, all tunnel processes are *elastic* by definition.

Both models, the single-level quantum dot and the metallic island with an infinite number of transverse channels, are related to generic models of many-body physics, the

single-channel and the multichannel-channel *Kondo model*, respectively. These systems have a complicated many-particle ground state which give rise to new behavior (*Kondo physics*) in comparison to the simple orthodox-theory picture. Predictions concerning the low-energy behavior of these models have been confirmed in recent experiments [49–53], thus combining questions of theoretical and practical relevance.

A discussion of this Kondo physics as well as a comparison with experiments is the central part of this thesis (Chapters 4 and 5). Kondo behavior arises from the *interplay* of charging effects and quantum fluctuations.

When do quantum fluctuations become relevant? For the quantum dot, deviations from sequential tunneling become visible when the finite width of the dot level can be resolved. This happens at temperatures lower than level width, $k_B T \lesssim \Gamma$. To see Kondo behavior the temperature has to be decreased further, $T \lesssim T_K$, where T_K is the Kondo temperature T_K. The stronger the tunnel coupling the better are these conditions satisfied. But the tunnel Hamiltonian description is only applicable if the transmission through the barrier for each channel is much smaller than unity. In metallic junctions with many transverse channels, however, it is possible to achieve a large total transmission, $\mathcal{T}_r = \sum_n \mathcal{T}_{r,n}$, with the transmission of each channel $\mathcal{T}_{r,n}$ being much smaller than unity. Quantum fluctuations become visible for $\mathcal{T}_r \gtrsim 1$ or $\alpha_0^r \gtrsim 1/4\pi^2$.

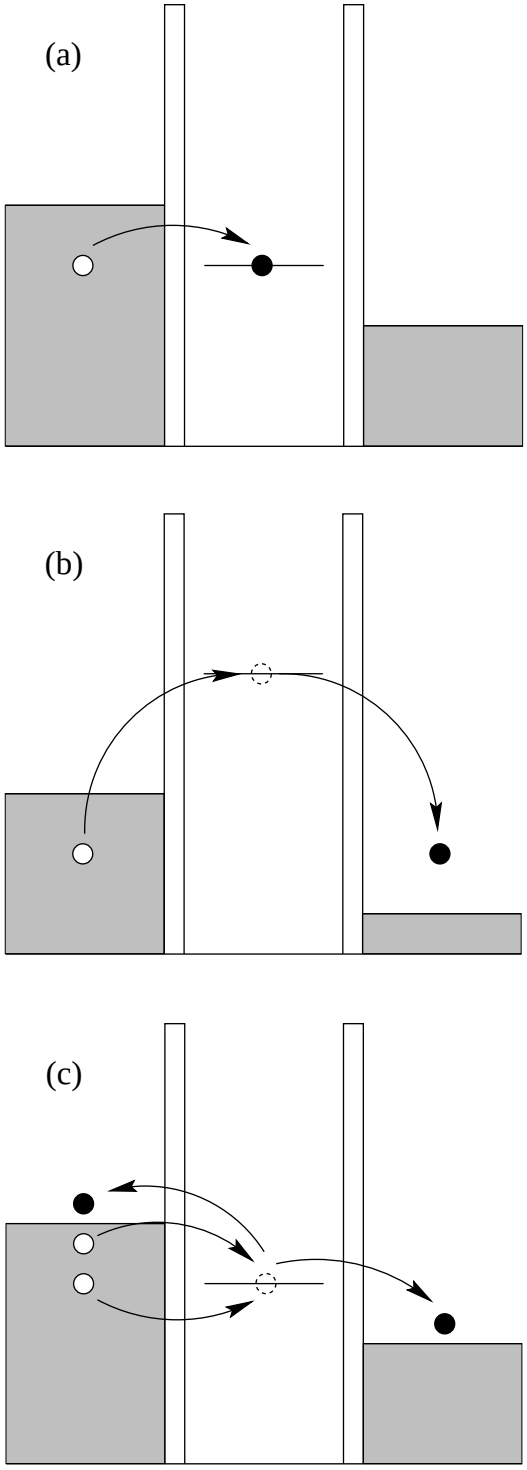

Figure 2.10: Tunneling processes in the quantum dot: a) sequential tunneling, b) cotunneling, and c) resonant tunneling. All processes are elastic.

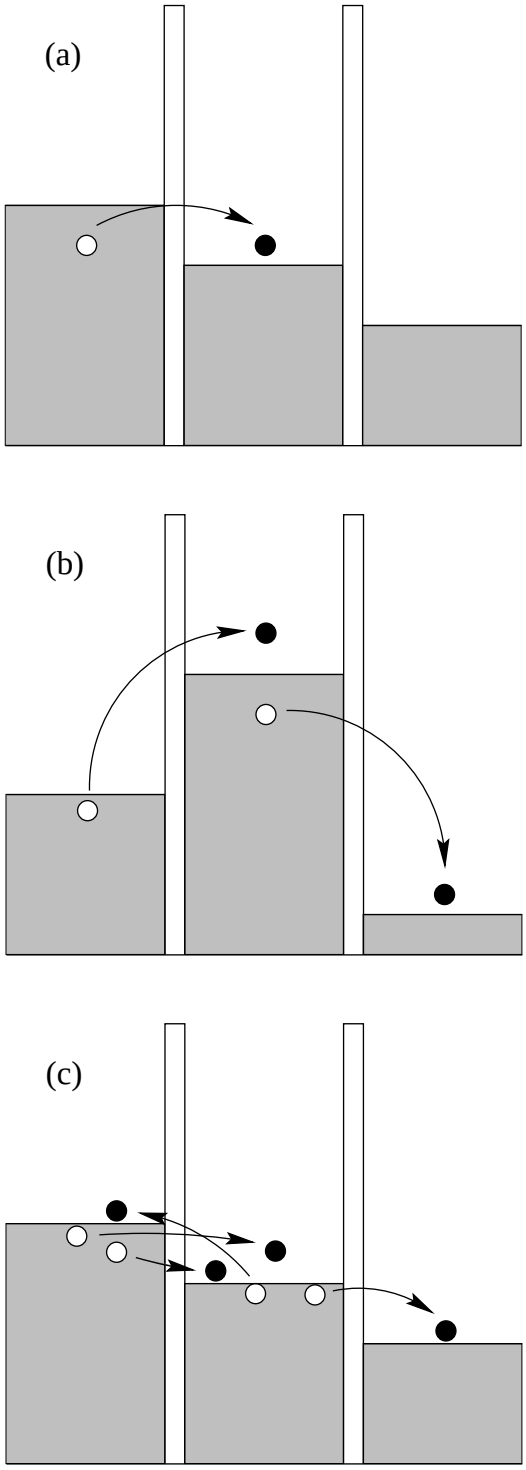

Figure 2.11: Tunneling processes in a metallic island: a) sequential tunneling, b) cotunneling, and c) resonant tunneling. Processes b) and c) are inelastic.

Chapter 3

Real-Time Transport Theory

We present a general transport theory based on a real-time diagrammatic approach [25–27, 30,31,39,40]. The latter is closely related to path-integral methods formulated in connection with dissipation [66–70] or tunneling in single metallic junctions [71, 72]. The basic idea is to integrate out all reservoir degrees of freedom and thus end up with a formally exact kinetic equation for the reduced density matrix of the dot states in the quantum dot or the charge states on the metallic island, respectively. The kernel of this integro-differential equation is represented as a sum over all irreducible diagrams and can be calculated in a systematic perturbation expansion in the tunneling strength. Each diagram has its physical interpretation as a specific tunnel process or renormalization term. Explicit calculations of the self-energy for the quantum dot and the metallic island within some approximation schemes for different regimes are given in Chapters 4 and 5.

In order to keep all formulas transparent, we put $\hbar = 1$ and $k_B = 1$ in the following chapters.

3.1 Diagrams

A quantum-statistical expectation value of an operator A at time t is given by

$$\langle A(t)\rangle = \mathrm{tr}[\rho_0 A(t)_H], \tag{3.1}$$

where $A(t)_H = \exp[iH(t-t_0)]A\exp[-iH(t-t_0)]$ is the operator in the Heisenberg picture with respect to the initial time t_0, and $\rho_0 = \rho(t_0)$. Permutation under the trace yields $\langle A(t)\rangle = \mathrm{tr}[\rho(t)A]$ with A in the Schrödinger picture. The density matrix $\rho(t)$ evolves in time via

$$\rho(t) = e^{-iH(t-t_0)}\rho(t_0)e^{iH(t-t_0)}\,. \tag{3.2}$$

We assume that the initial density matrix ρ_0 factorizes into parts for the dot electrons and the leads. Additionally, in the case of the metallic island, there is a part for the island-charge degrees of freedom N. We write

$$\rho_0 = \rho_0^D \prod_{r=L,R} \rho_0^r \qquad \text{and} \qquad \rho_0 = \rho_0^N \prod_{r=L,R,D} \rho_0^r \tag{3.3}$$

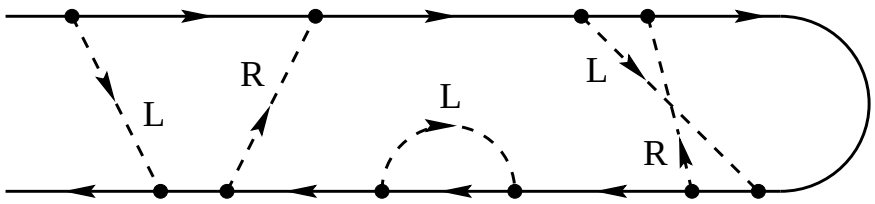

Figure 3.1: An example for the time evolution of the reduced density matrix. The upper and lower line represent the forward and backward propagator, respectively. There are tunneling lines (for the left and right reservoir) connecting vertices in pairs.

for the quantum dot and the metallic island, respectively. The leads and, in the case of the metallic island, the island electrons are treated as large equilibrium reservoirs with fixed electrochemical potentials $\mu_r = -eV_r$ (and $\mu_D = 0$). Therefore, we describe these electrons by Fermi functions $f_r(\omega)$ and the density matrix reads

$$\rho_0^r = \frac{1}{Z_0^r} e^{-\beta(H_r - \mu_r N_r)} \tag{3.4}$$

with the inverse temperature $\beta = 1/T$ and the number operator $N_r = \sum_{k\sigma} a^\dagger_{k\sigma r} a_{k\sigma r}$. The normalization factor Z_0^r is determined by $\mathrm{tr}\,\rho_0^r = 1$.

The remaining part, i.e., the dot electrons and the charge states of the island in the case of the quantum dot and the metallic island, respectively, is *not* described by equilibrium reservoirs. We only assume that their initial distribution is diagonal in some basis $\{|\chi\rangle\}$. In the quantum dot case, $|\chi\rangle$ labels some many-body dot states, which include the strong correlations within the island but are assumed to have fixed occupation numbers. We get

$$\rho_0^D = \sum_\chi P_\chi^0 |\chi\rangle\langle\chi| \tag{3.5}$$

with $\sum_\chi P_\chi^0 = 1$. For the metallic island, the initial distribution ρ_0^N is diagonal in the basis of the charge states, $|\chi\rangle = |N\rangle$. We will see later, that in the stationary limit, i.e., when t_0 is shifted to minus infinity, all the physical quantities are independent of the choice of P_χ^0.

In the following, it is convenient to change to the interaction picture with respect to H_0. This implies $A(t)_H = \tilde{T} \exp\left(-i \int_t^{t_0} dt'\, H_T(t')_I\right) A(t)_I\, T \exp\left(-i \int_{t_0}^t dt'\, H_T(t')_I\right)$ in which T is the time-ordering and $\tilde{T}$ denotes the anti-time-ordering operator. We write the integrals as one contour integral $\int_K dt' \ldots$ over the *Keldysh contour*. It is parameterized by the "time" t' which first runs forward from t_0 to t and then backward from t to t_0. In the diagrammatic language, the Keldysh contour is represented by horizontal lines running from the left to the right and then back to the left (see Fig. 3.1).

We find

$$\langle A(t)\rangle = \mathrm{tr}\left[\rho_0\, T_K \exp\left(-i \int_K dt' H_T(t')_I\right) A(t)_I\right]. \tag{3.6}$$

Here, we have introduced the Keldysh time-ordering operator T_K, which orders all following operators along the Keldysh contour such that the one with the later "time" along the

Keldysh contour appears at a further left position (without any sign change for an exchange of Fermi operators).

In the following we will encounter also higher-order correlation functions of the type $\langle T_K A_1(t_1)_I A_2(t_2)_I \dots A_n(t_n)_I \rangle$. The final time t is then given by $\max\{t_1, \dots, t_n\}$.

For a diagrammatic description we expand the exponential with respect to the tunneling Hamiltonian and obtain

$$\left\langle T_K \prod_{i=1}^{n} A_i(t_i) \right\rangle = \tag{3.7}$$
$$\mathrm{tr}\left[\rho_0 \sum_{m=0}^{\infty} (-i)^m \int_K dt_1' \int_K dt_2' \dots \int_K dt_m' \, T_K \left\{ H_T(t_1')_I H_T(t_2')_I \dots H_T(t_m')_I \prod_{i=1}^{n} A_i(t_i)_I \right\}\right]$$
$$t_1' > t_2' > \dots > t_m'$$

in which the relation $t_1' > t_2' > \dots > t_m'$ has to be understood with respect to the Keldysh contour. The time-ordering operator T_K acts also on the operators $A_i(t_i)_I$ and puts them on the correct place between the tunneling Hamiltonians. Both type of operators H_T and A are diagrammatically represented by vertices (see Fig. 3.1), either *internal* (for H_T) or *external* (for A_i) ones.

The next task is to perform the trace of each term of the expansion. We insert the tunnel Hamiltonian (2.10) or (2.14) and notice that the Hamiltonian H_0 is bilinear in the lead electron operators. Furthermore, H_0 for the metallic island is bilinear in the island-electron operators. For this reason, Wick's theorem holds for these degrees of freedom and the corresponding operators are contracted in pairs.[1] This includes contractions between pairs of field operators from H_T as well as contractions to electron operators which can be present in the operators A_i. The contractions are given by equilibrium distribution functions and are diagrammatically represented by tunneling lines (see Fig. 3.1). These lines are directed, indicating whether the particle number of the island is increased or decreased. Furthermore they are labeled by the reservoir index r. For the electrons in the quantum dot as well as for the charge degrees of freedom in the metallic island Wick's theorem does not hold since the Coulomb interaction is expressed by a quartic term of dot electron operators Eq. (2.9) and quadratic term in the charge Eq. (2.13), respectively. A product of those operators can not be contracted into pairs, but has to be treated explicitly.

3.2 Master Equation and Stationary Probabilities

The central object of this chapter is the quantum-mechanical transition rate $\Sigma_{\chi',\chi}(t',t)$ from a state χ' at time t' to a state χ at time t. This rate will serve as an input for

[1] In the quantum dot case only one tunneling line enters or leaves each vertex. For the metallic island, there are contractions both for the lead and the island electrons. But in the limit of a large number of channels, "simple loop" configurations dominate where the two fermion operators of one term H_T are contracted with the corresponding two operators from one other term H_T. We represent these loops by a single tunneling line.

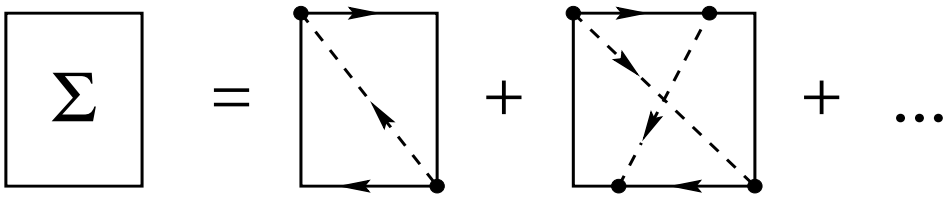

Figure 3.2: The irreducible self-energy Σ.

a formally exact and time-dependent master equation which, in principle, could be used to calculate all probabilities P_χ for the states χ as a function of time for an arbitrary initial distribution. Similar master equations are well-known and successfully applied in connection with macroscopic quantum coherence phenomena in spin Bose models [70, 73].

A matrix element of the reduced density matrix of the dot at time t, $P^{\chi_1}_{\chi_2}(t)$, is given by the quantum-statistical expectation value of the projector $|\chi_2\rangle\langle\chi_1|(t)$

$$P^{\chi_1}_{\chi_2}(t) = \left\langle |\chi_2\rangle\langle\chi_1|(t) \right\rangle , \tag{3.8}$$

i.e., we have to set $n = 1$ and $A_1 = |\chi_2\rangle\langle\chi_1|$ in Eq. (3.7). The matrix element $P^{\chi_1}_{\chi_2}(t)$ can be expressed by the reduced propagator $\Pi^{\chi_1',\chi_1}_{\chi_2',\chi_2}(t',t)$ from χ_1' at time t' forward to χ_1 at time t and then from χ_2 at time t backward to χ_2' at time t',

$$P^{\chi_1}_{\chi_2}(t) = \sum_{\chi_1',\chi_2'} P^{\chi_1'}_{\chi_2'}(t')\Pi^{\chi_1',\chi_1}_{\chi_2',\chi_2}(t',t) \ . \tag{3.9}$$

The propagator is the sum of all diagrams with the given states at the ends and can be expressed by an irreducible self-energy part $\Sigma^{\chi_1',\chi_1}_{\chi_2',\chi_2}(t',t)$, defined as the sum of all diagrams in which any vertical cut through them crosses at least one tunneling line (see Fig. 3.2). The propagators for the four lines attached to the self-energy are not included in $\Sigma^{\chi_1',\chi_1}_{\chi_2',\chi_2}(t',t)$. We obtain an iteration in the style of a Dyson equation (see Fig. 3.3),

$$\begin{aligned} \Pi^{\chi_1',\chi_1}_{\chi_2',\chi_2}(t',t) &= \Pi^{(0)\,\chi_1}_{\chi_2}(t',t)\delta_{\chi_1,\chi_1'}\delta_{\chi_2,\chi_2'} \\ &+ \sum_{\chi_1'',\chi_2''}\int_{t'}^{t} dt_2 \int_{t'}^{t_2} dt_1\, \Pi^{\chi_1',\chi_1''}_{\chi_2',\chi_2''}(t',t_1)\, \Sigma^{\chi_1'',\chi_1}_{\chi_2'',\chi_2}(t_1,t_2)\, \Pi^{(0)\,\chi_1}_{\chi_2}(t_2,t) \ , \end{aligned} \tag{3.10}$$

where $\Pi^{(0)\,\chi_1}_{\chi_2}(t',t) = \exp\left[-i(\epsilon_{\chi_1} - \epsilon_{\chi_2})(t-t')\right]$ is the propagator of the isolated dot or island charge subsystem, respectively. Multiplying this equation with $P^{\chi_1'}_{\chi_2'}(t')$, summing over the states χ_1', χ_2' and differentiating with respect to t, we obtain together with Eq. (3.9) and setting $t' = t_0$

$$\frac{d}{dt}P^{\chi_1}_{\chi_2}(t) + i(\epsilon_{\chi_1} - \epsilon_{\chi_2})P^{\chi_1}_{\chi_2}(t) = \sum_{\chi_1',\chi_2'}\int_{t_0}^{t} dt'\, P^{\chi_1'}_{\chi_2'}(t')\Sigma^{\chi_1',\chi_1}_{\chi_2',\chi_2}(t',t) \ . \tag{3.11}$$

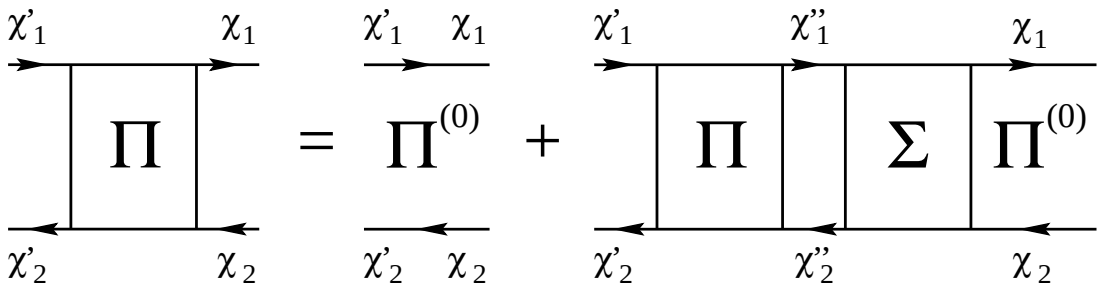

Figure 3.3: Iteration of the irreducible self-energy Σ for the propagator Π.

This formally exact equation is the most general kinetic equation for the reduced density matrix. No assumption is necessary for the initial state, and the integral kernel Σ on the right hand side shows that memory effects are fully taken into account.

The equation simplifies considerably if we assume that the initial density matrix is diagonal. In the general case, this does not imply that the reduced density matrix stays diagonal for all times. However, for the special cases of the Anderson model and the metallic island considered here, conservation of spin and transverse channel number implies that the reduced density matrix will be diagonal for all times $t > t_0$. Hence, we consider $\Sigma_{\chi',\chi} \equiv \Sigma^{\chi',\chi}_{\chi',\chi}$ and obtain from (3.11)

$$\frac{d}{dt}P_\chi(t) = \sum_{\chi'} \int_{t_0}^{t} dt'\, P_{\chi'}(t')\Sigma_{\chi',\chi}(t',t)\ , \tag{3.12}$$

where $P_\chi(t) \equiv P^\chi_\chi(t)$ denotes the probability to be in the state χ at time t. For a time-translational invariant system, the time-dependent rates $\Sigma_{\chi',\chi}(t',t)$ depend only on the time difference $\Sigma_{\chi',\chi}(t'-t)$. Performing the Laplace transform of Eq. (3.12) one can then study the time evolution of arbitrary initial probability distributions into the stationary state.

According to the diagrammatic rules, which we will discuss in detail in Chapters 4 and 5, the change of the position of the rightmost vertex from the upper to the lower propagator or vice versa yields a minus sign, and therefore $\sum_\chi \Sigma_{\chi',\chi}(t',t) = 0$. This allows us to rewrite Eq. (3.12) in the form

$$\frac{d}{dt}P_\chi(t) = \sum_{\chi'\neq\chi} \int_{t_0}^{t} dt'\, \left[P_{\chi'}(t')\Sigma_{\chi',\chi}(t',t) - P_\chi(t')\Sigma_{\chi,\chi'}(t',t)\right]\ . \tag{3.13}$$

We obtain the structure of a master equation with a gain and a loss term on the right hand side and transition rates given by the kernel $\Sigma_{\chi',\chi}(t',t)$.

The stationary distribution is given by

$$P_\chi = \lim_{t\to\infty} P_\chi(t) = \lim_{t_0\to-\infty} P_\chi(0) \tag{3.14}$$

and is *not* the equilibrium one if the electrochemical potentials of the leads are different. From (3.13) we obtain

$$0 = \sum_{\chi'} P_{\chi'} \Sigma_{\chi',\chi} = \sum_{\chi' \neq \chi} \left[P_{\chi'} \Sigma_{\chi',\chi} - P_{\chi} \Sigma_{\chi,\chi'} \right] , \tag{3.15}$$

for arbitrary χ, where

$$\Sigma_{\chi',\chi} = i \int_{-\infty}^{0} dt' \, \Sigma_{\chi',\chi}(t',0) \tag{3.16}$$

can be calculated directly by using our diagrammatic rules in energy space (see Chapters 4 and 5). For a well-defined perturbation expansion in powers of $|T|^2$, i.e., in powers of Γ and α_0 for the quantum dot and the metallic island, respectively, we can write

$$\Sigma_{\chi',\chi} = \sum_{k=1}^{\infty} \Sigma_{\chi',\chi}^{(k)} \qquad \text{and} \qquad P_{\chi} = \sum_{k=0}^{\infty} P_{\chi}^{(k)} , \tag{3.17}$$

and the stationary master equation (3.15) has to be satisfied in each order, i.e.,

$$0 = \sum_{\chi'} P_{\chi'}^{(0)} \Sigma_{\chi',\chi}^{(1)} \qquad \text{and} \qquad 0 = \sum_{\chi'} P_{\chi'}^{(0)} \Sigma_{\chi',\chi}^{(2)} + \sum_{\chi'} P_{\chi'}^{(1)} \Sigma_{\chi',\chi}^{(1)} \tag{3.18}$$

in first and second order. Thus, one can iteratively solve for $P_{\chi}^{(k)}$ with arbitrary k.

3.3 The Tunneling Current

The tunneling current flowing into reservoir r is related to the time derivative of the particle number, $I_r(t) = e \frac{d}{dt} \langle N_r(t) \rangle = ie \langle [H, N_r](t) \rangle$. This is equivalent to

$$I_r(t) = -ie \sum_{k\sigma} \left\{ T_k^r \langle (a_{k\sigma r}^{\dagger} c_{\sigma})(t) \rangle \, - \, T_k^{r*} \langle (c_{\sigma}^{\dagger} a_{k\sigma r})(t) \rangle \right\} \tag{3.19}$$

for the quantum dot and

$$I_r(t) = -ie \sum_{kqn} \left\{ T_{kq}^{rn} \langle (a_{knr}^{\dagger} c_{qn} e^{-i\varphi})(t) \rangle \, - \, T_{kq}^{rn*} \langle (c_{qn}^{\dagger} a_{knr} e^{i\varphi})(t) \rangle \right\} \tag{3.20}$$

for the metallic island. The procedure how to calculate the given expectation values follows from Section 3.1. The diagrams for the expectation values in Eqs. (3.19) and (3.20) have a vertex at time t. It has the same structure as the other tunneling vertices from H_T, and by attaching this vertex to the upper or lower propagator we can relate the rightmost irreducible part of the diagram to the self-energy Σ. We obtain

$$I_r(t) = e \sum_{\chi,\chi'} \int_{t_0}^{t} dt' P_{\chi'}(t') \Sigma_{\chi',\chi}^{r+}(t',t) = -e \sum_{\chi,\chi'} \int_{t_0}^{t} dt' P_{\chi'}(t') \Sigma_{\chi',\chi}^{r-}(t',t) \tag{3.21}$$

where we have introduced the partial self-energies $\Sigma^{r\pm}_{\chi',\chi}(t',t)$ as parts of the total self-energy

$$\Sigma_{\chi',\chi}(t',t) = \sum_r \left\{ \Sigma^{r+}_{\chi',\chi}(t',t) + \Sigma^{r-}_{\chi',\chi}(t',t) \right\} . \tag{3.22}$$

They, $\Sigma^{r+}_{\chi',\chi}$ (or $\Sigma^{r-}_{\chi',\chi}$) describe diagrams in which the rightmost tunneling line corresponds to reservoir r and is an outgoing (incoming) line if the rightmost vertex lies on the upper propagator or an incoming (outgoing) line if the rightmost vertex lies on the lower propagator. Their physical meaning is displayed by the current formula (3.21) which shows that they give the total contribution to the current rate. We can relate them to an intuitively more physical object, namely the rate $\Sigma^{rp}_{\chi',\chi}(t',t)$, $p = 0, \pm 1, \pm 2, \ldots$, which describes the transition rate where p particles are transferred to reservoir r. Within our graphical language $\Sigma^{rp}_{\chi',\chi}(t',t)$ is given by all diagrams where the number of tunneling lines with reservoir index r running from the forward to the backward propagator minus the number of tunneling lines with reservoir index r running from the backward to the forward propagator is given by p. We obtain the relation

$$\sum_\chi \Sigma^{r\pm}_{\chi',\chi}(t',t) = \pm \sum_\chi \sum_p p\, \Sigma^{rp}_{\chi',\chi}(t',t) \tag{3.23}$$

which is proven by combining those diagrams on the right-hand side of Eq. (3.23) with opposite vertical positions of the rightmost vertex (for details see [40]). The factor p shows clearly that $\Sigma^{r\pm}$ describes the contribution to the current rate. In contrast to lowest-order processes, i.e., the golden-rule rate, where p can only take the values ± 1, p can be arbitrary for higher-order processes. Nevertheless, Eq. (3.22) shows that the current rate can be calculated as a partial selection of diagrams already contained in the total transition rate $\Sigma_{\chi',\chi}$.

It is easy to prove [40] current conservation,

$$-e\frac{d}{dt}\langle N(t)\rangle = \sum_r I_r(t) , \tag{3.24}$$

where $-eN$ is the total island charge. This relation holds for any approximation scheme for the self-energy parts as long as diagrams with opposite vertical position of the rightmost vertex are both included or excluded.

We emphasize that the current formula (3.21) together with the master equation (3.12) constitutes a complete theory to describe time-dependent phenomena starting from an arbitrary diagonal initial state. The original problem has now been shifted to the evaluation of the various self-energy diagrams which correspond to transition and current rates. The self-energies are defined by a set of irreducible diagrams and thus their corresponding perturbation expansion in the number of tunneling lines is a well-defined series.

For time-translational invariant systems the current rates $\Sigma^{r\pm}_{\chi',\chi}(t',t)$ depend only on the time difference $t'-t$. To calculate the stationary current we define in analogy to (3.16)

$$\Sigma^{r\pm}_{\chi',\chi} = i\int_{-\infty}^{0} dt'\, \Sigma^{r\pm}_{\chi',\chi}(t',0) \tag{3.25}$$

which again can be calculated directly with our diagrammatic rules in energy space. The stationary current is then given by

$$I_r = -ie \sum_{\chi,\chi'} P_{\chi'} \Sigma^{r+}_{\chi',\chi} = ie \sum_{\chi,\chi'} P_{\chi'} \Sigma^{r-}_{\chi',\chi} \,. \tag{3.26}$$

It is straightforward to find a perturbation expansion in powers of $|T|^2$ (or, equivalently, in powers of Γ or α_0) of the current. The first and second order term describe sequential tunneling and cotunneling, respectively. They read

$$I_r^{seq} = -ie \sum_{\chi,\chi'} P^{(0)}_{\chi'} \Sigma^{r+\ (1)}_{\chi',\chi} \tag{3.27}$$

$$I_r^{cot} = -ie \sum_{\chi,\chi'} \left(P^{(0)}_{\chi'} \Sigma^{r+\ (2)}_{\chi',\chi} + P^{(1)}_{\chi'} \Sigma^{r+\ (1)}_{\chi',\chi} \right) \,. \tag{3.28}$$

It is important to note that for a systematic treatment not only the terms $P^{(0)}\Sigma^{(2)}$, which include higher-order transition rates, have to be taken into account but also terms with higher-order corrections for the stationary probabilities, namely $P^{(1)}\Sigma^{(1)}$.

Chapter 4

Quantum Dots and Kondo Physics

We apply the diagrammatic technique outlined in the previous chapter to quantum dots. The experimental study of electron transport through zero-dimensional states has recently received considerable interest [6,54–63]. Theoretical studies in the classical regime [7–10,74] are applicable at high temperature. At low temperature, however, quantum fluctuations have to be taken into account [15–21,39–43,75–79]. In this case, besides Coulomb blockade effects, resonant-tunneling phenomena and nonequilibrium generalizations of the Kondo effect are expected to occur. This leads to zero-bias anomalies in the differential conductance. They have been observed in ultrasmall charge traps [49] as well as in 2DEG quantum dots [50–52]. This is the experimental proof that quantum fluctuations give rise to new qualitative features which are not described within the orthodox theory of sequential tunneling.

In Section 4.1 we discuss the relation of the single-level quantum dot to the Kondo model. Then, in Section 4.2 we develop the diagrammatic technique in detail. We formulate the rules for a very general situation: The (spin-) degeneracy of the dot level may be lifted, e.g., by an applied magnetic field. Furthermore, in addition to the model described in Section 2.4.1 we include inelastic interactions with bosonic modes coupled to the dot. They describe applied time-dependent fields, interaction with phonons, or fluctuations in the electrodynamic environment.

In Section 4.3 we perform a systematic perturbation expansion for the linear conductance up to order Γ^2. Quantum fluctuations lead to cotunneling processes, where electrons tunnel through via a virtual state of the dot. Furthermore, the renormalization of the coupling strength and the dot-state energies will affect the transport characteristics.

For the explanation of the Kondo behavior seen in experiments a nonperturbative treatment is needed. This will be done in Section 4.4 within the *resonant-tunneling approximation*. We discuss in detail how an applied magnetic field or a coupling of the dot electrons to bosons influence the Kondo effect. We find good agreement with experimental results [49].

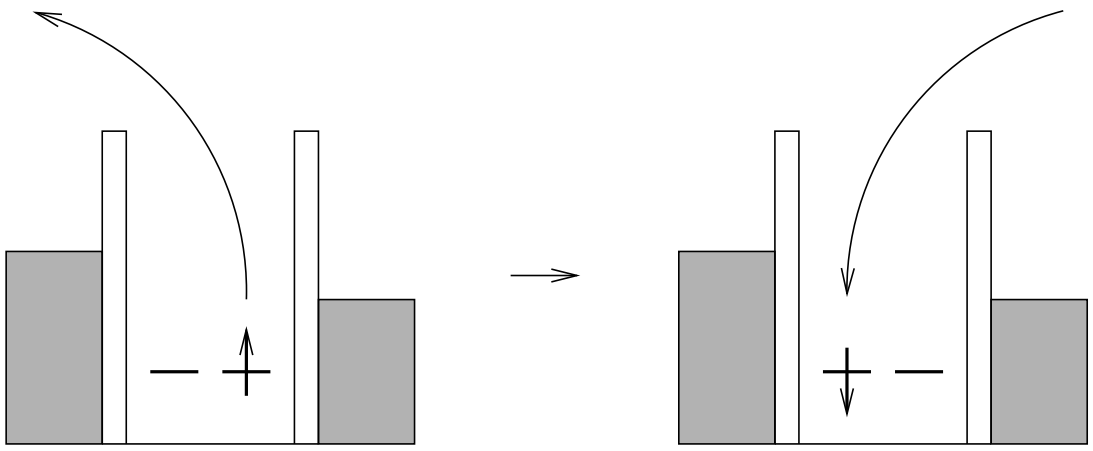

Figure 4.1: A spin flip in the Kondo model corresponds to tunneling of two electrons with the empty dot as a virtual intermediate state.

4.1 Relation to the Kondo Model

For a low-lying level $\epsilon_\sigma = \epsilon$ (with spin degeneracy $M = 2$) and strong Coulomb repulsion U, the Anderson model can be mapped onto the Kondo model by a Schrieffer-Wolff transformation (for details see, e.g., Refs. [80,81]). The Kondo model describes scattering of electrons in a metal by the spin of magnetic impurities (with $S = 1/2$). If the level lies far below the Fermi levels of the leads, the quantum dot will always be filled with one electron, either with up or down spin. The localized impurity spin in the Kondo model is mapped onto the spin of the dot electron. A spin flip during a scattering process corresponds to a spin flip due to tunneling of two electrons whereby an empty dot occurs as a virtual state (see Fig. 4.1). At low temperature, spin singlets are built, i.e., the local impurity will be screened by the conduction band electrons. This means that the scattering becomes resonant, which leads to an increase of the resistivity (Kondo effect). In the Anderson model the spin of the dot electron is screened by the reservoir electrons. Here, the Kondo effect shows up as an increase of the transmittivity through the dot, expressed by a spectral density with a sharp resonance near the Fermi level of the leads.

What is the mechanism of the Kondo effect in a quantum dot? To get a qualitative understanding let us first consider a simple model with two electrons distributed on two levels: one dot level at ϵ and one "reservoir" level at ϵ_F. This finite system can be diagonalized exactly. For zero coupling, $\Gamma = 0$, the total energy is either $2\epsilon_F$ or $\epsilon_F + \epsilon$, the latter being 4-fold degenerate. Double occupancy is forbidden due to Coulomb repulsion. At finite coupling, $\Gamma \neq 0$, the degeneracy is lifted since the formation of a spin singlet leads to an energy gain. Let us assume that for a large number of reservoir electrons each of them try to build up a singlet with the dot electron. In order to do so the partner with opposite spin has to be lifted above the Fermi level (see Fig. 4.2), which costs energy. This energy has to be lower than the energy gain due to the formation of the spin singlet (which is per definition the Kondo temperature T_K). As a consequence only the electrons near

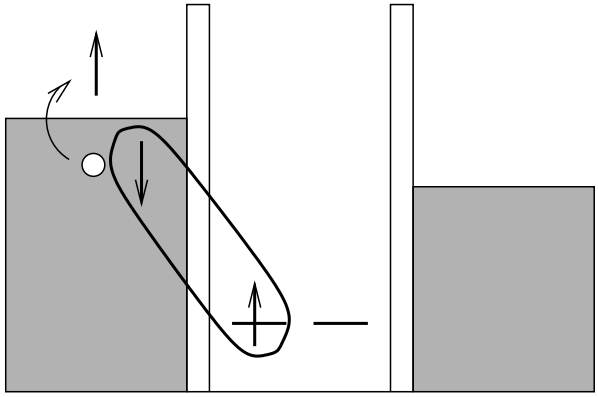

Figure 4.2: The reservoir electrons screen the dot electron spin by formation of a spin-singlet.

the Fermi level participate in the screening of the dot electron spin. This explains why the Kondo effect shows up in the spectral density as a sharp peak of width T_K around the Fermi levels.

There is also a mathematically exact argument for an enhanced transmission through the quantum dot. From Friedel's sum rule one can derive the Langreth formula [15, 82]

$$G|_{T,V=0} = 2\frac{e^2}{h}\frac{4\Gamma_L\Gamma_R}{(\Gamma_L+\Gamma_R)^2}\sin^2(\pi\langle N_\sigma\rangle) \tag{4.1}$$

for the linear conductance at zero temperature. The maximal conductance is obviously achieved for $\langle N_\sigma\rangle = 1/2$. If the Coulomb interaction in the dot is neglected, $U = 0$, then this is satisfied at $\epsilon = \epsilon_F$. But in the opposite limit of large U, such that double occupancy of the dot level is forbidden, the condition is $\epsilon \to -\infty$. This is consistent with the fact that the mapping of the Anderson model onto the Kondo model is possible in the regime with a low-lying dot level.

One may conclude that the lower the dot level lies the more pronounced the Kondo effect is. But this is only the case at zero temperature. For temperatures larger than the Kondo temperature, $T \gtrsim T_K$, the Kondo effect disappears. Since according to the estimate [83, 84]

$$T_K \sim \frac{\sqrt{U\Gamma}}{2}\exp\left(\frac{\pi\epsilon(\epsilon+U)}{\Gamma U}\right) \tag{4.2}$$

for $U \gg |\epsilon|, \Gamma$ the Kondo temperature decreases exponentially with decreasing ϵ, the experimentally relevant regime for the observation of the Kondo effect is $\epsilon \lesssim -\Gamma$. Kondo temperatures of the order of 50 mK have been realized in quantum dots [51].

4.2 Hamiltonian and Diagrammatic Rules

In general, experimentally realizable quantum dots contain a lot of levels. If the level splitting is larger than temperature and bias voltage, then at most one level participates in

transport. Therefore, we discuss in the following a single-level quantum dot. The dot electrons are coupled to bosonic modes ω_q with electron-boson coupling g_q. The Hamiltonian reads $H = H_0 + H_T$ with $H_0 = H_L + H_R + H_D + H_{ch}$ and $H_T = H_{T,L} + H_{T,R}$,

$$H_r = \sum_{k\sigma} \epsilon_{k\sigma r} a^\dagger_{k\sigma r} a_{k\sigma r} \qquad \text{for} \qquad r = L, R \tag{4.3}$$

$$H_D + H_{ch} = \sum_\sigma \epsilon^{(0)}_\sigma c^\dagger_\sigma c_\sigma + U_0 \sum_{\sigma<\sigma'} N_\sigma N_{\sigma'} + \sum_q \omega_q d^\dagger_q d_q + N \sum_q g_q (d_q + d^\dagger_q) \tag{4.4}$$

$$H_{T,r} = \sum_{k\sigma} \left(T^r_k a^\dagger_{k\sigma r} c_\sigma + h.c. \right) \qquad \text{for} \qquad r = L, R \tag{4.5}$$

with $N_\sigma = c^\dagger_\sigma c_\sigma$ and $N = \sum_\sigma N_\sigma$. The bosonic modes can represent interaction with phonons [85–88] or fluctuations of the electrodynamic environment [89–92] very similar to the approach taken in the Caldeira-Leggett model [68,69]. For our theory no assumption is needed for the specific kind of the modes ω_q and the couplings g_q. In this way we are able to present a general result for the current which shows the influence of inelastic interactions for an arbitrary environment.

A unitary transformation [93] with $V = \exp(-iN\varphi)$ and $\varphi = i\sum_q (g_q/\omega_q)(d^\dagger_q - d_q)$ yields $\bar{H} = VHV^{-1} = \bar{H}_0 + \bar{H}_T$, where $\bar{H}_0 = H_R + H_L + \bar{H}_D + \bar{H}_{ch}$,

$$\bar{H}_D + \bar{H}_{ch} = \sum_\sigma \epsilon_\sigma N_\sigma + U \sum_{\sigma<\sigma'} N_\sigma N_{\sigma'} + \sum_q \omega_q d^\dagger_q d_q \tag{4.6}$$

and

$$\bar{H}_T = \sum_{k\sigma r} (T^r_k a^\dagger_{k\sigma r} c_\sigma e^{i\varphi} + h.c.) \,. \tag{4.7}$$

The electron-boson interaction renormalizes the level position and the Coulomb repulsion, $\epsilon_\sigma = \epsilon^{(0)}_\sigma - \sum_q g^2_q/\omega_q$ and $U = U_0 - 2\sum_q g^2_q/\omega_q$, and the tunneling term acquires phase factors $e^{\pm i\varphi}$ (in contrast to the Hamiltonian for the metallic island Eq. (2.14) the phase φ is not the canonical conjugate of the island charge but describes additional degrees of freedom).

In lowest-order perturbation theory the rates for tunneling in and out of the dot to reservoir r are

$$2\pi\gamma^\pm_r(\omega) = 2\pi \int_{-\infty}^{\infty} d\omega' \bar{\gamma}^\pm_r(\omega') P^\pm(\omega - \omega') \,, \tag{4.8}$$

where $2\pi\bar{\gamma}^\pm_r(\omega) = \Gamma_r(\omega) f^\pm_r(\omega)$ is the classical rate without bosons (cf. Eq. (2.11)) and

$$P^\pm(\omega) = \frac{1}{2\pi} \int_{-\infty}^{\infty} dt\, e^{i\omega t} \left\langle e^{i\varphi(0)} e^{-i\varphi(\pm t)} \right\rangle_0 \tag{4.9}$$

describes the probability that an electron absorbs (P^+) or emits (P^-) the boson energy ω [89–91]. The expectation value is taken with the free boson Hamiltonian. In the absence

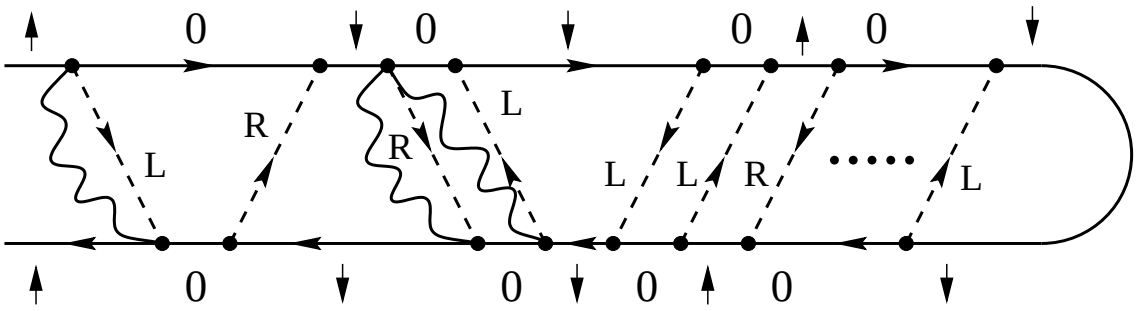

Figure 4.3: A diagram showing from left to right sequential tunneling in the left and right junction, cotunneling, and resonant tunneling. The dashed lines represent electron tunneling and the wiggly lines are due to coupling to bosons. We show only a few boson lines, but in general, each vertex has to be connected with each other vertex by a wiggly line.

of a bosonic field we have $P^{\pm}(\omega) = \delta(\omega)$. The probabilities satisfy the condition of detailed balance [94]

$$P^{-}(\omega) = P^{+}(-\omega) = e^{\beta\omega} P^{+}(\omega)\,. \tag{4.10}$$

In the following we will make use of the definitions $\Gamma = \sum_r \Gamma_r$, $\gamma^{\pm}(\omega) = \sum_r \gamma_r^{\pm}(\omega)$, $\gamma_r(\omega) = \gamma_r^{-}(\omega) + M\gamma_r^{+}(\omega)$, and $\gamma(\omega) = \gamma^{-}(\omega) + M\gamma^{+}(\omega)$ where M is the spin degeneracy.

4.2.1 Diagrams

With regard to the applications discussed in this thesis, it is sufficient to assume that the operators A_i (representing *external vertices*) in Eq. (3.7) depend on the lead and boson degrees of freedom only in the form

$$A_i = A_i \left(\sum_k T_k^r a_{k\sigma r}^{\dagger} c_\sigma e^{i\varphi}\,,\, \sum_k T_k^{r*} c_\sigma^{\dagger} a_{k\sigma r} e^{-i\varphi}\,,\, c_\sigma e^{i\varphi}\,,\, c_\sigma^{\dagger} e^{-i\varphi} \right)\,. \tag{4.11}$$

Each term of the expansion Eq. (3.7) can be represented by a diagram (see Fig. 4.3). In order to derive the diagrammatic rules we follow Section 3.1. Each internal vertex corresponds to a product of a lead and a dot electron operator and a phase factor $e^{\pm i\varphi}$. After integrating out the lead degrees of freedom, all vertices (either internal or external) containing a lead electron operator are connected in pairs by directed tunneling lines (dashed lines) $\bar{\gamma}_r^K(t,t')$ from t' to t, with $\bar{\gamma}_r^K(t,t') = \bar{\gamma}_r^{\pm}(t-t')$ for $t \lessgtr t'$ with respect to the Keldysh contour, and $\bar{\gamma}_r^{\pm}(t) = \int_{-\infty}^{\infty} d\omega\, e^{-i\omega t} \bar{\gamma}_r^{\pm}(\omega)$. These tunneling lines represent contractions of lead electron operators.

There are vertices from which a tunneling line leaves (representing $a_{k\sigma r}^{\dagger}(t) c_\sigma(t) e^{i\varphi(t)}$ which removes a dot electron with spin σ) and others to which a tunneling line enters (representing $c_\sigma^{\dagger}(t) a_{k\sigma r}(t) e^{-i\varphi(t)}$ which adds a dot electron with spin σ). Fermi statistics, furthermore, yield a minus sign for each crossing of tunneling lines.

In the interaction picture the dot electron operators acquire exponential factors which contain the energies ϵ_χ of the many-body dot states χ given by $\epsilon_\chi|\chi\rangle = H_D|\chi\rangle$. The order of the electron operators may induce, furthermore, a minus sign due to Fermi statistics.

The trace over the boson operators gives rise to a factor of the form

$$\begin{aligned} C_B(t_1, t_2, \ldots, t_m, t_1', t_2', \ldots, t_{m'}') \qquad (4.12) \\ &= \left\langle T_K \left[e^{-i\varphi(t_1)} e^{-i\varphi(t_2)} \ldots e^{-i\varphi(t_m)} e^{i\varphi(t_1')} e^{i\varphi(t_2')} \ldots e^{i\varphi(t_{m'}')} \right] \right\rangle \\ &= \prod_{i<j} P^K(t_i, t_j)^{-1} \prod_{i<j} P^K(t_i', t_j')^{-1} \prod_{i,j} P^K(t_i, t_j') \,. \end{aligned}$$

The latter equality follows from the fact that φ is linear in the boson operators. We write $P^K(t,t') = P^+(t,t')$ for $t < t'$ and $P^K(t,t') = P^-(t,t')$ for $t > t'$ on the Keldysh contour with $P^\pm(t) = \int_{-\infty}^{\infty} d\omega\, e^{-i\omega t} P^\pm(\omega)$. In the diagrammatic language, we represent the factors P^K by boson lines connecting each vertex with each other.

4.2.2 Rules in Time Space

In summary each term of the expansion Eq. (3.7) with operators A_i of the form Eq. (4.11) can be calculated according to the following rules:

1. Draw all topologically different diagrams with directed tunneling lines connecting pairs of internal or external vertices containing lead electron operators. Assign a reservoir index r and a spin index σ to each of these lines. Connect all vertices containing boson operators in all possible ways by boson lines. Assign states χ and the corresponding energy ϵ_χ to each element of the Keldysh contour connecting two vertices.

2. The propagation from t' to t with $t' < t$ on the Keldysh contour implies a factor $\exp[-i\epsilon_\chi(t-t')]$.

3. The state χ which is assigned to the leftmost part of the diagram implies a factor $P_\chi(t_0)$ from the initial density matrix. Each vertex containing a dot operator B gives rise to a matrix element $\langle\chi'|B|\chi\rangle$ where χ (χ') is the dot state entering (leaving) the vertex with respect to the Keldysh contour.

4. Each directed tunneling line with index r running from t' to t implies $(-1)^v \bar{\gamma}_r^K(t,t')$ with v being the number of electron operators (due to external vertices) on the part of the Keldysh contour from t' to t. The line corresponds to a tunneling process in reservoir r. Each boson line connecting vertices at times t and t' implies $P^K(t,t')$ if the phase factors at these vertices have different sign. Otherwise, the boson line has the value $P^K(t,t')^{-1}$.

5. Each diagram carries a prefactor $(-i)^m(-1)^c$, where m is the total number of internal vertices and c the number of crossings of tunneling lines. There may be a further

minus sign due to the order of dot electron operators which emerges from the matrix elements $\langle\chi'|B|\chi\rangle$ discussed in rule 3.

6. Integrate over the internal times along the Keldysh contour without changing their ordering and sum over the reservoir and spin indices.

We emphasize that these diagrammatic rules hold for arbitrary dot Hamiltonians $\bar{H}_D = \sum_\chi \epsilon_\chi |\chi\rangle\langle\chi|$, i.e., the states χ can be many-body eigenfunctions of $\bar{H}_D$ containing complicated correlations due to, e.g., Coulomb interaction, magnetic fields, or geometric setups. Such eigenfunctions have been calculated for special situations [95,96] and can be used as an input for our diagrammatic language. In this thesis, however, we will concentrate on the dot Hamiltonian (4.6) where the states χ are trivially known. For this special case, the matrix elements $\langle\chi'|B|\chi\rangle$ from rule 3 can only give rise to minus signs.

Furthermore, we note that the same diagrammatic rules even hold for arbitrary time-dependent dot Hamiltonians $\bar{H}_D(t)$ which are not diagonal in the states χ. In this case one has to assign two states χ' and χ to the beginning and the end of each element of the Keldysh contour, respectively. The factor $\exp[-i\epsilon_\chi(t-t')]$ from rule 2 is, then, replaced by the matrix element $\langle\chi|U_D(t,t')|\chi'\rangle$ where U_D denotes the time-evolution operator of $\bar{H}_D$ and t (t') are the times at the end (beginning) of the element of the Keldysh contour.

4.2.3 Rules in Energy Space

In order to calculate stationary transport properties it is convenient to change to an energy representation. Without loss of generality we assume that the times $t_1, \ldots, t_n$ of the correlation function (3.7) are ordered on the real axis according to $t_n < t_{n-1} < \ldots < t_1 = t$. This may be different to the ordering on the Keldysh contour which depends on whether the times lie on the upper or lower branch. In the stationary limit we can set $t_0 = -\infty$ and $t = t_1 = 0$.

We consider the Laplace transform

$$C(\omega_2, \omega_3, \ldots, \omega_n) = (-i)^{n-1} \int_{-\infty}^{0} dt_2 \int_{-\infty}^{t_2} dt_3 \ldots \int_{-\infty}^{t_{n-1}} dt_n \, e^{i\omega_2 t_2} e^{i\omega_3 t_3} \ldots e^{i\omega_n t_n} \times \langle T_K A_1(0) A_2(t_2) \ldots A_n(t_n)\rangle \, . \quad (4.13)$$

We will account for the exponential factors $\exp(i\omega_i t_i)$ $(i = 2, \ldots, n)$ by drawing directed virtual lines from the external vertices with time t_i to the last vertex with time $t_1 = 0$ and assigning the energy ω_i to this virtual line.

After expanding the expectation value in Eq. (4.13) we order the times of all internal (m) and external vertices (n) from left to right and label them by τ_j with $j = 1, 2, \ldots, m+n$ (with $\tau_{m+n} = 0$), irrespective on which branch they are. The Keldysh contour integrals are now written as ordinary integrals. This includes a minus sign for each internal vertex on the backward propagator. If the initial density matrix is diagonal we then encounter

expressions of the type

$$\int_{-\infty}^{0} d\tau_1 \int_{\tau_1}^{0} d\tau_2 \ldots \int_{\tau_{m+n-2}}^{0} d\tau_{m+n-1}\, e^{0^+\tau_1} e^{-i\Delta E_1(\tau_1-\tau_2)} e^{-i\Delta E_2(\tau_2-\tau_3)} \ldots e^{-i\Delta E_{m+n-1}\tau_{m+n-1}}$$
$$= i^{m+n-1} \frac{1}{\Delta E_1 + i0^+} \cdot \frac{1}{\Delta E_2 + i0^+} \cdots \frac{1}{\Delta E_{m+n-1} + i0^+} \,. \qquad (4.14)$$

Here ΔE_j is the difference of all energies going to the left minus all energies going to the right in each segment limited by τ_j and τ_{j+1}. This includes the energies of the propagators and – if present – the energies of the tunneling, boson and virtual lines. The convergence factor $e^{0^+\tau_1}$ is related to an adiabatic switching on of the tunneling term $\bar{H}_T$. The factor i^{m+n-1} cancels with the factor $(-i)^m$ from rule 5 above together with the prefactor $(-i)^{n-1}$ from the definition Eq. (4.13). Therefore, the corresponding rules in energy representation read:

1'. Draw all topologically different diagrams with fixed ordering of the vertices along the real axis, i.e., irrespective on which branch they are. The vertices are connected by tunneling and boson lines as in time space. In addition to the energy ϵ_χ assigned to the propagators, assign an energy ω to each tunneling line. For each boson line choose a direction (arbitrarily) and assign also an energy ω. The external vertices are connected by virtual lines with energies ω_i $(i = 2, \ldots, n)$ as described above.

2'. For each segment derived from $\tau_j \leq \tau \leq \tau_{j+1}$ with $j = 1, 2, \ldots, m+n-1$ assign a resolvent $1/[\Delta E_j + i0^+]$ where ΔE_j is the difference of the leftgoing minus the rightgoing energies (including the energies of the tunneling, boson and virtual lines).

3'. See rule 3 in time space.

4'. For each coupling of vertices write $(-1)^v \bar{\gamma}_r^+(\omega)$, if the tunneling line of reservoir r is going backward and $(-1)^v \bar{\gamma}_r^-(\omega)$, if it is going forward with respect to the closed time path (definition of v see rule 4 in time space). For each boson line write $P^+(\omega)$, if it is going backward and $P^-(\omega)$, if it is going forward with respect to the closed time path.

5'. The prefactor is given by $(-1)^b(-1)^c$, where b is the total number of internal vertices on the backward propagator and c the number of crossings of tunneling lines. There may be a further minus sign due to the order of dot electron operators which emerges from the matrix elements $\langle\chi'|B|\chi\rangle$ discussed in rule 3.

6'. Integrate over the energies of the tunneling and boson lines and sum over the reservoir and spin indices.

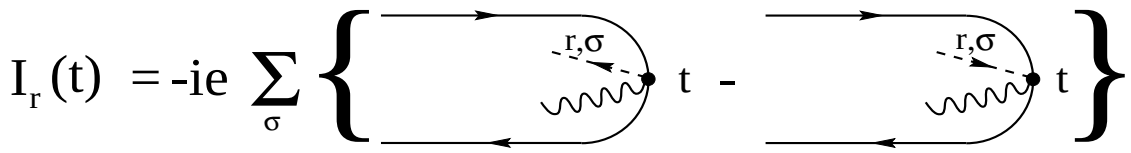

Figure 4.4: Graphical representation of the current I_r through lead r. Internal vertices are not indicated.

4.2.4 Green's Functions and the Current

After the unitary transformation with $V = \exp(-iN\varphi)$ the Green's functions of the dot electrons read

$$C^{>}_{\sigma}(t,t') = -i\langle (c_\sigma e^{i\varphi})(t)(c^\dagger_\sigma e^{-i\varphi})(t')\rangle \tag{4.15}$$

$$C^{<}_{\sigma}(t,t') = i\langle (c^\dagger_\sigma e^{-i\varphi})(t')(c_\sigma e^{i\varphi})(t)\rangle\,. \tag{4.16}$$

Here $C^{>}_\sigma$ and $C^{<}_\sigma$ are independent quantities since we do not assume equilibrium. For time-translational invariant systems, the Green's functions depend only on the time difference $C(t,t') = C(t-t')$. The Fourier transform $C(\omega) = \int_{-\infty}^{\infty} dt\, e^{i\omega t} C(t)$ can be written in the form

$$C^{>}_{\sigma}(\omega) = 2i\,\mathrm{Im}\,(-i)\int_{-\infty}^{0} dt e^{-i\omega t}\langle T_K (c_\sigma e^{i\varphi})(0)(c^\dagger_\sigma e^{-i\varphi})(t^+)\rangle \tag{4.17}$$

$$C^{<}_{\sigma}(\omega) = -2i\,\mathrm{Im}\,(-i)\int_{-\infty}^{0} dt e^{-i\omega t}\langle T_K (c_\sigma e^{i\varphi})(0)(c^\dagger_\sigma e^{-i\varphi})(t^-)\rangle\,, \tag{4.18}$$

where $t^\pm$ means that the time t lies on the upper (lower) branch of the Keldysh contour. Note that the time ordering is defined here by a pure ordering along the Keldysh contour without any sign change if we interchange fermion operators. The integrals can be calculated like Eq. (4.13), whereby instead of assigning the energy $-\omega$ to the virtual line connecting the external vertices one can change the direction of the line and assign the energy ω.

In order to relate the current to the Green's functions of the dot we consider the first diagram on the right hand side of Fig. 4.4 (the second one is just the complex conjugate). The external vertex can be either contracted by a tunneling line to the upper or lower propagator and we recover immediately the structure of the Green's functions $C^>$ and $C^<$, respectively (see Fig. 4.5). As a consequence the stationary current is related to the Green's functions by [17, 19, 97]

$$I_r = -ie\sum_\sigma \int_{-\infty}^{\infty} d\omega \left\{\gamma^+_r(\omega) C^{>}_\sigma(\omega) + \gamma^-_r(\omega) C^{<}_\sigma(\omega)\right\}. \tag{4.19}$$

If the couplings to the leads have the same energy dependence, $\Gamma_r(\omega)/\Gamma_{r'}(\omega) = \lambda_{r,r'}$, this can be written in the form (which was already derived in Ref. [19]),

$$I_r = e\sum_{r'}\sum_\sigma \int_{-\infty}^{\infty} d\omega\, \frac{\Gamma_r(\omega)\Gamma_{r'}(\omega)}{\sum_{r''}\Gamma_{r''}(\omega)} A_\sigma(\omega)[f^+_{r'}(\omega) - f^+_r(\omega)]\,. \tag{4.20}$$

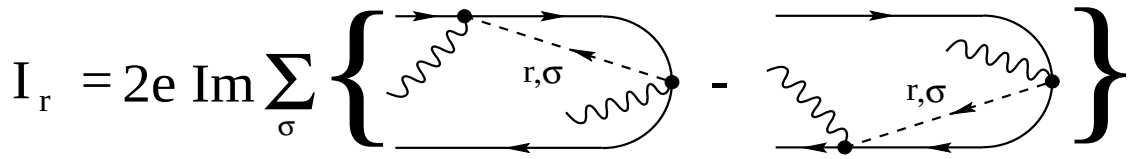

Figure 4.5: Graphical representation of the relation between the current and the Green's functions. Here, the line connecting the external vertices is a real one. Internal vertices are not indicated.

Here, we used the relation between the Green's functions $C_\sigma^<, C_\sigma^>$ and spectral density $A_\sigma \equiv (C_\sigma^< - C_\sigma^>)/2\pi i$. Using Eq. (4.19) or (4.20) we obtain the term $I_r^{(k+1)}$ for a systematic perturbation expansion from $C_\sigma^{(k)}(\omega)$ or $A_\sigma^{(k)}(\omega)$. To calculate the differential conductance $G = \partial I/\partial V$ with $I = I_L = -I_R$ from Eq. (4.20) in the linear response regime, $V = 0$, one only needs the spectral density $A_\sigma(\omega)$ in equilibrium.

4.3 Finite-Order Perturbation Theory

In general, we can not sum up *all* possible diagrams. Therefore, we have to find a systematic criterion which diagrams should be retained and summed.

One possibility is to perform a systematic perturbation expansion in the tunneling coupling Γ as outlined in Section 3.3. In lowest order (*sequential tunneling*) all diagrams in which two or more tunneling lines overlap in time are neglected (see the leftmost diagram parts in Fig. 4.3). This is a good description at high temperature, $\Gamma \ll T$ since in this regime thermal fluctuations dominate over quantum fluctuations, which can, therefore, be neglected.

In situations when sequential tunneling is suppressed by Coulomb blockade, the lowest-order contribution to the current arises due to *cotunneling*. The rates for a process in which an electron enters the dot from the left lead and leaves to right one is described by diagrams with two overlapping lines (see the diagram part in the middle of Fig. 4.3).

In this section we discuss sequential tunneling and cotunneling in linear response for a single-level quantum dot with spin degeneracy $M = 2$ (but we allow for a finite Zeeman energy, $\epsilon_\sigma \neq \epsilon_{\bar\sigma}$). We consider the case of strong Coulomb repulsion U, i.e., we restrict ourselves to the states with $N = 0, 1$. Diagrams in which a higher occupancy occurs do not contribute since they have resolvents of the order $1/U$. Furthermore, we set $P(\omega) = \delta(\omega)$, i.e., the coupling to bosonic fields is not included.

The generalization to finite bias voltage, higher spin degeneracy, multiple occupancy and finite electron-boson coupling is straightforward. It turns out, however, that the formulas for the cotunneling conductance become lengthy and non-transparent.

4.3.1 Sequential Tunneling

The equilibrium probabilities of an empty and singly occupied dot are in lowest order in Γ given by $P_0^{(0)} = 1/Z$ and $P_\sigma^{(0)} = \exp(-\beta\epsilon_\sigma)/Z$, respectively, with $Z = 1 + \sum_\sigma \exp(-\beta\epsilon_\sigma)$ and the spectral density reads

$$A_\sigma^{(0)}(\omega) = \left(P_0^{(0)} + P_\sigma^{(0)}\right) \delta(\omega - \epsilon_\sigma) \,. \tag{4.21}$$

As a consequence we obtain the linear conductance

$$\frac{G^{(1)}}{G_{as}} = \sum_\sigma \left(P_0^{(0)} + P_\sigma^{(0)}\right) \frac{\pi\Gamma}{T} \frac{1}{8\cosh^2(\beta\epsilon_\sigma/2)} \,. \tag{4.22}$$

Here, the conductance is normalized to the maximal conductance for each channel σ, namely $G_{as} = (e^2/h)\, 4\Gamma_L\Gamma_R/\Gamma^2$ with $\Gamma = \Gamma_L + \Gamma_R$. This asymptotic value follows from the Lagreth formula Eq. (4.1).

4.3.2 Cotunneling

The spectral density $A_\sigma(\omega)$ in next order is given by the sum of three terms $A_\sigma^{(1)}(\omega) = \sum_{i=1}^3 A_{\sigma,i}^{(1)}(\omega)$ with

$$\begin{aligned} A_{\sigma,1}^{(1)}(\omega) &= \Big[\left(P_0^{(0)} + P_\sigma^{(0)}\right)\left[\gamma^+(\omega) + \gamma^-(\omega)\right] + P_\sigma^{(0)}\gamma^+(\omega + \epsilon_{\bar\sigma} - \epsilon_\sigma) \\ &\qquad + P_{\bar\sigma}^{(0)}\gamma^-(\omega + \epsilon_{\bar\sigma} - \epsilon_\sigma)\Big] \times \mathrm{Re}\, \frac{1}{(\omega - \epsilon_\sigma + i0^+)^2} \end{aligned} \tag{4.23}$$

$$A_{\sigma,2}^{(1)}(\omega) = \left(\frac{\partial}{\partial\epsilon_\sigma} A_\sigma^{(0)}(\omega)\right) \mathrm{Re}\, \sigma^\sigma(\epsilon_\sigma) + \left(\frac{\partial}{\partial\epsilon_{\bar\sigma}} A_\sigma^{(0)}(\omega)\right) \mathrm{Re}\, \sigma^{\bar\sigma}(\epsilon_{\bar\sigma}) \tag{4.24}$$

$$A_{\sigma,3}^{(1)}(\omega) = A_\sigma^{(0)}(\omega) \left(\frac{\partial}{\partial\omega} \mathrm{Re}\, \sigma^\sigma(\omega)\right)\Big|_{\omega=\epsilon_\sigma} \tag{4.25}$$

and the definition

$$\sigma^\sigma(\omega) = \int_{-\infty}^{\infty} d\omega' \left[\frac{\gamma^-(\omega')}{\omega - \omega' + i0^+} + \sum_{\sigma'} \frac{\gamma^+(\omega')}{\omega - \omega' + \epsilon_{\sigma'} - \epsilon_\sigma + i0^+}\right] . \tag{4.26}$$

If the energy dependence of the coupling can be neglected, $\Gamma(\omega) = \Gamma$, we obtain

$$\mathrm{Re}\, \sigma^\sigma(\omega) = \frac{\Gamma}{2\pi}\left[\ln\left(\frac{\beta E_C}{2\pi}\right) - \mathrm{Re}\, \Psi\left(\frac{1}{2} + i\frac{\beta(\omega + \epsilon_{\bar\sigma} - \epsilon_\sigma)}{2\pi}\right)\right] . \tag{4.27}$$

Here, Ψ denotes the digamma function and we have chosen in the energy integral a Lorentzian cutoff at E_C. The introduction of a high-energy cutoff is required since we have neglected doubly occupancy. The corresponding states have energies which are of the order of E_C larger than the states which are taken into account.

The first term, Eq. (4.23), accounts for the usual elastic and inelastic cotunneling processes. This is the only contribution in the Coulomb blockade regime, where sequential tunneling is suppressed. At resonance, however, also Eqs. (4.24) and (4.25) become important. They describe the effect of the renormalization of level ϵ_σ, $\epsilon_{\bar\sigma}$, and Γ on sequential tunneling through level σ.

Using Eq. (4.20) and performing the integral analytically we find for the linear conductance $G^{(2)} = \sum_{i=1}^{3} G_i^{(2)}$,

$$\begin{aligned}\frac{G_1^{(2)}}{G_{as}} &= \frac{\pi\Gamma}{2}\sum_\sigma \Big\{ -\left(P_0^{(0)} + P_\sigma^{(0)}\right)\partial^2\phi(\epsilon_\sigma) \\ &\quad + P_\sigma^{(0)}\frac{\partial}{\partial\epsilon_\sigma}\left[n(\epsilon_{\bar\sigma}-\epsilon_\sigma)\left(\partial\phi(\epsilon_\sigma)-\partial\phi(\epsilon_{\bar\sigma})\right)\right] \\ &\quad - P_{\bar\sigma}^{(0)}\frac{\partial}{\partial\epsilon_\sigma}\left[\left(n(\epsilon_{\bar\sigma}-\epsilon_\sigma)+1\right)\left(\partial\phi(\epsilon_\sigma)-\partial\phi(\epsilon_{\bar\sigma})\right)\right]\Big\} \qquad (4.28)\end{aligned}$$

$$G_2^{(2)} = \sum_\sigma\left[\frac{\partial G_\sigma^{(1)}}{\partial\epsilon_\sigma}\mathrm{Re}\,\sigma^\sigma(\epsilon_\sigma) + \frac{\partial G_\sigma^{(1)}}{\partial\epsilon_{\bar\sigma}}\mathrm{Re}\,\sigma^{\bar\sigma}(\epsilon_{\bar\sigma})\right] \qquad (4.29)$$

$$G_3^{(2)} = -\sum_\sigma G_\sigma^{(1)}\partial\phi(\epsilon_{\bar\sigma}) \qquad (4.30)$$

with the Bose function $n(\omega) = 1/[\exp(\beta\omega)-1]$ and the abbreviations

$$\phi(\omega) = \frac{\Gamma}{2\pi}\mathrm{Re}\,\Psi\left(\frac{1}{2}+i\frac{\beta\omega}{2\pi}\right) \qquad \text{and} \qquad \partial^n\phi(\omega) = \frac{\partial^n\phi(\omega)}{\partial\omega^n}\,. \qquad (4.31)$$

In Fig. 4.6 we show the total conductance (sequential plus cotunneling) as well as all contributions Eqs. (4.28) - (4.30) to the cotunneling. For comparison, we also show the sequential-tunneling result, which is dominated by transport through level ϵ_1 since the other level ϵ_2 is far away. The existence of level ϵ_2, however, influences the cotunneling conductance. The term $G_1^{(2)}$ accounts for the elastic and inelastic cotunneling processes. They give a finite contribution in the Coulomb blockade regime, where sequential tunneling is exponentially suppressed, and lead to algebraic tails of the peak in Fig. 4.6. But at resonance the renormalization of the level positions ϵ_σ and the coupling Γ become important. We conclude from the structure of the term $G_2^{(2)}$ that the level position ϵ_σ is shifted by $\mathrm{Re}\,\sigma^\sigma(\epsilon_\sigma)$. The renormalization of the coupling Γ is accounted for by $G_3^{(2)}$.

4.3.3 Without Spin Conservation

The cotunneling conductance can also be calculated if spin is not conserved during tunneling or if σ labels some other non-conserved quantum number. In this case the tunneling part of the Hamiltonian Eq. (4.5) has to be replaced by

$$H_{T,r} = \sum_{k\sigma}\left(T_k^r a_{kr}^\dagger c_\sigma + h.c.\right)\,. \qquad (4.32)$$

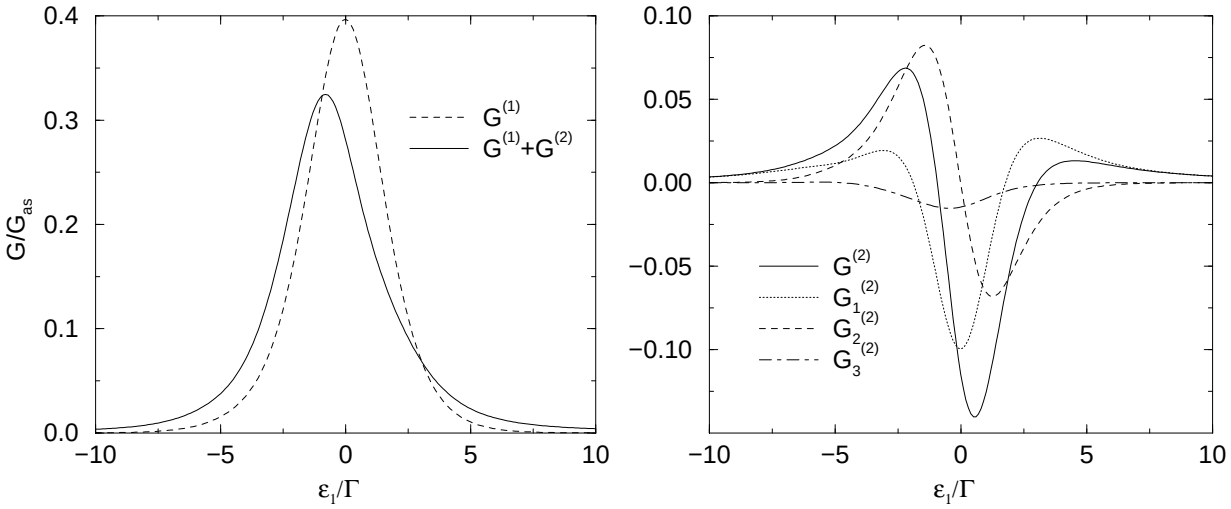

Figure 4.6: The linear conductance as a function of the lower level position with fixed level splitting $\Delta\epsilon = \epsilon_2 - \epsilon_1 = 5\Gamma$ for $\Gamma_L = \Gamma_R = \Gamma/2$, $T = \Gamma$, and $E_C = 100\Gamma$. Spin is conserved. Left-hand side: sequential tunneling and sequential plus cotunneling. Right-hand side: cotunneling and its contributions Eqs. (4.28) - (4.30).

This has the consequence that the density matrix does not remain diagonal even if the initial distribution has been so. The stationary matrix elements of the reduced density matrix $P^{\chi_1}_{\chi_2}$ with $\chi = 0, 1, 2$ (dot empty or filled up with level 1, 2) are described by the relation

$$(\epsilon_{\chi_1} - \epsilon_{\chi_1}) P^{\chi_1}_{\chi_2} + \sum_{\chi_1', \chi_2'} P^{\chi_1'}_{\chi_2'} \Sigma^{\chi_1', \chi_1}_{\chi_2', \chi_2} = 0\,, \tag{4.33}$$

which we derive from Eq. (3.11).

It turns out that the sequential-tunneling current is not modified. But for the cotunneling contribution in addition to the terms given in the previous section, there are off-diagonal Green's functions which lead to $G^{(2)} = \sum_{i=1}^{5} G_i^{(2)}$ with

$$\frac{G_4^{(2)}}{G_{as}} = \pi\Gamma P_0^{(0)} \frac{\partial\phi(\epsilon_{\bar\sigma}) - \partial\phi(\epsilon_\sigma)}{\epsilon_\sigma - \epsilon_{\bar\sigma}} \tag{4.34}$$

$$G_5^{(2)} = 2\frac{G_{\bar\sigma}^{(1)} \mathrm{Re}\,\sigma^\sigma(\epsilon_\sigma) - G_\sigma^{(1)} \mathrm{Re}\,\sigma^{\bar\sigma}(\epsilon_{\bar\sigma})}{\epsilon_\sigma - \epsilon_{\bar\sigma}}\,. \tag{4.35}$$

In Fig. 4.7 we show the total current and the new contributions $G_4^{(2)}$ and $G_5^{(2)}$ for the same parameters as in Fig. 4.6.

4.4 Resonant Tunneling

In order to describe the Kondo regime, we need a nonperturbative treatment of the tunneling, where quantum fluctuations yield finite life-time broadening and renormalization

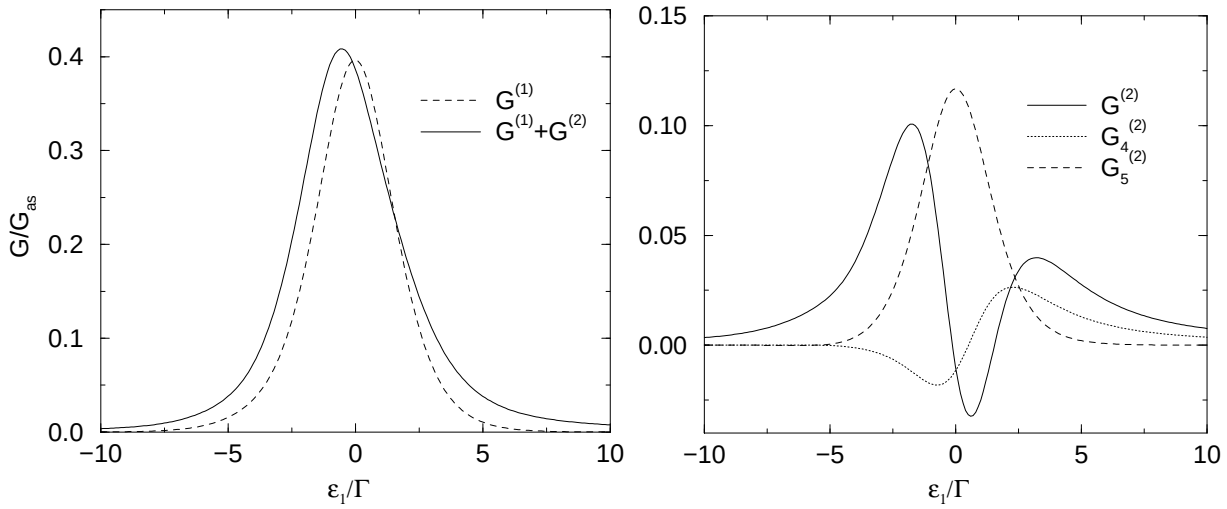

Figure 4.7: The linear conductance as a function of the lower level position with fixed level splitting $\Delta\epsilon = \epsilon_2 - \epsilon_1 = 5\Gamma$ for $\Gamma_1 = \Gamma_2 = \Gamma/2$, $T = \Gamma$, and $E_C = 100\Gamma$. Spin is not conserved. Left-hand side: sequential tunneling and sequential plus cotunneling. Right-hand side: cotunneling and its contributions Eqs. (4.34) and (4.35). For the other contributions Eqs. (4.28) - (4.30) see Fig. 4.6.

effects of the dot levels. As an illustration we first assume that (for $B = 0$) the broadening is given by the sum of the classical transition rates, Eq. (4.8). Using Kramers-Kronig we deduce the renormalization and obtain for the self-energy

$$\sigma(\omega) = \int_{-\infty}^{\infty} d\omega' \, \frac{M\gamma^+(\omega') + \gamma^-(\omega')}{\omega - \omega' + i0^+}. \tag{4.36}$$

In this section we will test and extend this simple physical picture within a systematic and conserving theory, which we call *resonant-tunneling approximation*, for all Green's functions and the current. In the generalization to cotunneling, we have to take into account irreducible diagrams with an arbitrary number of correlated tunneling processes.

In this section we formulate the theory for arbitrary spin degeneracy M and allow for a general electron-boson coupling. But we still concentrate on strong Coulomb repulsion U, i.e., we restrict ourselves to states with $N = 0, 1$. Per definition, the index σ labels the singly occupied state with spin $\sigma = 1, \ldots M$. The label χ additionally allows an empty dot, $\chi = 0, 1, \ldots M$.

In the resonant-tunneling approximation we take into account non-diagonal matrix elements of the total density matrix up to the difference of one electron-hole pair excitation in the leads. The graphical representation of this constriction is that only diagrams in which any vertical line will cut at most two tunneling lines are taken into account. As discussed in Section 3.3 resonant tunneling is a conserving approximation.

We give two arguments why this class of diagrams is the most important one. Firstly, since we treat the leads as large equilibrium reservoirs there should be a tendency of the

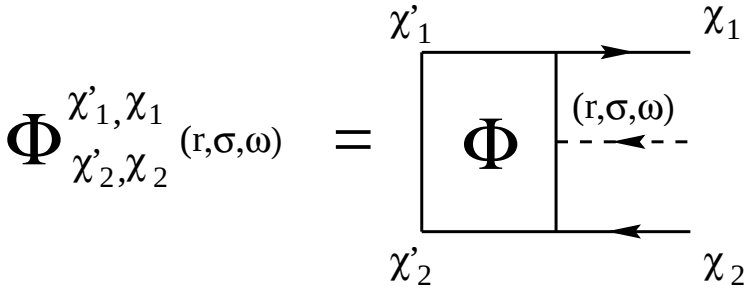

Figure 4.8: Definition of ϕ. It denotes a part of a diagram with an open tunneling line entering from the right.

system to stay close to diagonal states. Secondly, our approximation contains the exact solution for the noninteracting limit $U = 0$: if there is no electron-electron interaction in the dot, electrons with different spin do not influence each other, so that this limit is described within our model by choosing $M = 1$. In this case, the selected diagrams are the only ones that contribute. The sum of all other, more complicated, diagrams is zero.

Furthermore, we include only boson lines between vertices which are already connected by tunneling lines, i.e.,

$$C_B(t_1, t_2, \ldots, t_m, t_1', t_2', \ldots, t_m') \approx \prod_{i=1}^{m} P^K(t_i, t_i') \,. \tag{4.37}$$

where the pairs t_i, t_i' are already coupled by tunneling lines running from t_i' to t_i. This amounts to a dressing of the tunneling lines $\bar{\gamma} \to \gamma$. This approximation, while neglecting many diagrams, describes well the spectral density of the dot at resonance points. The reason is that position and value of the peaks of the spectral density are determined by a self-energy σ (see Eq. (4.43)) which is calculated here in lowest-order perturbation theory in Γ including the bosons.

The first task is to evaluate the rates $\Sigma_{\chi',\chi}$, which are purely imaginary. This can be seen by changing the vertical positions of all vertices on the Keldysh contour (without changing their horizontal position) and reversing the direction of all tunneling and boson lines. Consequently, only the energy differences ΔE_j from rule 2' will change sign. Since the number of vertices is even (all tunneling vertices are coupled in pairs by tunneling lines), there is no sign change due to rule 5' and the number of resolvents is odd. Thus, the whole diagram has been changed to its complex conjugate up to a sign.

We relate the rate $\Sigma_{\chi',\chi}$ to an irreducible diagram labeled by $\phi^{\chi_1',\chi_1}_{\chi_2',\chi_2}(r, \sigma, \omega)$ (see Fig. 4.8). It has an open tunneling line associated with tunneling of an electron with spin σ in the junction r carrying the energy ω. The line is directed from the right to the left and its value together with the corresponding resolvent is included in ϕ. The self-energy is then constructed by attaching the open tunneling line of these diagrams to the upper and lower

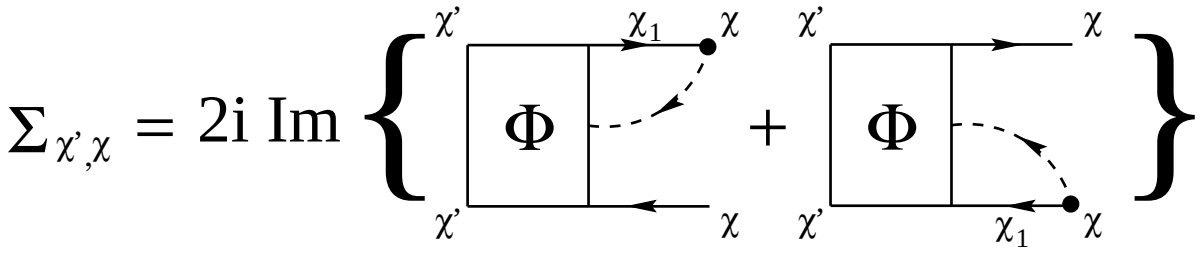

Figure 4.9: The irreducible self energy is obtained by attaching the open tunneling line of ϕ and ϕ^* to the upper and lower propagator.

propagator (see Fig. 4.9) with the result

$$\begin{aligned}\Sigma_{\chi',\chi} &= 2i\,\mathrm{Im}\int_{-\infty}^{\infty} d\omega \sum_{\sigma,r}\sum_{\chi_1}\left\{\langle\chi|c_\sigma|\chi_1\rangle\phi^{\chi',\chi_1}_{\chi',\chi}(r,\sigma,\omega) - \langle\chi_1|c_\sigma|\chi\rangle\phi^{\chi',\chi}_{\chi',\chi_1}(r,\sigma,\omega)\right\} \\ &= \sum_r \left\{\Sigma^{r+}_{\chi',\chi} + \Sigma^{r-}_{\chi',\chi}\right\}\,, \end{aligned} \tag{4.38}$$

where the current rates $\Sigma^{r\pm}_{\chi',\chi}$ correspond to the first and second term, respectively. We have made use of the fact that a diagram becomes the complex conjugate if we change the vertical position of all vertices and the direction of all tunneling and boson lines. As pointed out in Section 3.3 any approximation for ϕ will lead to a current conserving theory.

We construct the diagram ϕ by iteration (see Figs. 4.10 and 4.11). To do so, we need the diagram $\pi(\omega)$ which is the propagator while a tunneling line with energy ω is running in parallel from the right to the left. This diagram can also be expressed as an iteration in the style of a Dyson equation (see Fig. 4.12)

$$\pi^{\chi_1',\chi_1}_{\chi_2',\chi_2}(\omega) = \pi^{(0)}{}^{\chi_1'}_{\chi_2'}(\omega)\delta_{\chi_1',\chi_1}\delta_{\chi_2',\chi_2} + \sum_{\chi_1'',\chi_2''} \pi^{\chi_1',\chi_1''}_{\chi_2',\chi_2''}(\omega)\,\sigma^{\chi_1'',\chi_1}_{\chi_2'',\chi_2}(\omega)\,\pi^{(0)}{}^{\chi_1}_{\chi_2}(\omega)\,. \tag{4.39}$$

In analogy to Σ, the self-energy $\sigma(\omega)$ denotes the sum of all irreducible diagrams with a tunneling line going backward in time. Here, the free propagator in energy space is given by

$$\pi^{(0)}{}^{\chi_1}_{\chi_2}(\omega) = \frac{1}{\omega - (\epsilon_{\chi_1} - \epsilon_{\chi_2}) + i0^+}\,. \tag{4.40}$$

Hence, we can solve Eq. (4.39) and find in matrix notation the general relation

$$\pi(\omega) = [[\pi^{(0)}(\omega)]^{-1} - \sigma(\omega)]^{-1}\,. \tag{4.41}$$

Because of the restriction to two charge states, only the matrix elements $\pi^\sigma(\omega) \equiv \pi^{\sigma,\sigma}_{0,0}(\omega)$ of $\pi(\omega)$ and $\sigma^\sigma(\omega) \equiv \sigma^{\sigma,\sigma}_{0,0}(\omega)$ of $\sigma(\omega)$ are involved, and we deduce from Eq. (4.41)

$$\pi^\sigma(\omega) = \frac{1}{\omega - \epsilon_\sigma - \sigma^\sigma(\omega)}\,. \tag{4.42}$$

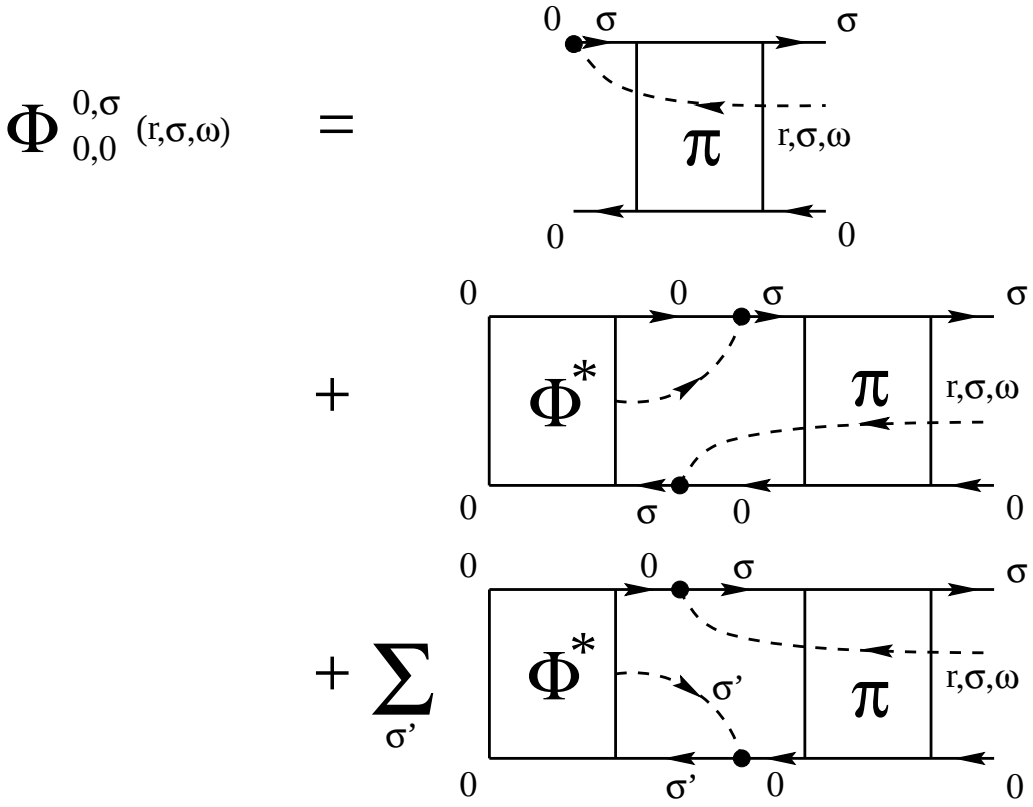

Figure 4.10: Graphical representation of the self-consistent equation for ϕ beginning with an empty dot state.

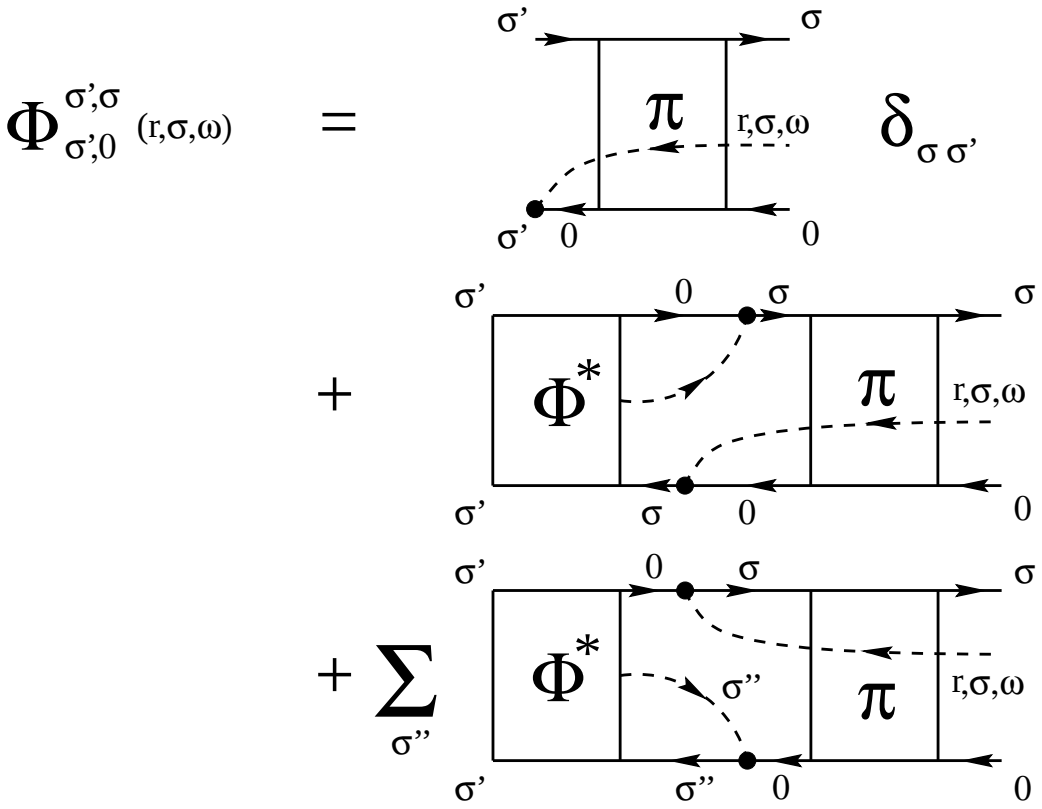

Figure 4.11: Graphical representation of the self-consistent equation for ϕ beginning with an occupied dot state.

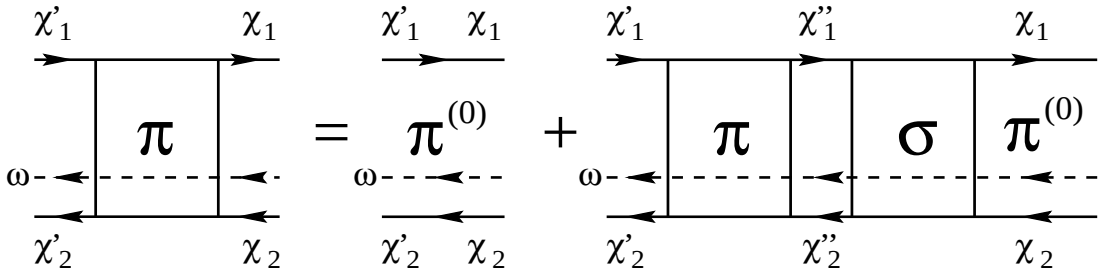

Figure 4.12: The iteration of processes for the propagator π with a tunneling line running in parallel from the right to the left.

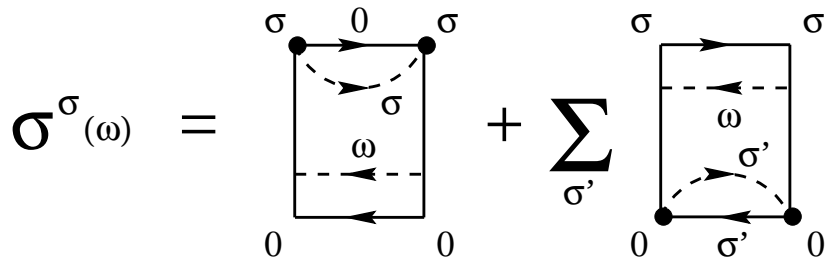

Figure 4.13: In our approximation, the diagram for the irreducible self-energy $\sigma^\sigma(\omega)$ contains one tunneling line in addition to the backward running line.

Since at most two tunneling lines are allowed at once, the irreducible self-energy $\sigma^\sigma(\omega)$ consists of only one tunneling line. We calculate all contributions, which are depicted in Fig. 4.13, and get

$$\sigma^\sigma(\omega) = \int_{-\infty}^{\infty} d\omega' \left[\frac{\gamma^-(\omega')}{\omega - \omega' + i0^+} + \sum_{\sigma'} \frac{\gamma^+(\omega')}{\omega - \omega' + \epsilon_{\sigma'} - \epsilon_\sigma + i0^+} \right] . \tag{4.43}$$

In the spin degenerate case, this is exactly the relation (4.36) which we found from intuitive arguments.

According to our rules, Figs. 4.10 and 4.11 lead to the self-consistent equation for the diagram $\phi(r, \sigma, \omega)$

$$\begin{aligned} \phi^{0,\sigma}_{0,0}(r, \sigma, \omega) = \pi^\sigma(\omega) \Bigg[& \gamma_r^+(\omega) - \gamma_r^-(\omega) \sum_{r'} \int_{-\infty}^{\infty} d\omega' \frac{1}{\omega - \omega' + i0^+} \, \phi^{*0,\sigma}_{0,0}(r', \sigma, \omega') \\ & - \gamma_r^+(\omega) \sum_{\sigma'} \sum_{r'} \int_{-\infty}^{\infty} d\omega' \frac{1}{\omega - \omega' + \epsilon_{\sigma'} - \epsilon_\sigma + i0^+} \, \phi^{*0,\sigma'}_{0,0}(r', \sigma', \omega') \Bigg] \end{aligned} \tag{4.44}$$

and

$$\begin{aligned} \phi^{\sigma',\sigma}_{\sigma',0}(r, \sigma, \omega) = \pi^\sigma(\omega) \Bigg[& -\gamma_r^-(\omega) \delta_{\sigma\sigma'} - \gamma_r^-(\omega) \sum_{r'} \int_{-\infty}^{\infty} d\omega' \frac{1}{\omega - \omega' + i0^+} \, \phi^{*\sigma',\sigma}_{\sigma',0}(r', \sigma, \omega') \\ & - \gamma_r^+(\omega) \sum_{\sigma''} \sum_{r'} \int_{-\infty}^{\infty} d\omega' \frac{1}{\omega - \omega' + \epsilon_{\sigma'} - \epsilon_\sigma + i0^+} \, \phi^{*\sigma',\sigma''}_{\sigma',0}(r', \sigma'', \omega') \Bigg] . \end{aligned} \tag{4.45}$$

The stationary probabilities and the current are derived from Eqs. (3.15) and (3.26). To calculate the rates we specify Eq. (4.38) and obtain

$$\Sigma^{r+}_{\chi',0} = 2i \, \mathrm{Im} \sum_{\sigma} \int_{-\infty}^{\infty} d\omega \, \phi^{\chi',\sigma}_{\chi',0}(r, \sigma, \omega) , \tag{4.46}$$

$$\Sigma^{r-}_{\chi',\sigma} = -2i \, \mathrm{Im} \int_{-\infty}^{\infty} d\omega \, \phi^{\chi',\sigma}_{\chi',0}(r, \sigma, \omega) , \tag{4.47}$$

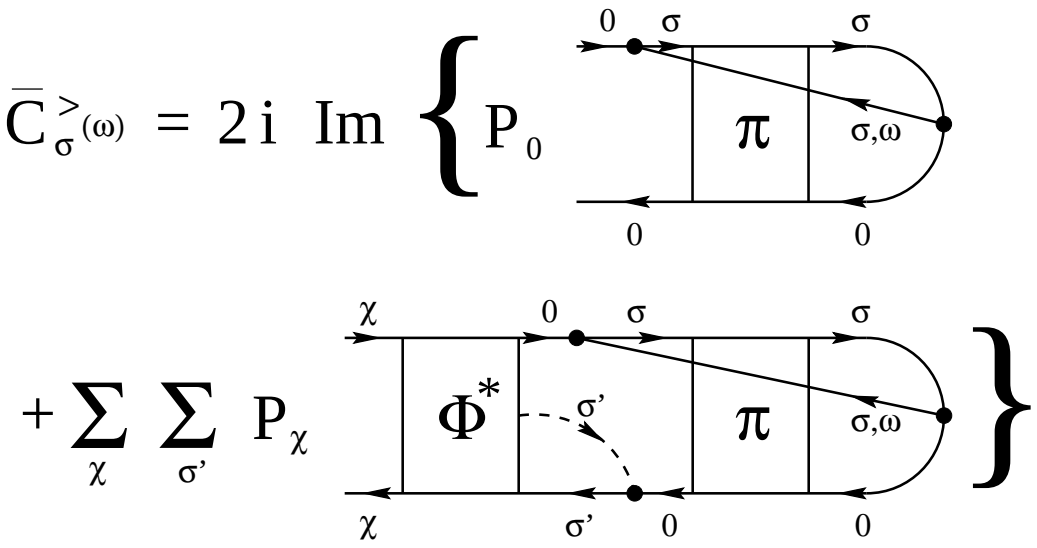

Figure 4.14: Graphical representation of $\bar{C}^{>}_{\sigma}(\omega)$.

whereas all other rates are zero.

The correlation functions can be calculated from the diagrams shown in Figs. 4.14 and 4.15. We have to consider only the latest (i.e. rightmost) correlated part of the diagram. The processes before end up with probability P_χ in a diagonal state χ. We have used the same criterion as for the calculation of the density matrix, with one exception. If a vertical line lies between the external vertices we allow a cut through at most one tunneling line. Here we have used the fact that such a vertical line will in addition always cut the virtual line connecting the external vertices. The sum of all these diagrams gives (where we can combine always two diagrams to the imaginary part of one of them)

$$C^{>}_{\sigma}(\omega) = \int_{-\infty}^{\infty} d\omega' \, \bar{C}^{>}_{\sigma}(\omega') P^{+}(\omega' - \omega) \tag{4.48}$$

$$C^{<}_{\sigma}(\omega) = \int_{-\infty}^{\infty} d\omega' \, \bar{C}^{<}_{\sigma}(\omega') P^{-}(\omega' - \omega) \tag{4.49}$$

with

$$\bar{C}^{>}_{\sigma}(\omega) = 2i \, \mathrm{Im} \left\{ \pi^{\sigma}(\omega) \left[P_0 - \sum_r \sum_{\sigma'} \int_{-\infty}^{\infty} d\omega' \frac{P_0 \phi^{*\,0,\sigma'}_{0,0}(r,\sigma',\omega') + \sum_{\sigma''} P_{\sigma''} \phi^{*\,\sigma'',\sigma'}_{\sigma'',0}(r,\sigma',\omega')}{\omega - \omega' + \epsilon_{\sigma'} - \epsilon_{\sigma} + i0^{+}} \right] \right\} \tag{4.50}$$

$$\bar{C}^{<}_{\sigma}(\omega) = -2i \, \mathrm{Im} \left\{ \pi^{\sigma}(\omega) \left[P_\sigma + \sum_r \int_{-\infty}^{\infty} d\omega' \frac{P_0 \phi^{*\,0,\sigma}_{0,0}(r,\sigma,\omega') + \sum_{\sigma'} P_{\sigma'} \phi^{*\,\sigma',\sigma}_{\sigma',0}(r,\sigma,\omega')}{\omega - \omega' + i0^{+}} \right] \right\} . \tag{4.51}$$

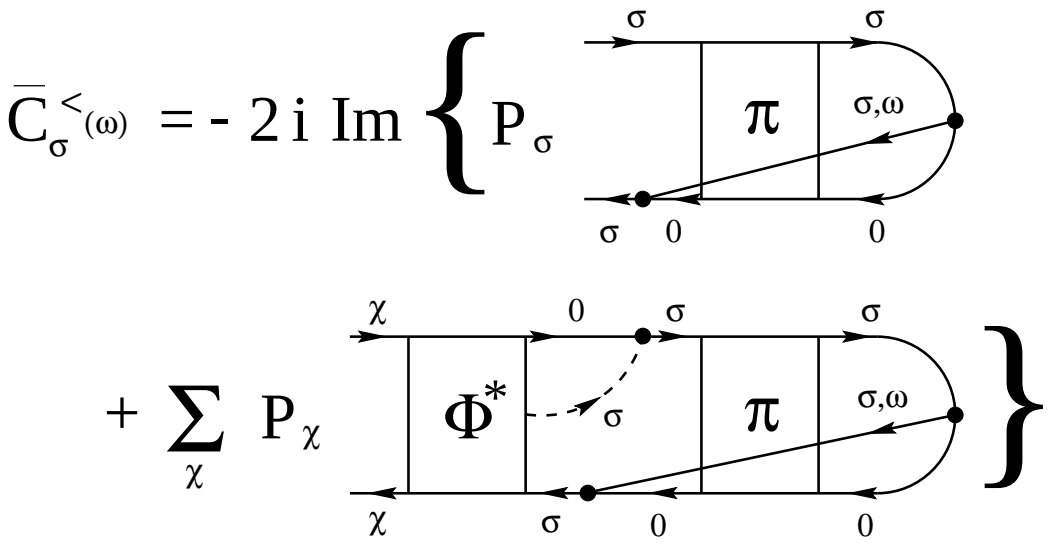

Figure 4.15: Graphical representation of $\bar{C}^{<}_{\sigma}(\omega)$.

In the following, we discuss for transparency the effect of the coupling to bosons and the presence of a magnetic field separately.

4.4.1 Boson-Assisted Tunneling

For zero magnetic field, i.e., $\epsilon_\sigma = \epsilon$ for all σ, we can perform the resummation of the corresponding diagrams for the rates and the Green's functions analytically. The result is given in Eq. (4.61).

Analytic Resummation

Defining the quantities $\pi(\omega) \equiv \pi^\sigma(\omega)$, $\sigma(\omega) \equiv \sigma^\sigma(\omega)$,

$$\phi_r^+(\omega) = \phi_{0,0}^{0,\sigma}(r,\sigma,\omega) \qquad \text{and} \qquad \phi_r^-(\omega) = \sum_{\sigma'} \phi_{\sigma,0}^{\sigma,\sigma'}(r,\sigma',\omega) \tag{4.52}$$

which are independent of σ. We get the integral equations

$$[\omega - \epsilon - \sigma(\omega)]\phi_r^\pm(\omega) = \pm\gamma_r^\pm(\omega) - \gamma_r(\omega)\int_{-\infty}^{\infty} d\omega' \frac{1}{\omega - \omega' + i0^+}\,\phi^{*\pm}(\omega') \tag{4.53}$$

where $\phi^\pm(\omega) = \sum_r \phi_r^\pm(\omega)$ and $\gamma_r(\omega) = \gamma_r^-(\omega) + M\gamma_r^+(\omega)$. Summing over r and taking the imaginary part we obtain the solution

$$\mathrm{Im}\,\phi^\pm(\omega) = \mp\pi\frac{\lambda^\pm}{\lambda}\gamma(\omega)|\pi(\omega)|^2 \tag{4.54}$$

with $\gamma(\omega) = \gamma^-(\omega) + M\gamma^+(\omega)$ and

$$\lambda^\pm = \int_{-\infty}^{\infty} d\omega\,\gamma^\pm(\omega)|\pi(\omega)|^2 \qquad \text{and} \qquad \lambda = \int_{-\infty}^{\infty} d\omega\,|\pi(\omega)|^2\,. \tag{4.55}$$

Furthermore, we obtain directly from (4.53) a relation between ϕ_r and ϕ,

$$\gamma(\omega)\phi_r^{\pm}(\omega) = \gamma_r(\omega)\phi^{\pm}(\omega) \pm \pi(\omega)[\gamma(\omega)\gamma_r^{\pm}(\omega) - \gamma^{\pm}(\omega)\gamma_r(\omega)] \tag{4.56}$$

Using Eqs. (4.46) and (4.47), the current rates follow from $\Sigma_{0,0}^{r+} = 2iM\int d\omega\,\mathrm{Im}\,\phi_r^+(\omega)$ and $\Sigma_{\sigma,0}^{r+} = 2i\int d\omega\,\mathrm{Im}\,\phi_r^-(\omega)$. With Eqs. (4.54) and (4.56), the result is

$$\Sigma_{0,0}^{r+} = -2\pi i M\left[\frac{\lambda^+}{\lambda}\lambda_r + \int_{-\infty}^{\infty} d\omega\,|\pi(\omega)|^2[\gamma^-(\omega)\gamma_r^+(\omega) - \gamma^+(\omega)\gamma_r^-(\omega)]\right] \tag{4.57}$$

$$\Sigma_{\sigma,0}^{r+} = 2\pi i\left[\frac{\lambda^-}{\lambda}\lambda_r - M\int_{-\infty}^{\infty} d\omega\,|\pi(\omega)|^2[\gamma^-(\omega)\gamma_r^+(\omega) - \gamma^+(\omega)\gamma_r^-(\omega)]\right], \tag{4.58}$$

where $\lambda_r = \int d\omega\,\gamma_r(\omega)|\pi(\omega)|^2$.

Summing the current rates over r and using $\sum_r \lambda_r = \lambda^- + M\lambda^+ = 1$, we get the total transition rates (note that $\Sigma_{\chi',0}^{r-} = 0$)

$$\Sigma_{0,0} = -2\pi i M\frac{\lambda^+}{\lambda} \qquad \text{and} \qquad \Sigma_{\sigma,0} = 2\pi i\frac{\lambda^-}{\lambda} \tag{4.59}$$

and the solution of the stationary master equation (3.15) reads

$$P_0 = \lambda^- \qquad \text{and} \qquad P_\sigma = \lambda^+ \qquad \text{with} \qquad \lambda^- + M\lambda^+ = 1\,. \tag{4.60}$$

The stationary current follows from (3.26) $I_r = -ie[P_0\Sigma_{0,0}^{r+} + MP_\sigma\Sigma_{\sigma,0}^{r+}]$ (note that $\Sigma_{\chi',\sigma}^{r+} = 0$), which gives as the final result Eq. (4.61).

Result

The current is

$$I_r = 2\pi eM\sum_{r'}\int_{-\infty}^{\infty} d\omega\,[\gamma_r^-(\omega)\gamma_{r'}^+(\omega) - \gamma_{r'}^-(\omega)\gamma_r^+(\omega)]\,|\pi(\omega)|^2 \tag{4.61}$$

with $\pi(\omega) = \pi^\sigma(\omega)$. We can write this equation in a more intuitive way by inserting the definition (4.8) for $\gamma_r^\pm(\omega)$

$$I_r = \frac{e}{h}\sum_{r'}\int_{-\infty}^{\infty} d\omega\int_{-\infty}^{\infty} d\omega'\Big\{T_{r',r}(\omega',\omega)f_{r'}(\omega')\,[1-f_r(\omega)] - T_{r,r'}(\omega,\omega')f_r(\omega)\,[1-f_{r'}(\omega')]\Big\}, \tag{4.62}$$

where

$$T_{r,r'}(\omega,\omega') = M\Gamma_r(\omega)\Gamma_{r'}(\omega')\int_{-\infty}^{\infty} d\omega_1 P^+(\omega_1-\omega)P^-(\omega_1-\omega')|\pi(\omega_1)|^2 \tag{4.63}$$

can be interpreted as a transmission probability for an electron to start from reservoir r with energy ω and end in reservoir r' with energy ω'. From the detailed balance condition (4.10) we get

$$T_{r',r}(\omega',\omega) = e^{\beta(\omega'-\omega)}T_{r,r'}(\omega,\omega')\,. \tag{4.64}$$

This guarantees that the current is zero if the chemical potentials of all reservoirs are identical.

However, the interpretation of $T_{r,r'}$ as a one-particle transmission probability in analogy to a generalization of the Landauer-Büttiker formula to inelastic interactions [98,99] is not correct. We see that the transmission probability still depends on the Fermi distribution functions via the self-energy $\sigma(\omega)$ in the denominator of the propagator $\pi(\omega)$. This reflects the many-particle aspect of the electron-electron and electron-boson interaction in our model.

Comparing our result for $T_{r,r'}$, Eq. (4.62), with other approaches in the case $M = 1$ [85–88,92], we see that the energy dependence of $\sigma(\omega)$ has been neglected in all previous treatments. We find that even in the $M = 1$ case, the energy dependence of $\sigma(\omega)$ cannot been neglected if the temperature T and the typical frequency ω_B of the bosons are smaller than Γ.

Without bosons, the current formula is exact to order Γ^2, i.e., sequential and electron cotunneling are fully taken into account. With bosons, cotunneling is not described correctly since we have treated the bosons only by a dressing of the tunneling lines. This means that our approximation is not valid in regions where the current is very small. However, at resonance we believe our treatment to be correct since sequential tunneling will be only modified by a renormalization and broadening of the local state of the dot which is described by the self-energy $\sigma(\omega)$, which is calculated in lowest order in Γ here. Higher orders will be small for high tunneling barriers.

Finally, we calculate the Green's functions and find

$$C^{>}(\omega) = -2\pi i \int_{-\infty}^{\infty} d\omega' \, \gamma^{-}(\omega') P^{+}(\omega' - \omega) \, |\pi(\omega')|^2 \tag{4.65}$$

$$C^{<}(\omega) = 2\pi i \int_{-\infty}^{\infty} d\omega' \, \gamma^{+}(\omega') P^{-}(\omega' - \omega) \, |\pi(\omega')|^2 \, . \tag{4.66}$$

The sum rule $C^{>}(\omega) = -\exp(\beta\omega) C^{<}(\omega)$ for equilibrium situations, i.e., $\mu_r = 0$ for all r, is fulfilled. Furthermore, for the $M = 1$ case, particle-hole symmetry is satisfied. The spectral density has the form

$$A(\omega) = \int_{-\infty}^{\infty} d\omega' \left[\gamma^{+}(\omega') P^{-}(\omega' - \omega) + \gamma^{-}(\omega') P^{+}(\omega' - \omega) \right] |\pi(\omega')|^2 \, . \tag{4.67}$$

The effect of the resonant-tunneling processes is described by the resolvent $\pi(\omega)$ containing the self-energy $\sigma(\omega)$, Eq. (4.43). The real and imaginary part of the self-energy express energy renormalization and broadening and determine, therefore, the position and the width of the maxima in the spectral density.

To proceed we consider now a one-mode environment (Einstein model) with boson frequency $\omega_q = \omega_B$. Experimentally, realizations of this model are optical phonons [85–88] or fluctuations of an external LC-circuit with frequency $\omega_B = (LC)^{-1/2}$ [89–92]. The results for a general environment can be anticipated approximately from the one-mode case by

a superposition. Furthermore, we choose the special case of two reservoirs $r = L/R$ and constant level broadening $\Gamma/2 = \Gamma_L = \Gamma_R$.

Defining $g = \sum_q g_q^2/\omega_B^2$ we obtain $P^{\pm}(\omega) = \sum_n p_n \delta(\omega \pm n\omega_B)$, where p_n is the probability for the emission of n bosons with frequency ω_B. This probability is given by

$$p_n = e^{-g(1+2N_0(\omega_B))} e^{n\omega_B/2T_B} I_n\left(2gN_0(\omega_B)e^{\omega_B/2T_B}\right) . \tag{4.68}$$

Here, $N_0(\omega_B)$ is the Bose function and I_n the modified Bessel function. Using Eq. (4.43) we obtain

$$\mathrm{Re}\,\sigma(\omega) = \sum_{n,r}(Mp_n - p_{-n})\frac{\Gamma_r}{2\pi}\Big[\ln\left(\frac{E_C}{2\pi T}\right) - \mathrm{Re}\,\Psi\left(\frac{1}{2} + i\frac{\omega + n\omega_B - \mu_r}{2\pi T}\right)\Big] \tag{4.69}$$

$$\mathrm{Im}\,\sigma(\omega) = -\pi\sum_n p_n[M\bar{\gamma}^+(\omega + n\omega_B) + \bar{\gamma}^-(\omega - n\omega_B)] . \tag{4.70}$$

Here Ψ denotes the digamma function, and we have chosen in the energy integrals a Lorentzian cut-off at E_C.

The real part of $\sigma(\omega)$ renormalizes the level position to higher energies. Furthermore, it depends logarithmically on energy, temperature, voltage and frequency. These logarithmic terms are typical for the occurrence of Kondo peaks. Hence, we anticipate logarithmic singularities either for $M \geq 2$ or for $p_n \neq p_{-n}$. This includes not only the degenerate case but also the case of a single dot level without spin ($M = 1$) since the probabilities for absorption and emission of bosons are different. It is important to remark here, that for systems coupled to classical time-dependent fields [21] the situation is different since then both probabilities are equal. At low enough temperatures we obtain logarithmic peaks in $\sigma(\omega)$ at $\omega = \mu_r + n\omega_B$ ($n \neq 0$ for $M = 1$). They lead to maxima of the resolvent $\pi(\omega)$ at $\omega = \mu_r + n\omega_B$ ($n > 0$ for $M = 1$, $n \geq 0$ for $M > 1$) for $\epsilon < 0$ and at $\omega = \mu_r + n\omega_B$ ($n < 0$) for $\epsilon > 0$. The spectral density (4.67) shows resonances at the same points but, due to the additional $P^{\pm}$ functions in the integrand, they are shifted by multiples of ω_B. This boson-assisted tunneling is completely different from the influence of the bosons on the self-energy $\sigma(\omega)$.

The spectral density at different voltages for a low lying level $\epsilon < 0$ is depicted in Fig. 4.16. Without an applied bias voltage, we obtain (for $M = 2$) the usual Kondo peak near the Fermi level (which we choose as zero energy). The emission of bosons leads to additional resonances at multiples of ω_B. For $M = 1$ and $\epsilon < 0$, resonances occur for negative energies and in the case $\epsilon > 0$ we find resonances at positive energies. In these cases, the effects are less pronounced and are only visible for very low temperatures. At finite bias voltages all peaks split and decrease in magnitude.

The resonances in the spectral density can be probed by the nonlinear differential conductance as function of the bias voltage V, as shown in Fig. 4.17 for the case $\epsilon < 0$. The splitting of the Kondo peak leads to an overall decrease of the spectral density in the energy range $|\omega| < eV$ (see inset of Fig. 4.17). For this reason, the conductance shows the well-known [19–21, 49] maximum at zero bias. The emission of bosons produces a set of symmetric satellite maxima. They can be traced back to the fact that pairs of Kondo

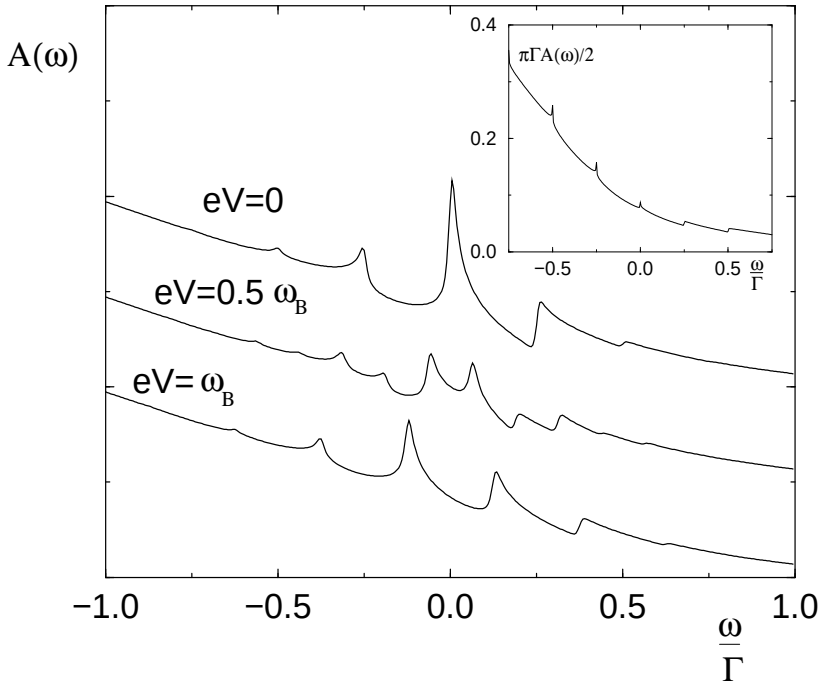

Figure 4.16: The spectral density for $M = 2$, $T = T_B = 0.005\Gamma$, $\epsilon = -2\Gamma$, $g = 0.2$, $\omega_B = 0.25\Gamma$ and $E_C = 50\Gamma$ at different voltages. For $V = 0$ there are resonances at multiples of ω_B, which split for finite bias voltage. Inset: spectral density for $M = 1$, $T = 0.00005\Gamma$, $T_B = 0.5\Gamma$, $\epsilon = -\Gamma$, $V = 0$, $g = 0.5$, $\omega_B = 0.25\Gamma$ and $E_C = 50\Gamma$.

peaks can merge if the bias voltage is a multiple of the boson frequency ω_B (see Fig. 4.16). This gives rise to pronounced Kondo peaks at $\omega = \pm eV/2$ and thus to an increase of the spectral density with bias voltage near these points.

Fig. 4.18 shows the differential conductance for $\epsilon \geq 0$ with and without bosons. A striking result is that the whole structure is inverted compared to the case $\epsilon < 0$, and we find a zero-bias anomaly although the Kondo peak at zero energy is absent. The coupling to bosons yields satellite steps at $|eV| = n\omega_B$. The contributions of sequential and co-tunneling lead, compared to resonant tunneling, only to a weak bias-voltage dependence of the differential conductance. This shows clearly that the influence of the logarithmic terms in $\sigma(\omega)$ are still important. The logarithmic peaks in $\mathrm{Re}\,\sigma(\omega)$ decrease with increasing bias voltage and approach the value of $\omega - \epsilon$ if ϵ is large enough. Thus the value of $\omega - \epsilon - \mathrm{Re}\,\sigma(\omega)$ decreases which in turn leads to an overall increase of the resolvent $\pi(\omega)$ and the spectral density $A(\omega)$ near zero energy (see the inset of Fig. 4.18).

Zero-bias minima are known from Kondo scattering from magnetic impurities [100]. They have been observed in recent experiments [101, 102] and have been interpreted as 2-channel Kondo scattering from atomic tunneling systems [103, 104]. Here we have shown that zero-bias minima can also arise due to resonant tunneling via local impurities if the level position is high enough such that we are in the mixed valence regime.

Finally, we investigate the differential conductance at fixed bias voltage as function of

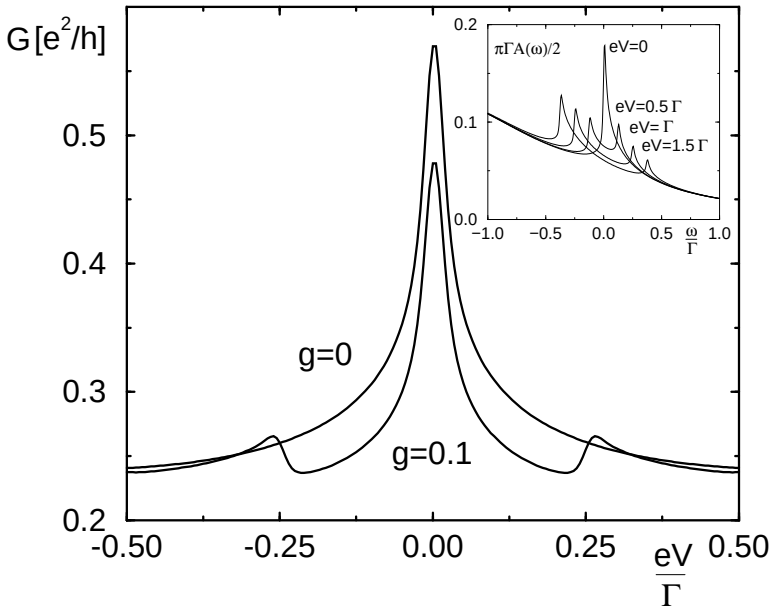

Figure 4.17: The differential conductance vs. bias voltage for $T = T_B = 0.005\Gamma$, $\epsilon = -2\Gamma$, $\omega_B = 0.25\Gamma$ and $E_C = 50\Gamma$. The curves show a maximum at zero bias and satellite maxima at multiples of ω_B for a finite electron-boson coupling. Inset ($g = 0$): increasing voltage leads to an overall decrease of the spectral density in the range $|\omega| < eV$.

the position of the dot level, which experimentally can be varied by a gate voltage coupled capacitively to the dot (see Fig. 4.19). The result shows a (classical) pair of peaks at $|\epsilon| = eV/2$ together with satellites (due to emission and absorption of bosons) and peaks for $|\epsilon| > eV/2$ (only due to absorption). The energy dependence of $\mathrm{Im}\,\sigma(\omega)$ gives rise to an asymmetry of the peak heights. The peak at $\epsilon = eV/2$ is higher than the one at $\epsilon = -eV/2$ since $|\mathrm{Im}\,\sigma(\omega)| = \pi|M\gamma^+(\omega) + \gamma^-(\omega)|$ is smaller for higher energies (except for $M = 1$ when particle-hole symmetry holds). This significant effect is due to the broadening of the spectral density by quantum fluctuations.

4.4.2 Magnetic-Field Dependence

In this section we discuss the effect of an applied magnetic field and do not take into account the coupling to bosons. Again we consider the case of two reservoirs and constant level broadenings. Since the energy levels ϵ_σ are now spin dependent, we can no longer solve the self-consistent equations analytically but have to solve them numerically.

We find Kondo resonances in the spectral density $A_\sigma(\omega)$ at energies $\omega = \mu_r + \epsilon_{\sigma'} - \epsilon_\sigma$ with $\sigma' \neq \sigma$. This is due to the fact that the correlation functions $C^<_\sigma(\omega)$ and $C^>_\sigma(\omega)$ are mainly determined by the resolvent $\pi^\sigma(\omega)$ (see Eqs. (4.50) and (4.51)) which contains via

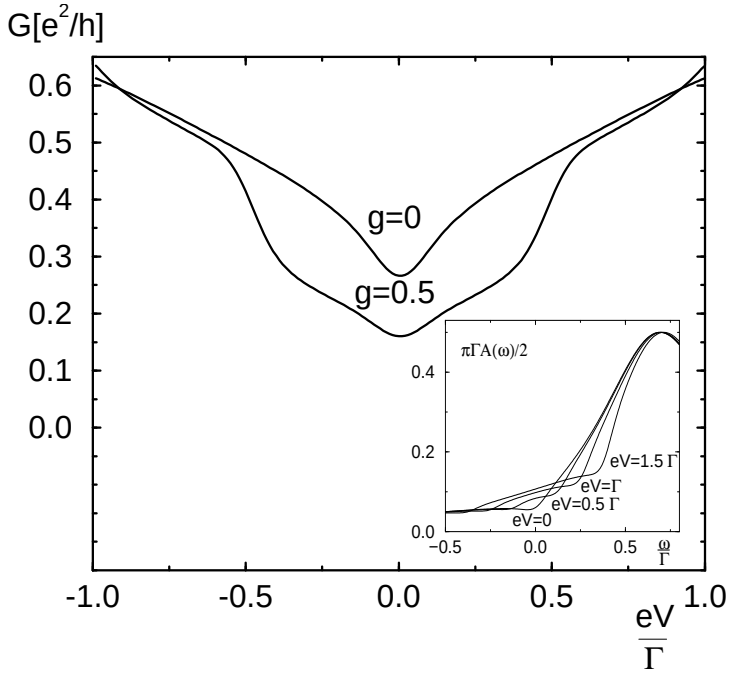

Figure 4.18: The differential conductance vs. bias voltage for $T = T_B = 0.025\Gamma$, $\epsilon = 0$, $\omega_B = 0.5\Gamma$ and $E_C = 50\Gamma$. The curves show a minimum at zero bias and steps at multiples of ω_B for a finite electron-boson coupling. Inset ($g = 0$): increasing voltage leads to an overall increase of the spectral density in the range $|\omega| < eV$.

the self-energy $\sigma^\sigma(\omega)$ logarithmic singularities at the corresponding energies,

$$\mathrm{Re}\,\sigma^\sigma(\omega) = \sum_r \frac{\Gamma_r}{2\pi} \sum_{\sigma' \neq \sigma} \left[\ln\left(\frac{E_C}{2\pi T}\right) - \mathrm{Re}\,\Psi\left(\frac{1}{2} + i\frac{\omega + \epsilon_{\sigma'} - \epsilon_\sigma - \mu_r}{2\pi T}\right) \right] \quad (4.71)$$

$$\mathrm{Im}\,\sigma^\sigma(\omega) = -\pi \left[\bar{\gamma}^-(\omega) + \sum_{\sigma'} \bar{\gamma}^+(\omega + \epsilon_{\sigma'} - \epsilon_\sigma) \right] . \quad (4.72)$$

From Eq. (4.20) we see that only energies within the window defined by the difference of the Fermi functions contribute to the current. For this reason, there is no Kondo-assisted tunneling at low transport voltage but sets on if transport voltage and level splitting are equal. Therefore, for low lying levels the conductance peak at zero bias found in the previous section now splits up into two peaks separated by the twice the level splitting [19, 20] (see Fig. 4.20).

Ralph and Buhrman recently measured Kondo-assisted tunneling via a single charge trap of a point contact tunnel barrier [49]. We follow the model proposed by the authors interpretating the experiment as a realization of the Anderson model with strong Coulomb repulsion such that double occupancy does not occur. However we think that the interaction energy U and not the conduction band width is the relevant cut-off in this situation.

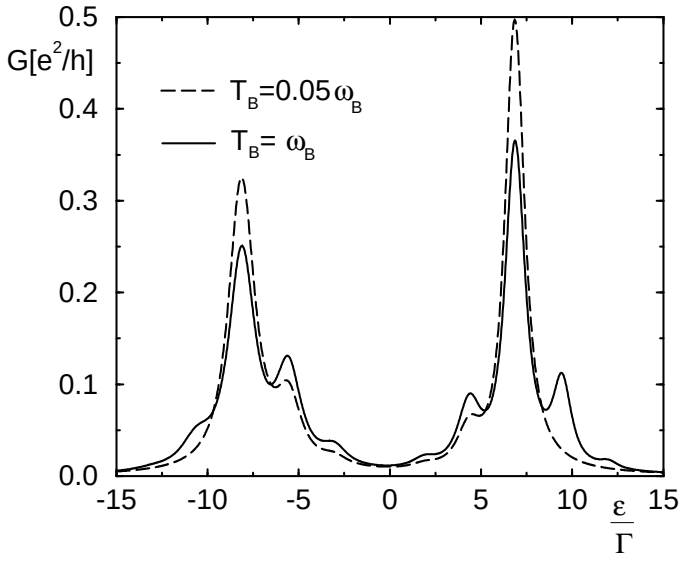

Figure 4.19: The differential conductance as a function of ϵ for $T = 0.125\Gamma$, $eV = 15\Gamma$, $g = 0.3$, $\omega_B = 2.5\Gamma$ and $E_C = 250\Gamma$.

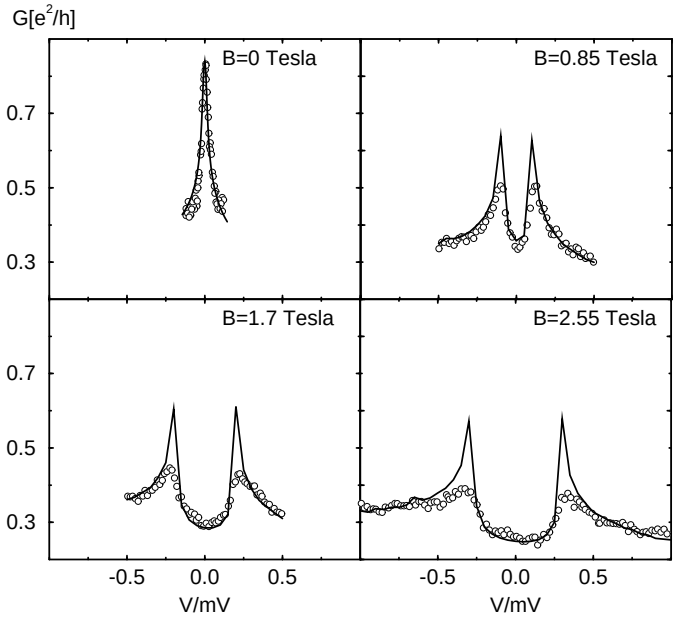

Figure 4.20: The differential conductance vs. bias voltage for $T = 4.3\mu$eV, $\epsilon_\sigma(B = 0) = -5.2$meV, $\Gamma = 3.4$meV, $a_c = 0.33$, and $E_C = 30$meV. The circles are experimental data from Ref. [49].

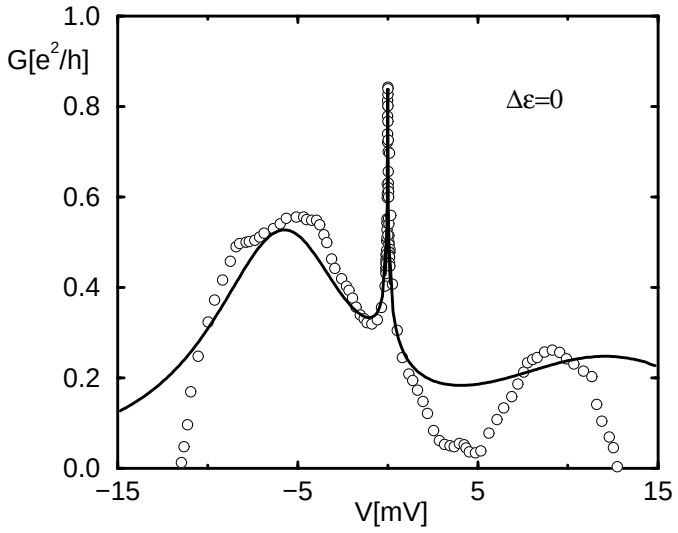

Figure 4.21: The differential conductance vs. bias voltage for $T = 4.3\mu$eV, $\epsilon_\sigma = -5.2$meV, $B = 0$, $\Gamma = 3.4$meV, $a_c = 0.33$, and $E_C = 30$meV. The circles are experimental data from Ref. [49].

A comparison of the experiment and our theory is given in Fig. 4.20, Fig. 4.21 and Fig. 4.22. We find a good agreement for the peaks induced by Kondo-assisted tunneling processes if we set the cut-off $U = 30$meV. The authors suspect the single charge trap to be a dangling bond, for which they expect $U = 100$meV. Our result agrees in the order of magnitude. It gives a hint however, that the state may have a larger extension than an ordinary dangling bond or that there is screening due to the copper electrodes or both. The peaks for larger magnetic fields show, however, a stronger broadening than predicted from our calculation. Nevertheless, our theory reproduces the experimental curves much better than the fits given in Ref. [49] using perturbation theory since we have taken into account nonperturbative effects which are obviously important here.

The model proposed by the authors of Ref. [49] explains the broad peaks at large voltages by the matching of the energies of the empty and the singly occupied dot. Our calculations for this case, however, lead to a broader and lower peak for positive voltages in comparison with experiment (see Fig. 4.21). We think, therefore, that due to the capacitance asymmetry the system becomes doubly occupied before the empty state is energetically favorable. The capacitance asymmetry a_c then makes the corresponding resonance peak sharper. An energy-dependent transparency of the barriers could then explain the different heights.

Finally, we consider the case when the energy level is above the Fermi energies of the leads. The zero-bias minimum found in the previous section splits for finite magnetic field into two minima separated by twice the level splitting (see Fig. 4.23).

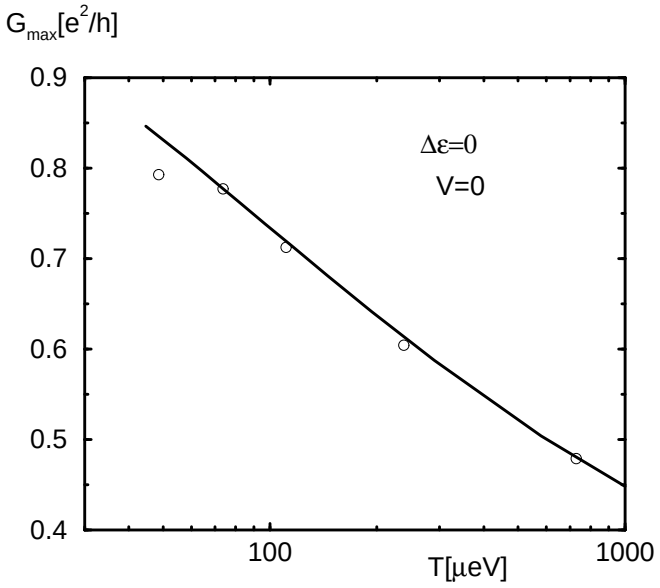

Figure 4.22: The maximal linear conductance vs. temperature for $\epsilon_\sigma = -5.2$meV, $B = 0$, $\Gamma = 3.4$meV, $a_c = 0.33$, and $E_C = 30$meV. The circles are experimental data from Ref. [49].

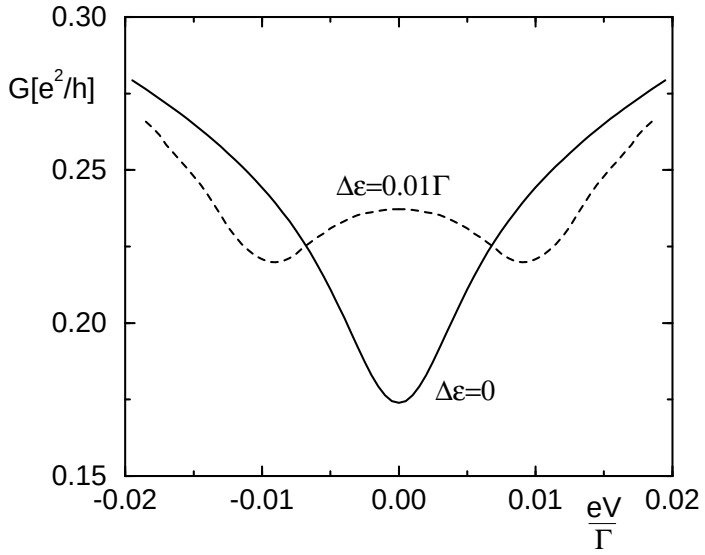

Figure 4.23: The differential conductance vs. bias voltage for $T = 0.001\Gamma$, $\epsilon_\sigma = 0.1\Gamma \pm \Delta\epsilon/2$, and $E_C = 10\Gamma$.

Chapter 5

Quantum Fluctuations in Metallic Islands

In some sense the realization of single-electron devices with metallic tunnel junctions constitutes the opposite limit to the quantum dots discussed in the previous chapter: typical overlap junctions of metallic single-electron devices accommodate a large number of transverse channels, and the density of island states is continuous. For this reason, quantum fluctuations will show up in a different way than in quantum dots. In addition, metallic single-electron transistors are related to a model with a complicated many-particle ground state: the *multi-channel* Kondo model (while the Anderson model is connected to the *single-channel* Kondo model). A qualitative understanding of this relation is presented in Section 5.1.

There are two equivalent ways to derive the diagrammatic rules for the metallic single-electron transistor: either to start directly from the Hamiltonian and proceed in the same way as we have done for the quantum dot or to reformulate first the problem in terms of an effective-action description using the path-integral language, as done in Section 5.2. The latter provides a generalization of a path-integral formulation of single junctions [71, 72] to the transistor. Of course, both approaches lead to the same rules given in Section 5.3.

In analogy to the previous chapter we then perform a systematic perturbation expansion up to order α_0^2 (*cotunneling*) in Sections 5.5 and 5.6 before we use the *resonant-tunneling approximation* for a non-perturbative treatment (Section 5.7). The quantum fluctuations lead to a renormalization of the charging-energy gap and the tunnel coupling. This indicates the relation to the Kondo model. We conclude in Section 5.8 with a discussion of these renormalization effects.

5.1 Relation to the Multi-Channel Kondo Model

Near resonance, when two charge states are almost degenerate, the metallic single-electron box (with junctions containing a large number of transverse channels) can be mapped onto the multi-channel Kondo model [110]. But the impurity spin in the Kondo model does not

correspond to a physical spin on the island. Spin up and down is rather mapped onto two charge states, say $N = 0, 1$. The "spin" flips when an electron tunnels and, thus, changes the charge state from 0 to 1 or vice versa. Higher charge states are neglected. A finite energy gap $\Delta_0 = E_{ch}(1) - E_{ch}(0)$ simulates a finite magnetic field in the Kondo model.

Renormalization-group studies of the single-electron box with a restriction to two charge states [24,110] predict a renormalization of the system parameters, which depends logarithmically on the dominant low-energy scale, temperature or energy gap, and on a high-energy cutoff. We reproduce the same result within the resonant-tunneling approximation.

For quantitative comparison with experiments, however, one should get rid of an adjustable cutoff. This is done by the inclusion of all relevant charge states and can not be achieved by the Kondo model, since only the charge states $N = 0, 1$ have spin-state counterparts. The renormalization already shows up in second-order perturbation theory. Since we include all relevant charge states the results are cutoff independent, and we can extract the argument of the leading logarithmic terms.

In order to describe also the single-electron transistor we generalize the results for the renormalization to nonequilibrium situations.

5.2 Path-Integral Formulation of the Problem

We reformulate the problem in terms of an effective-action description. Our aim is to study the time-evolution of the reduced density matrix for the island charge states. We sketch the main steps:

(i) The time evolution of the density matrix introduces two propagators, a forward and backward propagator, which get coupled when we trace out electron degrees of freedom of the reservoirs. The procedure is closely related to path-integral methods formulated in connection with dissipation [66–70] or tunneling in single metallic junctions [71, 72].

(ii) In order to describe the Coulomb interaction between the island electrons we introduce the electric potential of the island $V(t)$ as a macroscopic field via a Hubbard-Stratonovich transformation. The interaction between electrons is replaced in this way by an interaction with the collective variable $V(t)$.

(iii) We treat the leads as well as the electrons on the island as large equilibrium reservoirs. The electrochemical potentials of the reservoirs are fixed, $\mu_r = -eV_r$ for $r = L, R$. The only fluctuating field is the electric potential of the island $V(t)$. The definition $eV(t) \equiv -\dot{\varphi}(t)$ relates $V(t)$ to a phase $\varphi(t)$. Its quantum mechanical conjugate is the number of excess electrons $N(t)$ on the island. As a consequence of the procedure outlined so far, the macroscopic field $N(t)$ is independent of the microscopic degrees of freedom described by $c_{q\sigma}$ and $c^\dagger_{q\sigma}$. At this stage, the electronic degrees of freedom can be traced out.

(iv) The time evolution of the reduced density matrix $\rho(t; \varphi_1, \varphi_2)$, which depends only on the phase variable φ, can thus be expressed by a double path integral over the phases

corresponding to the forward and backward propagators φ_j $(j = 1, 2)$,

$$\rho_c(t_f;\varphi_{1f},\varphi_{2f}) = \int_{-\infty}^{\infty} d\varphi_{1i} \int_{-\infty}^{\infty} d\varphi_{2i} \int_{\varphi_{1i}}^{\varphi_{1f}} \mathcal{D}[\varphi_1(t)] \int_{\varphi_{2i}}^{\varphi_{2f}} \mathcal{D}[\varphi_2(t)] \exp\left(iS[\varphi_1(t),\varphi_2(t)]\right) \rho_c(t_i;\varphi_{1i},\varphi_{2i}) \,. \tag{5.1}$$

(v) The form (5.1) describes the situation where charges can take any continuous value and the phase is an extended variable. However, in our physical system the charge on the island is quantized in units of the electron charge e. In this case the phase variable is compact (i.e., the states φ and $\varphi+2\pi$ are equivalent), and we rewrite Eq. (5.1), introducing integer winding numbers $m_1, m_2 = 0, \pm1, \pm2, \ldots$,

$$\rho_d(t_f;\varphi_{1f},\varphi_{2f}) = \sum_{m_1,m_2} \int_{-\infty}^{\infty} d\varphi_{1i} \int_{-\infty}^{\infty} d\varphi_{2i} \int_{\varphi_{1i}}^{\varphi_{1f}+2\pi m_1} \mathcal{D}[\varphi_1(t)] \int_{\varphi_{2i}}^{\varphi_{2f}+2\pi m_2} \mathcal{D}[\varphi_2(t)] \exp\left(iS[\varphi_1(t),\varphi_2(t)]\right) \rho_d(t_i;\varphi_{1i},\varphi_{2i}) \,. \tag{5.2}$$

The two integrations can be combined to a single integral along the Keldysh contour, which runs forward and backward between t_i and t_f along the real-time axis. As a result the reduced propagator Π is written as a single path integral along this contour

$$\Pi = \mathrm{tr}\left[\rho_0\, T_K \exp\left(-i\int_K dt\, H(t)\right)\right] = \int \mathcal{D}[\varphi(t)] \exp\left(iS[\varphi(t)]\right). \tag{5.3}$$

Here the collective variable $\varphi(t)$ and the time integral are defined on the Keldysh contour K, and the time-ordering operator T_K orders the following operators accordingly.

The effective action entering the propagator is $S[\varphi(t)] = S_{ch}[\varphi(t)] + S_T[\varphi(t)]$. The first term represents the charging energy

$$S_{ch}[\varphi(t)] = \int_K dt \left[\frac{C}{2}\left(\frac{\dot\varphi(t)}{e}\right)^2 + n_x\dot\varphi(t)\right] , \tag{5.4}$$

and electron tunneling is described by $S_T[\varphi(t)]$, which, in the case of wide metallic junctions with a large number of channels N_{ch}, is expressed by the simplest electron loop connecting two times,[1]

$$S_T[\varphi(t)] = 2\pi i \sum_{r=L,R} \int_K dt \int_K dt'\, \alpha_r^K(t,t') e^{i\varphi(t)} e^{-i\varphi(t')} \,. \tag{5.5}$$

The kernels $\alpha_r^K(t,t') = \alpha_r^{\pm}(t-t')$ for $t < t'$ $(t > t')$ depend on the order of the times along the Keldysh contour. Their Fourier transforms are given by Eq. (2.17).

[1]Each loop acquires a factor N_{ch}. As a consequence, in $\mathcal{O}\left(\alpha_0^{(k)}\right)$ with $k \geq 2$ the value of diagrams containing k loops are by a factor $1/N_{ch}^{k-1}$ smaller than the contribution of diagrams which consist of one complicated loop.

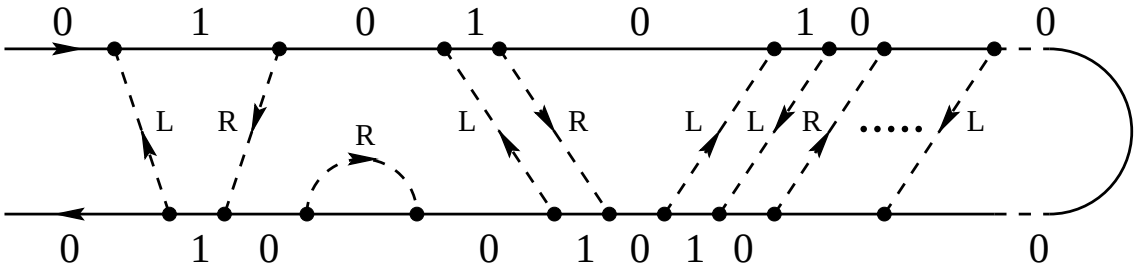

Figure 5.1: A diagram showing sequential tunneling in the left and right junction, cotunneling, and resonant tunneling.

(vi) For large systems, the phase behaves almost like a classical variable, whereas its conjugate variable, the charge, fluctuates strongly. A natural basis is then the phase representation. In the presence of strong Coulomb interaction, however, the situation is different: the phase undergoes strong fluctuations, while the time evolution of the charge is almost governed by classical rates. For this reason, we change from the phase to the charge representation. The time evolution of the density matrix in a charge representation depends on the propagator from N_1 forward to N_1' and on the backward branch from N_2' backward to N_2. It is given by the matrix element of the reduced propagator [30,31]

$$\Pi^{N_1,N_1'}_{N_2,N_2'} = \int_{-\infty}^{\infty} d\varphi_1 \int_{-\infty}^{\infty} d\varphi_1' \int_{-\infty}^{\infty} d\varphi_2' \int_{-\infty}^{\infty} d\varphi_2 \, e^{iN_1\varphi_1} e^{-iN_1'\varphi_1'} e^{iN_2'\varphi_2'} e^{-iN_2\varphi_2} \int_{\varphi_2,\varphi_2'}^{\varphi_1,\varphi_1'} \mathcal{D}[\varphi(t)] \int \mathcal{D}[N(t)] \exp\left(-iS_{ch}[N(t)] + iS_T[\varphi(t)] + i\int_K dt\, N(t)\dot{\varphi}(t) \right) . \tag{5.6}$$

In the charge representation the charging energy is simply given by

$$S_{ch}[N(t)] = \int_K dt\, E_C \left[N(t) - n_x\right]^2 . \tag{5.7}$$

A diagrammatic description is obtained by expanding the tunneling term $\exp\left(iS_T[\varphi(t)]\right)$ in the reduced propagator and integrating over φ. Each of the exponentials $\exp[\pm i\varphi(t)]$ describes tunneling of an electron at time t. These changes occur in pairs in each junction, $r = L, R$, and are connected by tunneling lines $\alpha_r^K(t,t')$. Each term of the expansion can be visualized by a diagram. Several examples are displayed in Fig. 5.1. The rules for the evaluation of the diagrams follow from the expansion of Eq. (5.6).

An alternative derivation starts directly from Eq. (3.7) on the Hamiltonian level and proceeds in the same way as for the quantum dot. Both approaches lead, of course, to the same rules.

5.3 Diagrammatic Rules

5.3.1 Rules in Time Space

These correspond to those in Section 4.2.2, but are now formulated for the metallic transistor:

1. Draw all topologically different diagrams with directed tunneling lines connecting pairs of internal or external vertices containing electron operators. Assign a reservoir index r to each of these lines. Assign charge states N and the corresponding energy $E_{ch}(N)$ to each element of the Keldysh contour connecting two vertices.

2. The propagation from t' to t with $t' < t$ on the Keldysh contour implies a factor $\exp[-iE_{ch}(N)(t-t')]$.

3. The state N which is assigned to the left most part of the diagram implies a factor $P_N(t_0)$ from the initial density matrix. Each vertex represents an exponential $\exp[\pm i\varphi(t)]$ of the tunneling contribution to the action. It changes the charge by ± 1.

4. Each directed tunneling line with index r running from t' to t implies $\alpha_r^K(t,t')$. The line corresponds to a tunneling process in reservoir r.

5. Each diagram carries a prefactor $(-i)^m$, where m is the total number of internal vertices.

6. Integrate over the internal times along the Keldysh contour without changing their ordering and sum over the reservoir indices.

5.3.2 Rules in Energy Space

In analogy to Section 4.2.3 we formulate the rules also in energy space:

1'. Draw all topologically different diagrams with fixed ordering of the vertices along the real axis, i.e., irrespective on which branch they are. The vertices are connected by tunneling lines as in time space. In addition to the energy $E_{ch}(N)$ assigned to the propagators we assign an energy ω to each tunneling line. The external vertices are connected by virtual lines with energies ω_i $(i = 2, \ldots, n)$.

2'. For each segment derived from $\tau_j \leq \tau \leq \tau_{j+1}$ with $j = 1, 2, \ldots, m+n-1$ assign a resolvent $1/[\Delta E_j + i0^+]$ where ΔE_j is the difference of the leftgoing minus the rightgoing energies (including the energies of the tunneling and virtual lines).

3'. See rule 3 in time space.

4'. For each coupling of vertices write $\alpha_r^+(\omega)$, if the tunneling line of reservoir r is going backward and $\alpha_r^-(\omega)$, if it is going forward with respect to the closed time path.

5'. The prefactor is given by $(-1)^b$, where b is the total number of internal vertices on the backward propagator.

6'. Integrate over the energies of tunneling and sum over the reservoir indices.

5.3.3 Green's Functions and the Current

The tunneling current I_r flowing into reservoir r can be expressed in terms of the correlation functions for the island charge

$$C^>(t,t') = -i\langle e^{-i\varphi(t)} e^{i\varphi(t')}\rangle\,, \tag{5.8}$$
$$C^<(t,t') = i\langle e^{i\varphi(t')} e^{-i\varphi(t)}\rangle\,. \tag{5.9}$$

Since the system is time-translationally invariant, the correlation functions depend only on the time difference $C(t,t') = C(t-t')$, and we can define the Fourier transforms $C(\omega) = \int_{-\infty}^{\infty} dt\, e^{i\omega t} C(t)$. Similar to Eq. (4.19) the tunneling current is

$$I_r = -ie \int_{-\infty}^{\infty} d\omega \left\{ \alpha_r^+(\omega) C^>(\omega) + \alpha_r^-(\omega) C^<(\omega) \right\}\,. \tag{5.10}$$

The diagrams for the correlation functions contain two external vertices (representing the $e^{\pm i\varphi}$ terms in Eqs. (5.8) and (5.9)) connected by a solid line. The value of the diagram is given by the probability of the states indicated on the left-hand side of the diagram, multiplied by the value of the irreducible diagram part. As discussed in Chapter 3, the probability P_N includes the sequence of preceding transitions which are disconnected from the latest irreducible part and can be determined by the stationary master equation Eq. (3.15).

To determine the probabilities P_N we can use an alternative set of equations which are equivalent to the master equation. For this task we introduce the quantities $C(\omega, N)$, $I_r(N)$ and $I(N) = \sum_r I_r(N)$ as the contribution to the correlation function and current in which the rightmost vertex describes a transition from N to $N+1$ or vice versa. We can prove current conservation not only for the total current $\sum_r I_r = 0$ but also for each part $I(N) = 0$,[2] i.e.,

$$\int_{-\infty}^{\infty} d\omega \left\{ \alpha^+(\omega) C^>(\omega, N) + \alpha^-(\omega) C^<(\omega, N) \right\} = 0\,. \tag{5.11}$$

The normalization condition $\sum_N P_N = 1$ together with Eq. (5.11) determine the probabilities P_N which can, then, be inserted in Eq. (5.10) to calculate the current.

The spectral density is related to the Green's functions by $A = (C^< - C^>)/2\pi i$.

[2] The master equation is equivalent to $I(N) = I(N+1) = \text{const.}$. To determine the constant we consider the limit $N \to \infty$ and find $I(N) = 0$.

5.4 Systematic Perturbation Expansion

For a systematic perturbation theory in powers of α_0 we write

$$P_N = \sum_{k=0}^{\infty} P_N^{(k)} \tag{5.12}$$

for the probabilities, and

$$C(\omega, N) = \sum_{k=0}^{\infty} C^{(k)}(\omega, N) = \sum_{k=0}^{\infty} \sum_{l=0}^{k} C^{(l,k-l)}(\omega, N) \tag{5.13}$$

for the correlation functions. The index k in $P_N^{(k)}$ and $C^{(k)}$ denotes the term of the order α_0^k in the expansion. The term $C^{(l,k-l)}$ is the contribution to the correlation function $C^{(k)}$ of the order k that is built up from a probability of the order l and an irreducible diagram part of the order $k-l$ with $0 \leq l \leq k$. (One may write $C^{(l,k-l)} \sim P^{(l)}\alpha^{\pm}(\omega_1)\ldots\alpha^{\pm}(\omega_{k-l})$ symbolically.)

The conservation rule Eq. (5.11) must hold in each order. This allows us to determine the probabilities recursively. If we know the probabilities $P_N^{(l)}$ of the order $l \leq k-1$, then we get $P_N^{(k)}$ from the $k+1$-th order term of the normalization condition $\sum_N P_N^{(k)} = \delta_{k,0}$ and Eq. (5.11),

$$P_N^{(k)}\alpha^+(\Delta_N) - P_{N+1}^{(k)}\alpha^-(\Delta_N) = \tag{5.14}$$
$$\frac{1}{2\pi i}\sum_{l=0}^{k-1}\int_{-\infty}^{\infty} d\omega \left[\alpha^+(\omega)C^{>(l,k-l)}(\omega, N) + \alpha^-(\omega)C^{<(l,k-l)}(\omega, N)\right] .$$

Here, we have used $\Delta_N = E_{ch}(N+1) - E_{ch}(N)$ and

$$C^{<(k,0)}(\omega, N) = 2\pi i\, P_{N+1}^{(k)}\, \delta(\omega - \Delta_N) \tag{5.15}$$
$$C^{>(k,0)}(\omega, N) = -2\pi i\, P_N^{(k)}\, \delta(\omega - \Delta_N) . \tag{5.16}$$

Having determined the probabilities up to $P_N^{(k)}$ we get for the $k+1$-th term of the current Eq. (5.10)

$$I_r^{(k+1)} = -ie\int_{-\infty}^{\infty} d\omega \left\{\alpha_r^+(\omega)C^{>(k)}(\omega) + \alpha_r^-(\omega)C^{<(k)}(\omega)\right\} . \tag{5.17}$$

5.5 Sequential Tunneling

In lowest order (sequential tunneling), we have $k=0$ in Eq. (5.14), i.e.,

$$P_N^{(0)}\alpha^+(\Delta_N) - P_{N+1}^{(0)}\alpha^-(\Delta_N) = 0 \tag{5.18}$$

with $\sum_N P_N^{(0)} = 1$. The solution in equilibrium is $P_N^{(0)} = \exp[-\beta E_{ch}(N)]/Z$ with $Z = \sum_N \exp[-\beta E_{ch}(N)]$. At low temperature (and voltage) at most two charge states ($N = 0, 1$) are important, and all other states are exponentially suppressed. Higher-order processes modify the occupation, and the probabilities for the other charge states are only algebraically suppressed, but not exponentially. This leads to correction terms $\langle N\rangle^{(k)}$ in the average occupation $\langle N\rangle = \sum_N N P_N = \sum_{k=0}^{\infty}\langle N\rangle^{(k)}$.

The current $I = I_L = -I_R$ follows from Eq. (5.17) and is given in lowest order by

$$I^{(1)} = \frac{4\pi^2 e}{h}\sum_N \left[P_N^{(0)} + P_{N+1}^{(0)}\right] \frac{\alpha_L(\Delta_N)\alpha_R(\Delta_N)}{\alpha(\Delta_N)} \left[f_R^+(\Delta_N) - f_L^+(\Delta_N)\right] \tag{5.19}$$

with the corresponding probabilities $P_N^{(0)}$ obtained from Eq. (5.18). We write down the differential conductance in the limit of zero bias, $V = 0$, or zero temperature, $T = 0$, explicitly. In the first case the linear conductance is

$$\left.\frac{G^{(1)}}{G_{as}}\right|_{V=0} = \sum_{N=-\infty}^{\infty} P_N^{(0)} \frac{\beta E_C(1 + 2(N - n_x))}{\exp\left[\beta E_C(1 + 2(N - n_x))\right] - 1} \tag{5.20}$$

with $P_N^{(0)} = \exp\left[-\beta E_C(N - n_x)^2\right] / \sum_{N'} \exp\left[-\beta E_C(N' - n_x)^2\right]$. The asymptotic high-temperature conductance is $G_{as} = 1/(R_L + R_R)$. At low temperatures, when processes involving only two charge states dominate, the maximal classical conductance saturates at one half of the asymptotic conductances at high temperatures. The width of the peaks scales linearly with temperature.

In the limit of zero temperature the result for symmetric tunnel barriers, $\alpha_0^L = \alpha_0^R$, and symmetric bias, $\mu_L = -\mu_R = eV/2$, reads

$$\left.\frac{G^{(1)}}{G_{as}}\right|_{T=0} = \left(\frac{1}{2} + \frac{2E_C^2(1 - 2n_x)^2}{(eV)^2}\right) \Theta\left(\frac{eV}{4E_C} - \left|\frac{1}{2} - n_x\right|\right) . \tag{5.21}$$

As a function of n_x it shows a series of structures of width $eV/2E_C$ with vertical steps at its edges. The width scales linearly with bias voltage.

5.6 Cotunneling

This section is devoted to the calculation of the next-order contribution, i.e., $k = 1$ in Eqs. (5.14) and (5.17). We first calculate the correlation functions $C^{(0,1)}(\omega, N)$, insert the result into Eq. (5.14) to get the corrections to the probabilities $P_N^{(1)}$. Then we have $C^{(1,0)}(\omega, N)$ and $C^{(1)}(\omega)$ from Eqs. (5.13), (5.15), and (5.16), and the current $I^{(2)}$ follows from Eq. (5.17).

The first task is to evaluate all diagrams contributing to the correlation functions $C^{(0,1)}(\omega, N)$. For $C^<$ and $C^>$ there are 32 diagrams each. They contain one tunnel line and two external vertices. In Fig. 5.2 we show two such diagrams which contribute to

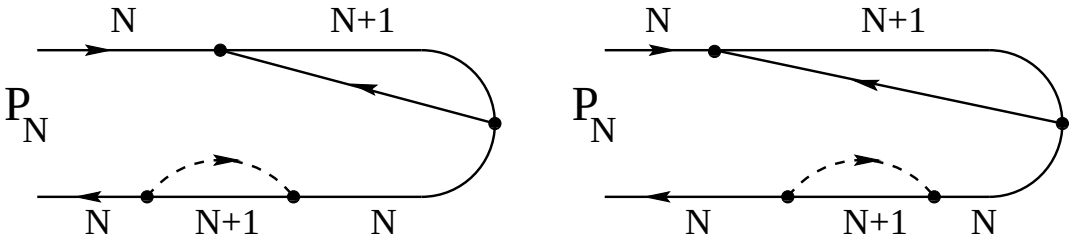

Figure 5.2: Two diagrams contributing to $C^{>(0,1)}(\omega, N)$.

$C^{>(0,1)}(\omega, N)$. The other diagrams are generated from these two by putting the right and/or the left vertex of the tunnel line on the opposite propagator and/or change the direction of the tunneling line. In each case we have to adjust the charge states at the propagators in such a way that the rightmost (external) vertex describes a transition from $N+1$ to N (or vice versa). By this procedure, we get in total 16 terms. The other 16 terms are obtained by mirroring the old diagrams with respect to a horizontal line and changing the direction of all lines. The diagrammatic rules imply that the mirrored diagrams are minus the complex conjugate of the old ones.

The first and second diagram in Fig. 5.2 have the values

$$P_N^{(0)} \int_{-\infty}^{\infty} d\omega' \, \alpha^+(\omega') \, \frac{1}{\Delta_N - \omega' + i0^+} \, \frac{1}{\omega - \omega' + i0^+} \, \frac{1}{\omega - \Delta_N + i0^+} \tag{5.22}$$

and

$$P_N^{(0)} \int_{-\infty}^{\infty} d\omega' \, \alpha^+(\omega') \, \frac{1}{\omega - \omega' + i0^+} \, \frac{1}{(\omega - \Delta_N + i0^+)^2} \, . \tag{5.23}$$

The integrands have poles. But these poles are regularized in a natural way (this follows from our theory and has *not* to be added by hand) as Cauchy principal values and delta functions, $1/(x + i0^+) = P[1/x] - i\pi\delta(x)$, and their derivative $1/(x + i0^+)^2 = -(d/dx)P[1/x] + i\pi\delta'(x)$. The integrals are well-defined at these points. Another condition for the existence of the integrals concerns the behavior at $|\omega'| \to \infty$. Since $\alpha(\omega')$ rises linearly at large energies, the integrands of some integrals may not decay fast enough at $|\omega'| \to \infty$ to ensure convergence for a single diagram. The sum of all diagrams, however, is convergent. To see this, we use for each diagram a Lorentzian cutoff $U^2/(U^2 + \omega'^2)$ with U larger than all relevant energy scales. Then, all intermediate results become convergent but may be U-dependent. To be more precise, the cutoff enters only in the form $W = \ln(\beta U/2\pi)$. While the W is present at some intermediate steps (even in the probabilities $P_N^{(1)}$), we find that the physical quantities like the average charge and the current are independent of W. This means that the divergences are only an artefact of considering single diagrams and are not present for the sum of all contributions.

Defining $\phi_{N,r} = \alpha_0^r(\Delta_N - \mu_r) \operatorname{Re} \Psi\left(i\beta(\Delta_N - \mu_r)/2\pi\right)$ and $\phi_N = \sum_r \phi_{N,r}$, where Ψ denotes the digamma function, and making use of $\Delta_{N+1} - \Delta_N = 2E_C$, we obtain the lengthy but complete result

$$
\begin{aligned}
C^{>(0,1)}(\omega,N) &= 2\pi i \qquad (5.24)\\
&\Big\{ -\left[P^{(0)}_{N-1}\alpha^+(\Delta_N+\Delta_{N-1}-\omega)+P^{(0)}_N\alpha^-(\omega)\right]\mathrm{Re}\left[\frac{1}{\omega-\Delta_N+i0^+}R_N(\omega)\right]\\
&+\left[P^{(0)}_N\alpha^+(\Delta_{N+1}+\Delta_N-\omega)+P^{(0)}_{N+1}\alpha^-(\omega)\right]\mathrm{Re}\left[\frac{1}{\omega-\Delta_N+i0^+}R_{N+1}(\omega)\right]\\
&+P^{(0)}_{N-1}\delta(\omega-\Delta_{N-1})\frac{\phi_N-\phi_{N-1}}{2E_C}+P^{(0)}_N\delta(\omega-\Delta_N)\frac{\phi_{N+1}-\phi_{N-1}}{2E_C}\\
&+P^{(0)}_{N+1}\delta(\omega-\Delta_{N+1})\frac{\phi_{N+1}-\phi_N}{2E_C}\\
&-\delta(\omega-\Delta_N)\left[P^{(0)}_{N-1}\partial\phi_{N-1}+P^{(0)}_N\partial(\phi_N+\phi_{N+1})+P^{(0)}_{N+1}\partial\phi_N\right]\\
&+P^{(0)}_N\delta'(\omega-\Delta_N)\left[2\phi_N-\phi_{N+1}-\phi_{N-1}\right]\\
&+\alpha_0 W P^{(0)}_{N-1}\left[\delta(\omega-\Delta_N)-\delta(\omega-\Delta_{N-1})\right]+\alpha_0 W P^{(0)}_{N+1}\left[\delta(\omega-\Delta_N)-\delta(\omega-\Delta_{N+1})\right]\Big\}\,.
\end{aligned}
$$

Here ∂ stands for $-(1/2E_C)(\partial/\partial n_x)$ and we have used the abbreviation

$$R_N(\omega)=\frac{1}{\omega-\Delta_N+i0^+}-\frac{1}{\omega-\Delta_{N-1}+i0^+}\,. \qquad (5.25)$$

The other contribution to $C^{>(1)}(\omega,N)=C^{>(0,1)}(\omega,N)+C^{>(1,0)}(\omega,N)$ involves probabilities in higher order, see Eq. (5.16) for $k=1$.

The expression for $C^{<(1)}(\omega,N)$ looks very similar. It is obtained from $C^{>(1)}(\omega,N)$ by changing the direction of all lines and adjusting the charge states. This implies $\alpha^+\leftrightarrow\alpha^-$, $\Delta_{N-1}\leftrightarrow\Delta_{N+1}$, $\phi_{N-1}\leftrightarrow\phi_{N+1}$, $2E_C\leftrightarrow-2E_C$, $P_{N-1}\leftrightarrow P_{N+2}$, $P_N\leftrightarrow P_{N+1}$, $R_N\leftrightarrow -R_{N+1}$, and, furthermore, there is a global minus sign.

We can solve Eq. (5.14) with the help of $C^{>(0,1)}(\omega,N)$ and $C^{<(0,1)}(\omega,N)$ for the probabilities $P^{(1)}_N$. Due to the last line of Eq. (5.24) the corrections of the probabilities, $P^{(1)}_N$, are W-dependent. But the W-dependence is of the form $-\alpha_0 W\left[2P^{(0)}_N-P^{(0)}_{N+1}-P^{(0)}_{N-1}\right]$. As a consequence, in $C^{(1)}(\omega)=\sum_N C^{(1)}(\omega,N)$ as well as in $\langle N\rangle^{(1)}$ the W-independent terms drop out, i.e., there is no divergence problem for the physical quantities.

Now we are ready to formulate the most important result of this section. Inserting the result for $C^{(1)}(\omega)$ in Eq. (5.17) with $k=1$, we obtain the cotunneling current $I^{(2)}$ which can be divided into four parts, $I^{(2)}=\sum_{i=1}^4 I^{(2)}_i$ with

$$I^{(2)}_1 = \sum_N P^{(0)}_N\int_{-\infty}^{\infty}d\omega\, B(\omega)\,\alpha(\omega)\,\mathrm{Re}\,R_N(\omega)^2\,, \qquad (5.26)$$

$$
\begin{aligned}
I^{(2)}_2 &= -\frac{1}{2}\sum_N\left(P^{(0)}_N+P^{(0)}_{N+1}\right)B(\Delta_N)\int_{-\infty}^{\infty}d\omega\,\alpha(\omega)\mathrm{Re}\left[R_N(\omega)^2+R_{N+1}(\omega)^2\right]\\
&\quad+\sum_N\left(\hat{P}_N+\hat{P}_{N+1}\right)B(\Delta_N)\,, \qquad (5.27)
\end{aligned}
$$

$$I_3^{(2)} = -\frac{1}{2}\sum_N \left(P_N^{(0)} + P_{N+1}^{(0)}\right) \frac{\partial B(\Delta_N)}{\partial \Delta_N} \int_{-\infty}^{\infty} d\omega\, \alpha(\omega) \mathrm{Re}\left[R_N(\omega) - R_{N+1}(\omega)\right] , \tag{5.28}$$

$$\begin{aligned} I_4^{(2)} = {} & \frac{4\pi^2 e}{h}\sum_N \int_{-\infty}^{\infty} d\omega \\ & \left\{ -P_{N-1}^{(0)} \alpha^+(\Delta_N + \Delta_{N-1} - \omega) \frac{\alpha_L^+(\omega)\alpha_R(\Delta_N)}{\alpha(\Delta_N)} \mathrm{Re}\left[\frac{1}{\omega - \Delta_N + i0^+} R_N(\omega)\right] \right. \\ & + P_{N+1}^{(0)} \alpha^-(\Delta_N + \Delta_{N-1} - \omega) \frac{\alpha_L^-(\omega)\alpha_R(\Delta_N)}{\alpha(\Delta_N)} \mathrm{Re}\left[\frac{1}{\omega - \Delta_N + i0^+} R_N(\omega)\right] \\ & + P_N^{(0)} \alpha^+(\Delta_{N+1} + \Delta_N - \omega) \frac{\alpha_L^+(\omega)\alpha_R(\Delta_N)}{\alpha(\Delta_N)} \mathrm{Re}\left[\frac{1}{\omega - \Delta_N + i0^+} R_{N+1}(\omega)\right] \\ & \left. - P_{N+2}^{(0)} \alpha^-(\Delta_{N+1} + \Delta_N - \omega) \frac{\alpha_L^-(\omega)\alpha_R(\Delta_N)}{\alpha(\Delta_N)} \mathrm{Re}\left[\frac{1}{\omega - \Delta_N + i0^+} R_{N+1}(\omega)\right] \right\} \\ & - (L \leftrightarrow R) . \end{aligned} \tag{5.29}$$

Here we have used the definitions

$$B(\omega) \equiv \frac{4\pi^2 e}{h} \frac{\alpha_L(\omega)\alpha_R(\omega)}{\alpha(\omega)} \left[f_R^+(\omega) - f_L^+(\omega)\right] \tag{5.30}$$

and

$$\hat{P}_N \equiv P_N^{(1)} + \alpha_0 W \left[2P_N^{(0)} - P_{N+1}^{(0)} - P_{N-1}^{(0)}\right] - (P_N^{(0)} - P_{N-1}^{(0)})\partial\phi_{N-1} + (P_{N+1}^{(0)} - P_N^{(0)})\partial\phi_N . \tag{5.31}$$

In the low-temperature limit, $B(\Delta_0)$ is the sequential-tunneling result. It enters in $I_1^{(2)}, I_2^{(2)}$, and $I_3^{(2)}$ in different ways.

The first term $I_1^{(2)}$ describes processes in which one electron enters and other one leaves the island coherently. In the Coulomb blockade regime only one charge state is occupied in lowest order at low temperature, $P_N^{(0)} = \delta_{N,0}$. At $T = 0$, the integrand is zero at the poles of $R_N(\omega)$, and we can omit the term $i0^+$. In this case, we recover from Eq. (5.26) the usual cotunneling result [47,48]. At finite temperature, however, the term $+i0^+$ is needed for regularization which is not provided by previous theories.[3] The result Eq. (5.26) is also well-defined for $T \neq 0$.

Furthermore, we are able to describe the system at resonance. In this regime, $I_2^{(2)}$ and $I_3^{(2)}$ become important. These terms describe the renormalization of the tunneling conductance α_0 and the energy gap Δ_0, respectively. They can be traced back to vertex correction and propagator renormalization diagrams (see Fig. 5.3). We will discuss these contributions in more detail in Sections 5.6.1 and 5.8.

At high temperature or bias voltage, there are processes in which two electrons enter or leave the island coherently. After such a process, the island charge has increased or decreased by $2e$. These processes are described by the fourth term $I_4^{(2)}$, Eq. (5.29).

[3] Usually, the value of the integral is approximated by replacing the denominators with an ω-independent term or by adding a constant lifetime in the denominator, see, e.g., Refs. [105–107].

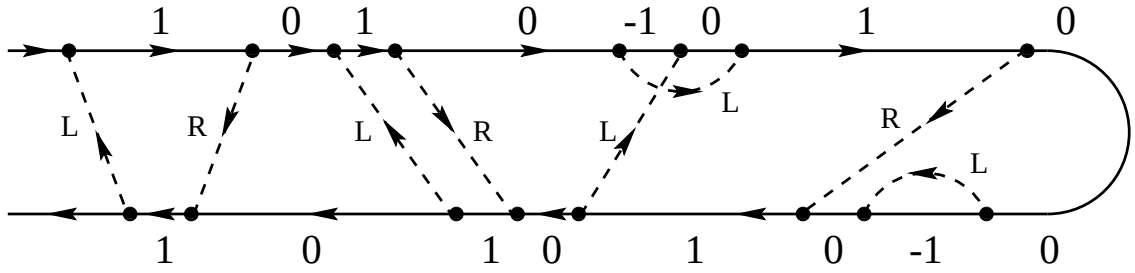

Figure 5.3: A diagram showing contributions to sequential tunneling ($\Sigma^{(1)}_{0,1}$ and $\Sigma^{(1)}_{1,0}$) and cotunneling: usual cotunneling with two electrons tunneling coherently (contribution to $\Sigma^{(2)}_{0,0}$), vertex correction ($\Sigma^{(2)}_{0,1}$), and propagator renormalization ($\Sigma^{(2)}_{1,0}$).

All integrals in Eqs. (5.26) - (5.29) can be performed analytically. We do not write down the lengthy results for the general case here. They can be found for the most interesting limits in Sections 5.6.1 and 5.6.2. The quantities $\hat{P}_N$ which enter Eq. (5.27) are determined by $\sum_N \hat{P}_N = 0$ and

$$
\begin{aligned}
&\hat{P}_N \alpha^+(\Delta_N) - \hat{P}_{N+1}\alpha^-(\Delta_N) = \qquad (5.32)\\
&\sum_{r,r'} \frac{P^{(0)}_{N-1} - e^{\beta(\Delta_N+\Delta_{N-1}-\mu_r-\mu_{r'})}P^{(0)}_{N+1}}{e^{\beta(\Delta_N+\Delta_{N-1}-\mu_r-\mu_{r'})}-1}\,\alpha^r_0\\
&\quad\times\left\{-\partial\left[(\Delta_N-\mu_r)\phi_{N-1,r'}+(\Delta_{N-1}-\mu_r)\phi_{N,r'}\right]-\frac{\Delta_{N-1}-\mu_r}{E_C}\phi_{N-1,r'}+\frac{\Delta_N-\mu_r}{E_C}\phi_{N,r'}\right\}\\
&+\sum_{r,r'} \frac{P^{(0)}_{N} - e^{\beta(\Delta_{N+1}+\Delta_N-\mu_r-\mu_{r'})}P^{(0)}_{N+2}}{e^{\beta(\Delta_{N+1}+\Delta_N-\mu_r-\mu_{r'})}-1}\,\alpha^r_0\\
&\quad\times\left\{-\partial\left[(\Delta_{N+1}-\mu_r)\phi_{N,r'}+(\Delta_N-\mu_r)\phi_{N+1,r'}\right]-\frac{\Delta_N-\mu_r}{E_C}\phi_{N,r'}+\frac{\Delta_{N+1}-\mu_r}{E_C}\phi_{N+1,r'}\right\}\\
&-\left[P^{(0)}_N\partial\alpha^+(\Delta_N)-P^{(0)}_{N+1}\partial\alpha^-(\Delta_N)\right]\left[2\phi_N-\phi_{N+1}-\phi_{N-1}\right].
\end{aligned}
$$

In principle, the problem is now solved. One can solve Eq. (5.32) for $\hat{P}_N$ numerically and will then get the average charge and the current. In Figs. 5.4 and 5.5 we show the differential conductance as a function of the transport voltage for two different values of the gate charge. There are steps at voltages at which new charge states become important. Due to cotunneling the steps are washed out. Furthermore, there is a finite conductance in the Coulomb blockade regime although the sequential-tunneling contribution is exponentially suppressed.

But we can do even better and find analytic expressions for the two most interesting cases. The first one (Section 5.6.1) covers the regime in which only two charge states are occupied in lowest order (then four charge states have corrections in first order). In this regime the Coulomb oscillations are most pronounced and the system is expected to behave like a multichannel Kondo model. But to study the crossover from the Coulomb blockade

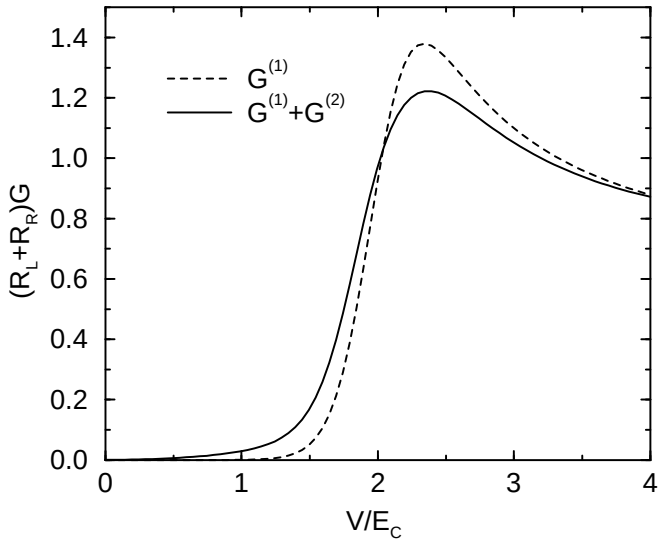

Figure 5.4: The differential conductance as a function of transport voltage for $T/E_C = 0.05$, $n_x = 0$, and $\alpha_0 = 0.01$: sequential tunneling and sequential plus cotunneling contribution.

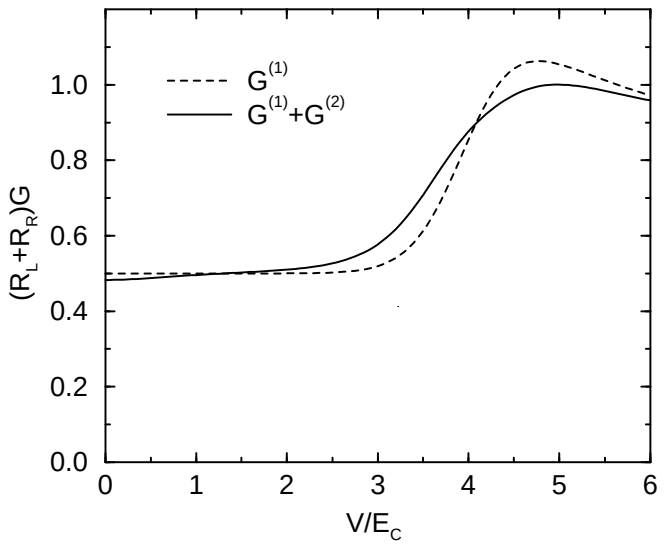

Figure 5.5: The differential conductance as a function of transport voltage for $T/E_C = 0.1$, $n_x = 0.5$, and $\alpha_0 = 0.01$: sequential tunneling and sequential plus cotunneling contribution.

to the classical (high temperature) regime, one has to allow for all temperatures. This is done in Section 5.6.2, in which we consider the linear response.

5.6.1 Low-Temperature Nonequilibrium Transport

At low temperature, $T \ll E_C$, and a transport voltage which may be finite but small enough, only two charge states ($N = 0, 1$) are occupied in lowest order, $P_N^{(0)} \approx 0$ for $N \neq 0, 1$.

Sequential tunneling gives for the average charge just $\langle N \rangle^{(0)} = P_1^{(0)} = \alpha^+(\Delta_0)/\alpha(\Delta_0)$, and the current is $I^{(1)} = B(\Delta_0)$.

The probabilities in next order, $P_N^{(1)}$, are determined by Eq. (5.14). In the low-temperature limit, the first and second term in Eq. (5.32) are exponentially small. We find

$$P_{-1}^{(1)} = -P_0^{(0)}\partial\phi_{-1} + P_0^{(0)}\alpha_0 W \tag{5.33}$$

$$P_0^{(1)} = P_0^{(0)}\partial\phi_{-1} - (P_1^{(0)} - P_0^{(0)})\partial\phi_0 + \partial P_0^{(0)}\left[2\phi_0 - \phi_{-1} - \phi_1\right] + (P_1^{(0)} - 2P_0^{(0)})\alpha_0 W \tag{5.34}$$

$$P_1^{(1)} = (P_1^{(0)} - P_0^{(0)})\partial\phi_0 + P_1^{(0)}\partial\phi_1 + \partial P_1^{(0)}\left[2\phi_0 - \phi_{-1} - \phi_1\right] + (P_0^{(0)} - 2P_1^{(0)})\alpha_0 W \tag{5.35}$$

$$P_2^{(1)} = -P_1^{(0)}\partial\phi_1 + P_1^{(0)}\alpha_0 W \tag{5.36}$$

while all other corrections vanish, and therefore

$$\langle N \rangle^{(1)} = -\frac{1}{2E_C}\frac{\partial}{\partial n_x}\left[P_0^{(0)}\left(\phi_{-1} - \phi_0\right) + P_1^{(0)}\left(\phi_0 - \phi_1\right)\right] . \tag{5.37}$$

The total second-order, cotunneling, current Eqs. (5.26) - (5.29) simplifies to

$$I_1^{(2)} = \int_{-\infty}^{\infty} d\omega\, B(\omega)\alpha(\omega)\,\mathrm{Re}\left[P_0^{(0)}R_0(\omega)^2 + P_1^{(0)}R_1(\omega)^2\right] , \tag{5.38}$$

$$I_2^{(2)} = -\frac{1}{2}B(\Delta_0)\int_{-\infty}^{\infty} d\omega\,\alpha(\omega)\,\mathrm{Re}\left[R_0(\omega)^2 + R_1(\omega)^2\right] , \tag{5.39}$$

$$I_3^{(2)} = -\frac{1}{2}\frac{\partial B(\Delta_0)}{\partial\Delta_0}\int_{-\infty}^{\infty} d\omega\,\alpha(\omega)\,\mathrm{Re}\left[R_0(\omega) - R_1(\omega)\right] , \tag{5.40}$$

and $I_4^{(2)} = 0$. All integrals in Eqs. (5.38) - (5.40) can be performed analytically. The result is

$$I_1^{(2)} = \frac{4\pi^2 e}{h}\alpha_0^R \sum_{N=0,1} P_N^{(0)}\left\{\frac{\Delta_{N-1} - \mu_R}{E_C}\phi_{N-1,L} - \frac{\Delta_N - \mu_R}{E_C}\phi_{N,L}\right. \tag{5.41}$$

$$\left. + \partial\left[(\Delta_{N-1} - \mu_R)\phi_{N-1,L} + (\Delta_N - \mu_R)\phi_{N,L}\right]\right\} - (L \leftrightarrow R) ,$$

$$I_2^{(2)} = B(\Delta_0)\left\{\frac{\phi_{-1} - \phi_1}{E_C} + \partial[2\phi_0 + \phi_{-1} + \phi_1]\right\} , \tag{5.42}$$

$$I_3^{(2)} = \left[\frac{\partial B(\Delta_0)}{\partial\Delta_0}\right](2\phi_0 - \phi_{-1} - \phi_1) . \tag{5.43}$$

In the Coulomb blockade regime, we have $P_0^{(0)} = 1$, $P_1^{(0)} = 0$ and $I^{(1)}(\Delta_0) = 0$, which yields $I_2^{(1)} = I_3^{(1)} = 0$. The only contribution is the term with $N = 0$ in Eq. (5.38). This gives the well-known result of inelastic cotunneling [47,48].

At resonance ($P_0^{(0)} \neq 0 \neq P_1^{(0)}$), the terms describing the renormalization of the tunneling conductance α_0 and the energy gap Δ_0, $I_2^{(2)}$ and $I_3^{(2)}$, become important. Suppose that the current can be expressed by the sequential-tunneling result with renormalized parameters $\tilde{\alpha}$ and $\tilde{\Delta}$ plus some regular terms, $I(\alpha_0, \Delta_0) = I^{(1)}(\tilde{\alpha}, \tilde{\Delta}) + \text{regular terms}$. The expansion up to $\mathcal{O}(\alpha_0^2)$ of

$$I^{(1)}(\tilde{\alpha}, \tilde{\Delta}) = \frac{\tilde{\alpha} - \alpha_0}{\alpha_0} I^{(1)}(\alpha_0, \Delta_0) + (\tilde{\Delta} - \Delta_0) \frac{\partial I^{(1)}(\alpha_0, \Delta_0)}{\partial \Delta_0} \,. \tag{5.44}$$

and the identification with Eqs. (5.42) and (5.43) yield the lowest-order corrections for the renormalized quantities.

In Fig. 5.6 we compare the first-order result for the differential conductance $G = \partial I / \partial V$ with the sum of the first and second order in the nonlinear regime (in the following we choose $\alpha_0^L = \alpha_0^R$). The deviation from sequential tunneling is significant and of the order 20%. In the inset we show the second-order contributions. The dimensionless conductance $\tilde{\alpha}$ as well as energy gap $\tilde{\Delta}$ is decreased in comparison to the unrenormalized values α_0 and Δ_0. For this reason, $G_2^{(2)}$ is negative since the conductance is reduced, and $G_3^{(2)}$ is positive since the system is effectively "closer" to the resonance.

In Fig. 5.7 shows the same for the nonlinear regime. There is in total a double peak structure (resonance with the Fermi levels of the left and right reservoir) instead of one peak like in the linear response regime. The cotunneling contribution leads again to a decrease of the peaks and a broadening.

5.6.2 Linear Response for Arbitrary Temperature

In the last section we discussed the effect of the quantum fluctuations at low temperature, when Coulomb oscillations are pronounced. In this case, at most two charge states are occupied classically. But also at high temperature, the asymptotic behavior shows deviations from the sequential-tunneling result. Furthermore, for a comparison with experiment, it is necessary to describe also the crossover between the low and the high temperature regime. In this section we discuss the linear response, i.e., we set $V = 0$, but we allow for all charge states.

The corrections to the probabilities are then

$$\begin{aligned} P_N^{(1)} = &\left(P_N^{(0)} - P_{N-1}^{(0)}\right) \partial\phi_{N-1} - \left(P_{N+1}^{(0)} - P_N^{(0)}\right) \partial\phi_N - \beta P_N^{(0)} \left(\phi_{N-1} - \phi_N\right) \\ &+\beta P_N^{(0)} \sum_{N'} P_{N'}^{(0)} \left(\phi_{N'-1} - \phi_{N'}\right) - \alpha_0 W \left(2P_N^{(0)} - P_{N+1}^{(0)} - P_{N-1}^{(0)}\right) \end{aligned} \tag{5.45}$$

which implies

$$\langle N \rangle^{(1)} = -\frac{1}{2E_C} \frac{\partial}{\partial n_x} \left[\sum_N P_N^{(0)} \left(\phi_{N-1} - \phi_N\right) \right] \,. \tag{5.46}$$

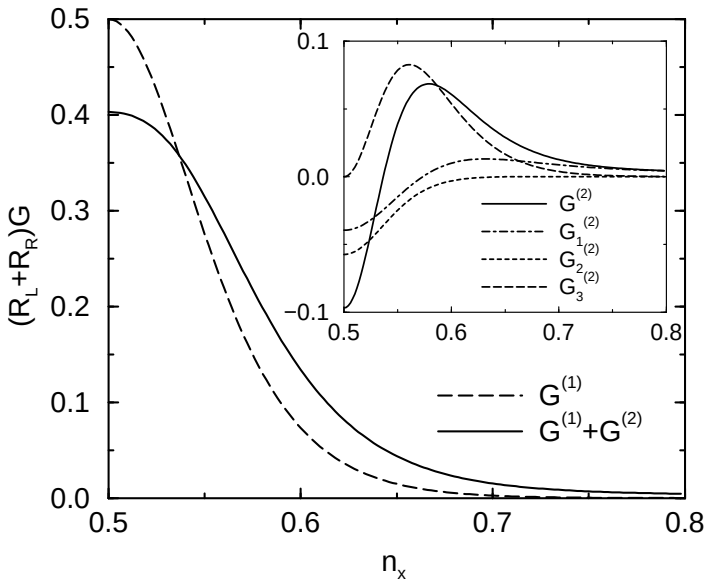

Figure 5.6: Differential conductance for $T/E_C = 0.05$, $\alpha_0 = 0.04$ and $V = 0$: sequential tunneling and sequential plus cotunneling. Inset: second-order contribution $G^{(2)} = \sum_{i=1}^{3} G_i^{(2)}$. All curves are symmetric around $n_x = 0.5$.

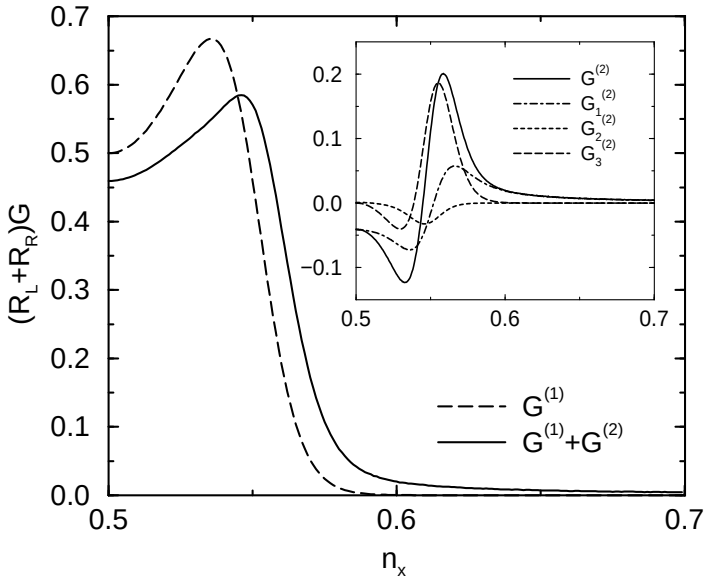

Figure 5.7: Differential conductance for $T/E_C = 0.01$, $\alpha_0 = 0.02$ and $eV/E_C = 0.2$: sequential tunneling and sequential plus cotunneling. Inset: second-order contribution $G^{(2)} = \sum_{i=1}^{3} G_i^{(2)}$. All curves are symmetric around $n_x = 0.5$.

A systematic perturbative expansion of the partition function (up to order α_0^2) was performed in Ref. [23]. The result Eq. (5.46) is identical to the result obtained there in order α_0, which at $T=0$ reads $\langle N\rangle^{(1)} = \alpha_0 \ln[(1+2n_x)/(1-2n_x)]$.

Using the definition $S(\Delta_N) = \partial B(\Delta_N)/\partial V$ we find the differential conductance $G^{(2)} = \partial I^{(2)}/\partial V = \sum_{i=1}^{4} G_i^{(2)}$ with

$$G_1^{(2)} = \int_{-\infty}^{\infty} d\omega\, S(\omega)\alpha(\omega) \sum_N P_N^{(0)} \mathrm{Re}\, R_N(\omega)^2\,, \tag{5.47}$$

$$G_2^{(2)} = -\frac{1}{2}\sum_N S(\Delta_N) \int_{-\infty}^{\infty} d\omega\, \alpha(\omega) \mathrm{Re}\left\{ \left(P_N^{(0)} + P_{N+1}^{(0)}\right)\left[R_N(\omega)^2 + R_{N+1}(\omega)^2\right] \right.$$
$$\left. +\beta P_N^{(0)} R_N(\omega) + \beta P_{N+1}^{(0)} R_{N+1}(\omega) - \beta\left(P_N^{(0)} + P_{N+1}^{(0)}\right) \sum_{N'} P_{N'}^{(0)} R_{N'}(\omega) \right\} \tag{5.48}$$

$$G_3^{(2)} = -\frac{1}{2}\sum_N \left(P_N^{(0)} + P_{N+1}^{(0)}\right) \frac{\partial S(\Delta_N)}{\partial \Delta_N} \int_{-\infty}^{\infty} d\omega\, \alpha(\omega) \mathrm{Re}\,\left[R_N(\omega) - R_{N+1}(\omega)\right] \tag{5.49}$$

$$G_4^{(2)} = \frac{4\pi^2 e^2}{h}\beta \sum_N \int_{-\infty}^{\infty} d\omega\, P_{N-1}^{(0)} \alpha_L^+(\Delta_N + \Delta_{N-1} - \omega)\alpha_R^+(\omega) \mathrm{Re}\, R_N(\omega)^2 \tag{5.50}$$

In comparison to the previous section, a new term, $G_4^{(2)}$, appears, which is related to new processes where the island charge is increased or decreased by $2e$. Again, all integrals Eq. (5.47) - (5.50) can be performed analytically. While the sequential-tunneling result gives

$$\frac{G^{(1)}}{G_{as}} = \sum_N \left[P_N^{(0)} + P_{N+1}^{(0)}\right] \frac{\beta\Delta_N/2}{\sinh \beta\Delta_N} \tag{5.51}$$

we find for the cotunneling

$$\frac{G_1^{(2)}}{G_{as}} = \sum_N P_N^{(0)} \times \tag{5.52}$$
$$\left\{ \Delta_{N-1}\partial^2\phi_{N-1} + \Delta_N \partial^2 \phi_N + \frac{\Delta_{N-1}\partial\phi_{N-1} - \Delta_N \partial\phi_N}{E_C} + \frac{\phi_N - \phi_{N-1}}{E_C} \right\}$$

$$\frac{G_2^{(2)}}{G_{as}} = \sum_N \left(\frac{\beta\Delta_N/2}{\sinh\beta\Delta_N}\right) \times \tag{5.53}$$
$$\left\{ \left(P_N^{(0)} + P_{N+1}^{(0)}\right)\left[\frac{\phi_{N-1} - \phi_{N+1}}{E_C} + \partial\left(2\phi_N + \phi_{N-1} + \phi_{N+1}\right)\right] - \beta P_N^{(0)}[\phi_{N-1} - \phi_N] \right.$$
$$\left. -\beta P_{N+1}^{(0)}[\phi_N - \phi_{N+1}] + \beta\left(P_N^{(0)} + P_{N+1}^{(0)}\right) \sum_{N'} P_{N'}[\phi_{N'-1} - \phi_{N'}] \right\}$$

$$\frac{G_3^{(2)}}{G_{as}} = \sum_N \left[\frac{\partial}{\partial\Delta_N}\left(\frac{\beta\Delta_N/2}{\sinh\beta\Delta_N}\right)\right]\left(P_N^{(0)} + P_{N+1}^{(0)}\right)[2\phi_N - \phi_{N-1} - \phi_{N+1}] \tag{5.54}$$

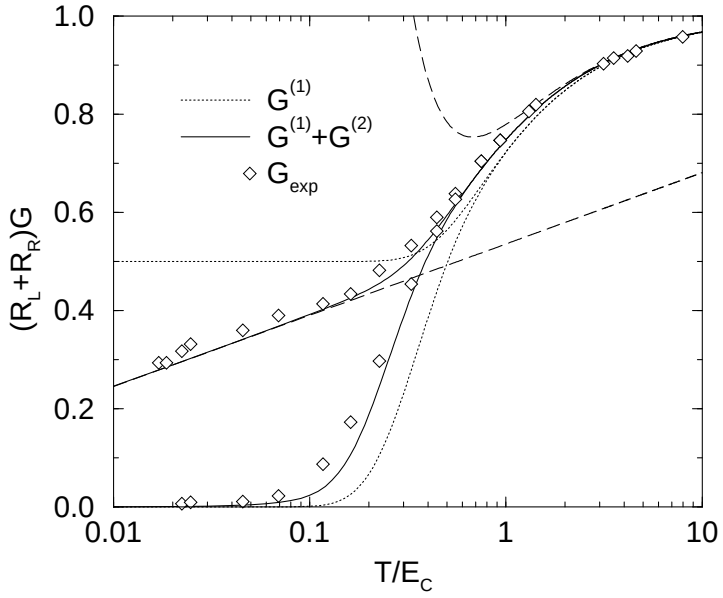

Figure 5.8: Maximal ($n_x = 0.5$) and minimal ($n_x = 0$) linear conductance for $E_C = 1K$ and $\alpha_0 = 0.063$. Dotted lines: first-order results. Solid lines: first plus second-order results. The upper lines are the results at $n_x = 0.5$, the lower lines at $n_x = 0$. Dashed lines: low- and high-temperature expansion. Diamonds: experimental data from Ref. [53].

$$\frac{G_4^{(2)}}{G_{as}} = \beta \sum_N \frac{P_{N-1}^{(0)} + P_{N+1}^{(0)}}{\sinh \beta \left(\Delta_{N-1} + \Delta_N\right)} \times \left\{ -\Delta_{N-1} \partial\phi_N - \Delta_N \partial\phi_{N-1} + \frac{\Delta_{N-1} + \Delta_N}{2E_C} [\phi_N - \phi_{N-1}] \right\} . \tag{5.55}$$

In Fig. 5.8 we compare our results with recent experiments [53]. The temperature dependence of the Coulomb oscillations were measured for a sample with a conductance $\alpha_0 = 0.063$. Our results in second-order perturbation theory agree very well in the whole temperature range.

We emphasize that only bare values for α_0 and E_C have been used here, as determined directly in the experiment, i.e., the solid lines in Fig. 5.8 represent a no-parameter fit to the experimental data. In contrast, the resonant-tunneling approximation with bare values of the charging energy would lead to a deviation from the experiment by about 10%. Thus, the inclusion of higher-order charge states within second-order perturbation theory, as presented in this section, is important for comparison with experiments.

While at resonance the new terms are crucial, the Coulomb blockade regime is sufficiently described by Eq. (5.38) which yields a good agreement between theory and experiment.

5.6.3 Asymptotic Behavior

In linear response, the whole temperature regime is covered by Eqs. (5.51) - (5.55). At high and low temperatures these formulas become very simple.

High-Temperature Expansion

At high temperature ($\beta E_C \ll 1$), Coulomb oscillations are washed out, i.e., there is no gate-charge dependence of the conductance, and using the Euler-MacLaurin formula we can replace the sum in Eq. (5.51) by an integral. In this way we average the conductance over all possible gate charges, loosing the information about the difference between minimal and maximal conductance. In linear response we have $P_N^{(0)} = \exp[-\beta E_C (N - n_x)^2]/Z$. We expand $(\beta\Delta_N)/\sinh(\beta\Delta_N)$ in $\beta\Delta$ and perform the integral which approximates Eq. (5.51). This yields $G^{(1)}/G_{as} = 1 - \beta E_C/3 + (\beta E_C)^2/15 + \mathcal{O}((\beta E_C)^3)$.

For the cotunneling contribution we expand the digamma functions which enter $\phi_N = \alpha_0 \Delta_N \mathrm{Re}\,\Psi\,(i\beta\Delta_N/2\pi)$ using $\mathrm{Re}\,\Psi(ix) = \mathrm{Re}\,\Psi(1+ix) = -\gamma + \zeta(3)x^2 - \zeta(5)x^4 + \mathcal{O}(x^6)$, and we find $G_1^{(2)} = G_2^{(2)} = G_4^{(2)} = 2\alpha_0(\beta E_C)^2\zeta(3)/\pi^2$ and $G_3^{(2)} = 0$, i.e.,

$$\frac{G}{G_{as}} = 1 - \frac{\beta E_C}{3} + (\beta E_C)^2 \left[\frac{1}{15} + \frac{6\zeta(3)}{\pi^2}\alpha_0\right] + \mathcal{O}\left((\beta E_C)^3\right) . \tag{5.56}$$

This result was also derived in Refs. [34, 108, 109].

Low-Temperature Expansion

At low temperature ($\beta E_C \gg 1$), Coulomb oscillations appear. The maximal conductance is reached at half integer values of n_x. In sequential tunneling the maximal conductance saturates at one half of the asymptotic high temperature value. The quantum fluctuations, however, lead to a further reduction. Approximating the digamma function by $\mathrm{Re}\,\Psi(ix) = \ln|x|$ for $x \neq 0$, we find $G_{1,max}^{(2)}/G_{as} = -\alpha_0$, $G_{2,max}^{(2)}/G_{as} = \alpha_0\,[1 - \gamma - \ln(\beta E_C/\pi)]$, and $G_{3,max}^{(2)} = G_{4,max}^{(2)} = 0$, i.e., in total

$$\frac{G_{max}}{G_{as}} = \frac{1}{2} - \alpha_0 \left[\gamma + \ln\left(\frac{\beta E_C}{\pi}\right)\right] + \mathcal{O}\left(\alpha_0^2\right) \tag{5.57}$$

with γ being Euler's constant. The peak conductance depends logarithmically on temperature. This result may be interpreted as a renormalization of G_{as} or α_0. It shows a typical logarithmic temperature dependence since, at least in the equilibrium situation, the low-energy behavior of the system is expected to be that of the multichannel Kondo model.

In Fig. 5.8 we compare the limiting expressions Eq. (5.56) and (5.57) with the full second-order result Eq. (5.51) - (5.55), which interpolates between the logarithmic behavior at low temperature and the high-temperature result.

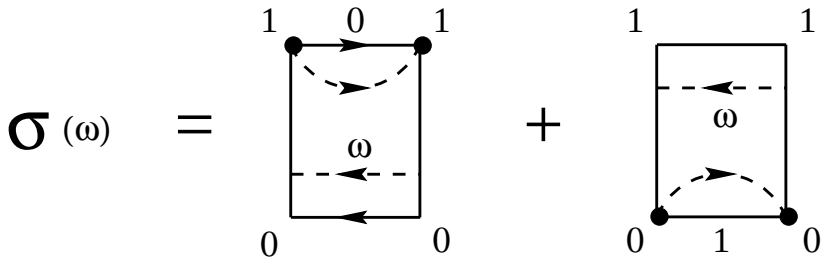

Figure 5.9: In our approximation, the diagram for the irreducible self-energy $\sigma(\omega)$ contains one tunneling line in addition to the backward running line.

5.7 Resonant Tunneling

The *resonant-tunneling approximation* discussed in Section 4.4 for the quantum dot can be also used for a nonperturbative treatment of the quantum fluctuations in metallic islands. We include processes of arbitrary high order, but we restrict ourselves to matrix elements of the density matrix which are at most two-fold off-diagonal. Furthermore, we allow only for two charge states $N = 0, 1$. Like in the quantum dot case, this provides a conserving approximation.

The advantage of the resonant-tunneling approximation over cotunneling is applicability at stronger coupling. Due to the nonperturbative treatment we find a structure of the renormalization of the energy gap and coupling constant similar to the results from renormalization-group techniques. Differences and similarities will be discussed in the next section.

The analytic resummation is very analogous to the derivation presented in Section 4.4.1. We get the following results:

The stationary probabilities are

$$P_0 = \lambda^- \qquad \text{and} \qquad P_1 = \lambda^+ \qquad \text{with} \qquad \lambda^\pm = \int_{-\infty}^{\infty} d\omega\, \alpha^\pm(\omega) |\pi(\omega)|^2 \,. \tag{5.58}$$

Again, the propagator $\pi(\omega)$ and the self-energy $\sigma(\omega)$ are diagram parts with one tunneling line running in parallel (see Figs. 4.12 and 5.9),

$$\pi(\omega) = [\omega - \Delta_0 - \sigma(\omega)]^{-1} \qquad \text{and} \qquad \sigma(\omega) = \int_{-\infty}^{\infty} d\omega' \, \frac{\alpha(\omega')}{\omega - \omega' + i0^+} \,. \tag{5.59}$$

We find for the current

$$I = \frac{4\pi^2 e}{h} \int_{-\infty}^{\infty} d\omega \, \frac{\alpha_L(\omega)\alpha_R(\omega)}{\alpha(\omega)} A(\omega)[f_R^+(\omega) - f_L^+(\omega)] \,. \tag{5.60}$$

with the spectral density

$$A(\omega) = \frac{\alpha(\omega)}{[\omega - \Delta_0 - \mathrm{Re}\,\sigma(\omega)]^2 + [\mathrm{Im}\,\sigma(\omega)]^2} \,. \tag{5.61}$$

In general, quantum fluctuations yield energy renormalization and broadening effects, which enter in the spectral density via the complex self-energy $\sigma(\omega)$ given in Eq. (5.59). In order to evaluate $\sigma(\omega)$ we introduce a Lorentzian cut-off which we choose equal to E_C (since the energy difference to charge states which are not taken into account here is of the order of the charging energy). In this case we find

$$\mathrm{Re}\,\sigma(\omega) = -\sum_r \alpha_0^r(\omega-\mu_r)\left[2\ln\left(\frac{E_C}{2\pi T}\right) - 2\mathrm{Re}\,\Psi\left(i\,\frac{\omega-\mu_r}{2\pi T}\right)\right] \tag{5.62}$$

$$\mathrm{Im}\,\sigma(\omega) = -\pi\alpha(\omega)\,. \tag{5.63}$$

The effect of the quantum fluctuations can be estimated from the spectral density in the limits $T \gg eV, |\omega|$ or $eV \gg T, |\omega|$. Then, the spectral density is

$$A(\omega) \approx \frac{Z^2\alpha(\omega)}{[\omega - Z\Delta_0]^2 + [\pi Z\alpha(\omega)]^2}\,, \tag{5.64}$$

with

$$Z^{-1} = 1 + 2\alpha_0 \ln\left(\frac{E_C}{\max\{eV/2, 2\pi T\}}\right). \tag{5.65}$$

We observe a renormalization of Δ_0 and α_0 by Z and a broadening given by $\pi Z\alpha(\omega)$.

A pronounced signature of quantum fluctuations is contained in the differential conductance $G = \partial I/\partial V$. In Figs. 5.10 and 5.11 we show our results in linear and nonlinear response, respectively. For comparison, we show also the sequential-tunneling result.

From Eq. (5.51) we see that at low temperatures, when processes involving only two charge states dominate, the maximal classical conductance saturates in linear response at one half of the asymptotic value $G_{as} = 1/(R_L + R_R)$. The width of the peaks scales linearly with temperature. The situation changes when resonant-tunneling processes are taken into account. The maximal conductance and the peak width are renormalized by Z and Z^{-1} which depend logarithmically on temperature (see Fig. 5.10). For this reason, the conductance peak does not reach one half of the high temperature limit and decreases with lower temperatures, while the peak width is increased compared to the lowest-order perturbation theory result. For an estimate of the maximal conductance, we can use the spectral density in the form of Eq. (5.64) and perform the integral Eq. (5.60) analytically,

$$\frac{G_{max}(T)}{G_{as}} \approx Z\left[\frac{1}{2} - \frac{1}{\pi}\arctan\left(\frac{(\pi Z\alpha_0)^2 - 1}{2\pi Z\alpha_0}\right)\right]. \tag{5.66}$$

(The results shown in Fig. (5.10), however, were obtained by numerical analysis based on Eq. (5.61).)

The effects of quantum fluctuations are even more pronounced in the nonlinear differential conductance when the transport voltage dominates over temperature. In Fig. 5.11 we compare the results of perturbation theory and resonant tunneling at $T = 0$ assuming that for $eV < 2E_C$ only two charge states $N = 0, 1$ are involved. The conductance in sequential tunneling, Eq. (5.21), shows as a function of n_x a series of structures of width $eV/2E_C$

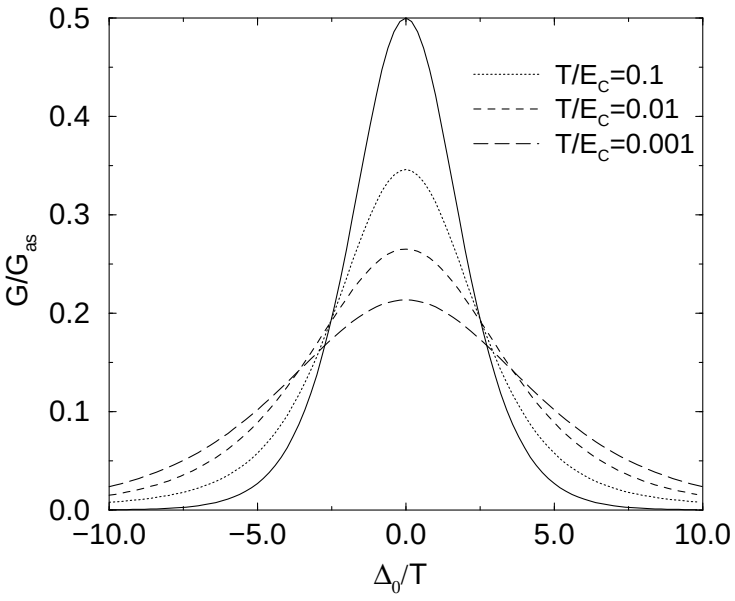

Figure 5.10: The differential conductance in linear response, $V = 0$, as a function of the energy gap Δ_0 normalized to the temperature T with $\alpha_0^L = \alpha_0^R = 0.05$ for different values of T/E_C. For comparison we show the sequential-tunneling result (solid line), which is independent of the temperature.

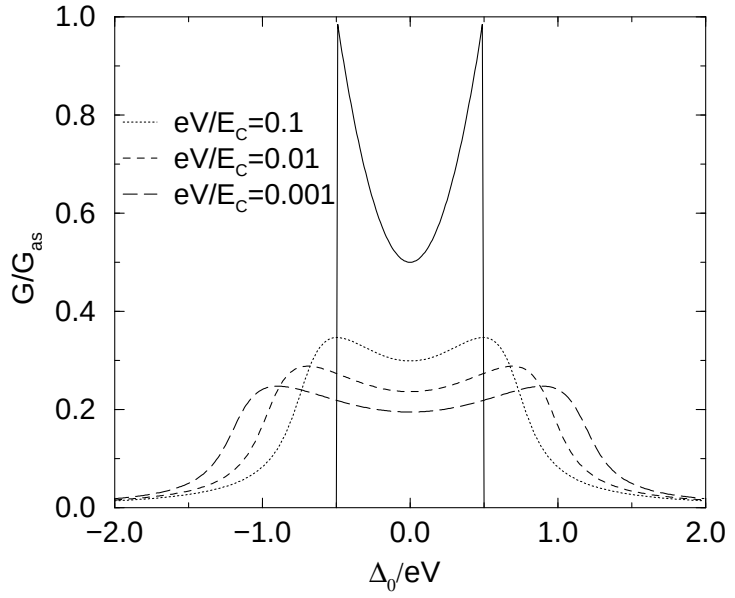

Figure 5.11: The differential conductance at zero temperature, $T = 0$, as a function of the energy gap Δ_0 normalized to the transport voltage eV with $\alpha_0^L = \alpha_0^R = 0.05$ for different values of eV/E_C. For comparison we show the sequential-tunneling result (solid line), which is independent of the transport voltage eV.

with vertical steps at its edges. The width scales linearly with bias voltage. Resonant tunneling leads to a renormalization of the height and width by Z and Z^{-1} respectively, which depends now logarithmically on the voltage (see Fig. 5.11). For this reason, the height of the structure is below the sequential-tunneling result and further decreases at lower voltages, while the width is enhanced. Furthermore, the sharp edges are smeared out even in the absence of thermal fluctuations (since $T = 0$).

5.8 Renormalization Effects

Renormalization-group techniques have been applied for the single-electron box (which is equivalent to the transistor at zero bias voltage) including two charge states [24, 110]. Starting with some initial high-energy cutoff (which is of the order of the charging energy E_C), one integrates out the high-energy modes. This leads to a renormalization of the system parameters. This procedure has to be performed until the cutoff reaches the largest energy scale ω_C which is important for the lowest order tunneling processes. This leads to

$$\frac{\tilde{\alpha}}{\alpha_0} = \frac{\tilde{\Delta}}{\Delta_0} = \frac{1}{1 + 2\alpha_0 \ln(E_C/\omega_C)}. \tag{5.67}$$

Of course, the result is rather qualitative, since the numerical coefficient of the high-energy cutoff and, therefore, the constant in the argument of the logarithm remains unknown. Furthermore, Eq. (5.67) does not describe the situation when two candidates for ω_C (e.g. Δ and T) are of the same order of magnitude.

Using the resonant-tunneling approximation, Eqs. (5.61) - (5.63), we are able to generalize Eq. (5.67) to non-equilibrium situations and find (for E_C larger than any other energy scale)

$$\tilde{\alpha} = \frac{\alpha_0}{1 + 2\sum_r \alpha_0^r \left[\ln\left(\frac{\beta E_C}{2\pi}\right) - \mathrm{Re}\,\Psi\left(i\frac{\beta(\tilde{\Delta}-\mu_r)}{2\pi}\right)\right]} \tag{5.68}$$

$$\tilde{\Delta} = \frac{\Delta_0 + 2\sum_r \alpha_0^r \mu_r \left[\ln\left(\frac{\beta E_C}{2\pi}\right) - \mathrm{Re}\,\Psi\left(i\frac{\beta(\tilde{\Delta}-\mu_r)}{2\pi}\right)\right]}{1 + 2\sum_r \alpha_0^r \left[\ln\left(\frac{\beta E_C}{2\pi}\right) - \mathrm{Re}\,\Psi\left(i\frac{\beta(\tilde{\Delta}-\mu_r)}{2\pi}\right)\right]}. \tag{5.69}$$

In contrast to Eq. (5.67), this result applies also in intermediate regimes, e.g., $\beta\Delta \sim 1$. But still the constants in the arguments of the logarithms remain unknown, since the high-energy cutoff was put by hand. This is improved by the cotunneling theory, in which we have taken all relevant charge states into account, i.e., the cutoff is provided naturally by the energy of the adjacent charge states and has not to be introduced by hand. Therefore, we can extract the complete arguments from Eqs. (5.42) and (5.43),

$$\tilde{\alpha} = \alpha_0 - 2\alpha_0 \sum_r \alpha_0^r \left[-1 + \ln\left(\frac{\beta E_C}{\pi}\right) - \frac{\partial}{\partial \Delta_0}\left((\Delta_0 - \mu_r)\mathrm{Re}\,\Psi\left(i\frac{\beta(\Delta_0-\mu_r)}{2\pi}\right)\right)\right] \tag{5.70}$$

$$\tilde{\Delta} = \Delta_0 - 2\sum_r \alpha_0^r (\Delta_0 - \mu_r)\left[1 + \ln\left(\frac{\beta E_C}{\pi}\right) - \mathrm{Re}\,\Psi\left(i\frac{\beta(\Delta_0-\mu_r)}{2\pi}\right)\right]. \tag{5.71}$$

In the following we discuss different limits.

5.8.1 Linear Response

At zero bias voltage the system is "on resonance" if $\beta\Delta_0 \ll 1$ and "off resonance" if $\beta\Delta_0 \gg 1$.

While the resonant-tunneling formula yields "on resonance"

$$\frac{\tilde{\alpha}}{\alpha_0} = \frac{\tilde{\Delta}}{\Delta_0} = \frac{1}{1 + 2\alpha_0 \left[\gamma + \ln\left(\frac{\beta E_C}{2\pi}\right)\right]} \tag{5.72}$$

with Euler's constant $\gamma = 0.577216\ldots$, we get from cotunneling

$$\tilde{\alpha} = \alpha_0 \left[1 - 2\alpha_0 \left(-1 + \gamma + \ln\left(\frac{\beta E_C}{\pi}\right)\right)\right] \tag{5.73}$$

$$\tilde{\Delta} = \Delta_0 \left[1 - 2\alpha_0 \left(1 + \gamma + \ln\left(\frac{\beta E_C}{\pi}\right)\right)\right] . \tag{5.74}$$

We see that the temperature is the relevant energy scale which determines the renormalization.

In the opposite case, i.e., "off resonance" the resonant-tunneling approximation leads to

$$\frac{\tilde{\alpha}}{\alpha_0} = \frac{\tilde{\Delta}}{\Delta_0} = \frac{1}{1 + 2\alpha_0 \ln\left(\frac{E_C}{|\Delta|}\right)} , \tag{5.75}$$

and the cotunneling yields

$$\tilde{\alpha} = \alpha_0 \left[1 - 2\alpha_0 \left(-2 + \ln\left(\frac{2E_C}{|\Delta_0|}\right)\right)\right] \tag{5.76}$$

$$\tilde{\Delta} = \Delta_0 \left[1 - 2\alpha_0 \left(1 + \ln\left(\frac{2E_C}{|\Delta_0|}\right)\right)\right] . \tag{5.77}$$

Now, the energy gap itself provides the energy at which the renormalization procedure stops.

The conductance as well as the energy gap is reduced during the renormalization, i.e., the system is effectively "closer" to the resonance but with higher tunnel barriers than the bare system.

5.8.2 Nonlinear Response

At finite bias voltage a new energy scale comes into play. Furthermore, since the Fermi levels of the reservoirs are separated, the relevant energy scale may depend on which reservoir is responsible for the renormalization. For $\mu_R - \mu_L = eV \gg T$, being "on resonance" with the left Fermi level means that $T \gg |\Delta_0 - \mu_L|$, i.e., that again the

temperature provides the dominant energy scale for the left reservoir, but $|\Delta_0 - \mu_R| \approx eV$ is the relevant energy for the right one.

The resonant-tunneling formula leads to

$$\tilde{\alpha} = \frac{\alpha_0}{1 + 2\alpha_0^L \left[\gamma + \ln\left(\frac{\beta E_C}{2\pi}\right)\right] + 2\alpha_0^R \ln\left(\frac{E_C}{eV}\right)} \tag{5.78}$$

$$\tilde{\Delta} - \mu_L = \frac{\Delta_0 - \mu_L + 2\alpha_0^R \, eV \ln\left(\frac{E_C}{eV}\right)}{1 + 2\alpha_0^L \left[\gamma + \ln\left(\frac{\beta E_C}{2\pi}\right)\right] + 2\alpha_0^R \ln\left(\frac{E_C}{eV}\right)}, \tag{5.79}$$

and the cotunneling gives

$$\tilde{\alpha} = \alpha_0 \left[1 - 2\alpha_0^L \left(-1 + \gamma + \ln\left(\frac{\beta E_C}{\pi}\right)\right) - 2\alpha_0^R \left(-2 + \ln\left(\frac{2E_C}{eV}\right)\right)\right] \tag{5.80}$$

$$\tilde{\Delta} - \mu_L = \Delta_0 - \mu_L - 2\alpha_0^L (\Delta_0 - \mu_L)\left[1 + \gamma + \ln\left(\frac{\beta E_C}{\pi}\right)\right] + \alpha_0^R eV\left[1 + \ln\left(\frac{2E_C}{eV}\right)\right] \tag{5.81}$$

In the opposite case, i.e., $|\Delta_0 - \mu_L| \gg T$ and $|\Delta_0 - \mu_R| \gg T$ ("off resonance") the resonant tunneling yields

$$\tilde{\alpha} = \frac{\alpha_0}{1 + 2\sum_r \alpha_0^r \ln\left(\frac{E_C}{|\tilde{\Delta} - \mu_r|}\right)} \tag{5.82}$$

$$\tilde{\Delta} = \frac{\Delta_0 + 2\sum_r \alpha_0^r \, \mu_r \ln\left(\frac{E_C}{|\tilde{\Delta} - \mu_r|}\right)}{1 + 2\sum_r \alpha_0^r \ln\left(\frac{E_C}{|\tilde{\Delta} - \mu_r|}\right)} \tag{5.83}$$

in comparison to cotunneling,

$$\tilde{\alpha} = \alpha_0 \left[1 - 2\sum_r \alpha_0^r \left(-2 + \ln\left(\frac{2E_C}{|\Delta_0 - \mu_r|}\right)\right)\right] \tag{5.84}$$

$$\tilde{\Delta} = \Delta_0 - 2\sum_r \alpha_0^r (\Delta_0 - \mu_r)\left[1 + \ln\left(\frac{2E_C}{|\Delta_0 - \mu_r|}\right)\right] . \tag{5.85}$$

The renormalization of the energy gap differs qualitatively from that in the linear response regime, since now there is a competition between the renormalization of the system towards the left and the right Fermi level. This effect is displayed in Fig. 5.12 which shows the differential conductance as a function of the external gate charge. The position at which the system is in resonance with the left Fermi level is shifted towards the right Fermi level with increasing coupling strength to the right reservoir.

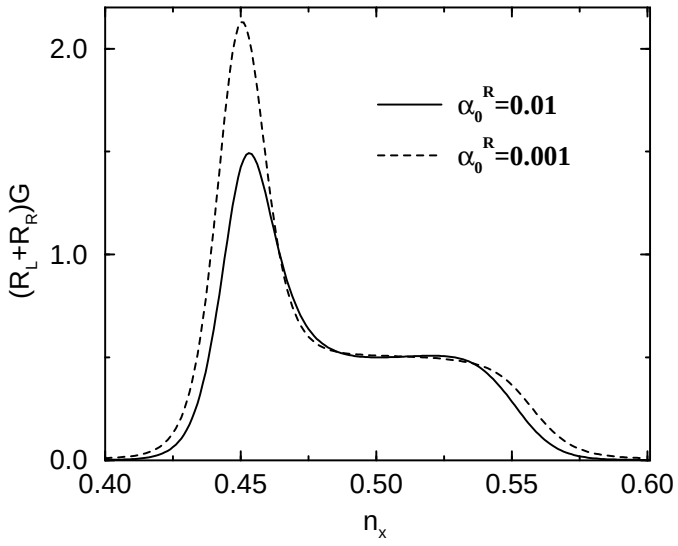

Figure 5.12: The differential conductance $T/E_C = 0.01$, $eV/E_C = 0.2$, $\alpha_0^L = 0.0001$, $\alpha_0^R = 0.01$ (solid line) and $\alpha_0^R = 0.001$ (dashed line).

Chapter 6

Renormalization-Group Method

The diagrammatic technique used so far in this thesis is a transparent tool to describe the various tunneling processes in terms of the corresponding diagrams. In different regimes a certain choice of included diagrams, either a systematic perturbation theory or a nonperturbative partial resummation, allows for a quantitative or qualitative comparison with experiments and describes the dominating aspects of the underlying theoretically interesting models. In order to increase the covered regime, more contributions have to be taken into account. This means for a systematic perturbation theory that one has to perform a cumbersome summing up of a large number of diagrams. On the other hand, the success of a partial resummation of a certain diagram class depends on the solution of some self-consistency equation which may require extended numerical work.

In this chapter we work out an alternative approach. We develop a new renormalization-group analysis of the single-electron box. Thereby, similar to the resummation of certain diagram classes, the nonperturbative treatment includes contributions of arbitrary high order. It turns out, however, that the RG treatment is a more efficient tool for a quantitative description over a large range of the coupling parameter.

6.1 Introduction

In the *weak tunneling* regime, i.e., when the transmission $\mathcal{T} = h/e^2R$ of the barrier is much less than unity, the average charge of the box (see Fig. 2.3) can be described within the orthodox theory, which means that the energy for charge N on the island is given by the classical expression

$$E_N(n_x) = E_C(N - n_x)^2 \,, \tag{6.1}$$

with $E_C = e^2/2(C_J + C_G)$ and $en_x = C_G V_G$. The ground-state energy E_G is the periodic continuation of the parabola $E_0(n_x)$ for $-1/2 < n_x < 1/2$. Furthermore, at zero temperature, the average charge is given by

$$\langle N \rangle(n_x) = n_x - \frac{1}{2E_C}\frac{\partial E_G}{\partial n_x}(n_x) \,, \tag{6.2}$$

and increases in steps at half-integer values of n_x.

In this chapter we analyze the smearing of $E_G(n_x)$ and $\langle N\rangle(n_x)$ in the whole regime from weak to strong tunneling up to $\mathcal{T} \sim 50$ due to quantum fluctuations (in recent experiments $\mathcal{T} \sim 33$ was achieved [111]).

Another quantity of recent interest is the renormalized charging energy

$$E_C^*(n_x) = \frac{1}{2}\frac{\partial^2 E_G}{\partial n_x^2}(n_x) = E_C\left(1 - \frac{C_\mu}{C_G}\right) , \tag{6.3}$$

with the electrochemical capacitance $C_\mu = \partial Q/\partial V_G$ [112].

Perturbative approaches, see Refs. [23, 113] and Section 5.6, in $\alpha = \mathcal{T}/(4\pi^2)$ up to α^3 [113] can describe $E_C^*(0)$ up to $\mathcal{T} \sim 15$.[1] However, within this approach, the range of allowed values for $\mathcal{T}$ decreases considerably for $n_x \to 1/2$, and the average charge turns out to be divergent at $n_x = 1/2$.

Therefore, nonperturbative approaches have been developed to describe the system near the degeneracy point of adjacent charge states either within a "non-crossing" expansion scheme [22] or using an effective two-state system, Refs. [24, 110] and Section 5.7. But for $\mathcal{T} \gtrsim 1$ the broadening $\hbar/(RC) \sim \mathcal{T}E_C/\pi$ of the charge states is of the same order as the energy gap E_C, i.e., all charge states become important. And even for weaker coupling the results from a renormalization-group (RG) treatment [24, 110] depend on both a high-energy and a low-energy cutoff. The first one, of the order of the charging energy, accounts for the neglected higher charge states. The second one is provided by the dominant low-energy scale, energy gap or temperature. As a result, quantitative statements depend on adjustable parameters.

For very strong coupling, $\mathcal{T} \gg 1$, instanton methods have been developed, which predict an exponential decrease of Coulomb blockade phenomena: $E_C^*(0)/E_C \sim \mathcal{T}^\eta \exp(-\mathcal{T}/2)$, [114,115]. However, the exponent η is still controversial. Poor man scaling methods in $1/\mathcal{T}$ reveal a strong renormalization of $\mathcal{T}$ to smaller values [24,116]. This analysis is performed in the phase representation for the topological sector with winding number zero. However, for decreasing $\mathcal{T}$ all winding numbers become important. Consequently, a quantitative matching to the two-charge state approximation is not possible [34].

Even recent quantum Monte Carlo (QMC) simulations [113,116–118] have led to different results for $E_C^*(0)$ in the regime $\mathcal{T} > 15$. Furthermore, the error bars and the computing time are very large for $\mathcal{T} \gg 1$ and/or $n_x \to 1/2$ and extrapolation to zero temperature in order to describe ground-state properties becomes difficult. As a consequence, a large gap still remains between the small and large $\mathcal{T}$-regions, the latter being even controversial.

The RG method presented in this chapter covers self-consistently level renormalization and -broadening together with vertex corrections, and includes all charge states without the need of initial or final energy cutoffs. In contrast to QMC simulations our theory works also at zero temperature. For $E_C^*(0)$ we find good agreement with the QMC simulation of Refs. [113, 116]. We also find agreement with the exponential behavior of $E_C^*(0)$ for

[1] In this chapter we omit the subscript in α_0 since we will define α_N as the renormalized couplings for charge state N.

$\mathcal{T} \gtrsim 20$, as predicted in Refs. [114, 115] but with a different preexponent. We calculate $\langle N \rangle(n_x)$ for all n_x and predict that for $\mathcal{T} > 27$ charge quantization will be suppressed such that the deviation from a straight line is less than 1%. We find that the slope of $\langle N \rangle$ at $n_x = 1/2$ is always infinite.

6.2 Model

The system is modeled by the Hamiltonian $H = H_0 + H_T$, in which

$$H_0 = \sum_{kn} \epsilon_{kn} a^\dagger_{kn} a_{kn} + \sum_{qn} \epsilon_{qn} c^\dagger_{qn} c_{qn} + \sum_N E_N |N\rangle\langle N| \tag{6.4}$$

describes the box without tunneling. The operators $a^{(\dagger)}$ and $c^{(\dagger)}$ annihilate (create) electrons in the lead and island electrode, respectively. The tunneling coupling is given by

$$H_T = \sum_N \sum_{\sigma=\pm} g^\sigma_N |N+\sigma\rangle\langle N| J_\sigma \tag{6.5}$$

with $J_- = \sum_{kqn} T^n_{kq} a^\dagger_{kn} c_{qn}$ and $J_+ = J^\dagger_-$. The channel number $n = 1, \ldots, N_{ch}$ accounts for both the transverse wave number and the spin and is conserved during a tunnel process. We assume here a wide metallic junction with a large number of transverse channels. The matrix elements T^n_{kq} are assumed to be independent of the states k and q. They are related to the tunnel resistance by $1/R = (2\pi e^2/\hbar) \sum_n N_L(0) N_I(0) |T^n|^2$, where $N_{L/I}(0)$ are the density of states of the lead and the island. The factor g^σ_N describes the relative strength of the tunnel coupling. At the beginning, we have $g^\sigma_N \equiv 1$ for all N and σ. But under the renormalization-group procedure, the coupling will indeed depend on the charge state N and on σ. We define $\alpha_N = \alpha g^+_N g^-_{N+1}$.

6.3 Renormalization-Group Procedure

The invariant quantity under the RG is the S-matrix $S = T \exp(-i \int dt\, H(t))$. The idea of the RG is to start with some high-energy cutoff, then to reduce it by integrating out the corresponding degrees of freedom, and end up with an effective low-energy theory. All the energies and coupling constants will be renormalized, and, simultaneously, new terms which are not present in the original Hamiltonian may be generated. We will proceed in three steps. (i) We introduce a time cutoff t_c. (ii) The cutoff is increased $t_c \to t_c + dt_c$, thus flowing from t^0_c to t^f_c. The invariance condition for the S-matrix demands

$$T e^{-i \int dt\, H(t)}\big|_{t_c} = T e^{-i \int dt\, H'(t)}\big|_{t_c + dt_c} \tag{6.6}$$

for each RG step. (iii) We take $t^0_c \to 0$ and $t^f_c \to \infty$.

(i) After changing to the interaction picture we write the S-matrix in the form $S = T \exp(-i \int dt\, H_0) T \exp(-i \int dt\, H_T(t)_I)$, where $H_T(t)_I$ is the tunnel part of the Hamiltonian

in the interaction picture with respect to H_0. The expansion of the second exponential yields

$$S = Te^{-i\int dt\, H_0} \sum_{n=0}^{\infty} (-i)^n \int\limits_{t_1>t_2>\ldots>t_n} H_1 \ldots H_n, \tag{6.7}$$

where $H_i \equiv H_T(t_i)_I$. Next, we perform a normal ordering of the fermion operators $c^{(\dagger)}$ and $a^{(\dagger)}$ involved in H_i,

$$H_1 = :H_1: \tag{6.8}$$

$$H_1H_2 = :H_1H_2: + \overbrace{H_1H_2} \tag{6.9}$$

$$H_1H_2H_3 = :H_1H_2H_3: + \overbrace{H_1H_2}H_3 + \overbrace{H_1H_2H_3} + H_1\overbrace{H_2H_3} \tag{6.10}$$

where $:\ldots:$ stands for normal ordering and $\overbrace{H_1H_2}$ represents contractions of all the fermion operators $c^{(\dagger)}$ and $a^{(\dagger)}$ in H_1 and H_2 with the relative time $t_1 - t_2$. In principle the two fermion operators of H_i may be contracted with fermion operators of different $H_{i'}$'s. For a large number of channels, $N_{ch} \to \infty$, however, these contributions are negligible. The only combination of contractions which enter here is (at zero temperature)

$$\langle J_\pm(t_1) J_\mp(t_2)\rangle_{eq} = -\frac{\alpha}{(t_1-t_2)^2} + i\alpha\pi\delta'(t_1-t_2)\,. \tag{6.11}$$

This is nothing but the tunneling rate $\alpha^+(t)$ or $\alpha^-(-t)$ (see Eq. (2.17)) in time space. We now introduce a time cutoff t_c by multiplying the right hand side of Eq. (6.11) with $\Theta(|t_1 - t_2| - t_c)$. Consequently, via Eqs. (6.7)-(6.10), the S-matrix is well-defined with a sharp cutoff t_c.

(ii) The increase of the cutoff $t_c' = t_c + dt_c$ leads to correction terms $\overbrace{H_1\overset{\times}{H_2}}$, $\overbrace{H_1\overset{\times}{H_2}H_3}$, etc. The cross indicates that the time difference is between t_c and t_c'. We interpret such many-time objects as clusters with *one* time argument for the time ordering (we choose t_2). It is possible to reexponentiate the sum of terms and correction terms. The renormalized exponent reads

$$-i\int H_1' = -i\int H_1 + (-i)^2 \int\limits_{t_1>t_2} \overbrace{H_1\overset{\times}{H_2}} + (-i)^3 \int\limits_{t_1>t_2>t_3} \left\{\overbrace{H_1\overset{\times}{H_2}H_3} - H_2\overbrace{H_1\overset{\times}{H_3}}\right\} \tag{6.12}$$

plus higher-order correction terms which we truncate. This is the central equation since it determines the renormalization of all quantities. The second term (propagator renormalization) can be absorbed in a change of the energies, while the third term (vertex corrections) renormalize the coupling strength.

(iii) The limit $t_c^0 \to 0$ is possible if we take into account all charge states. There are no divergences like in a two-state approximation. After performing the limit $t_c^f \to \infty$ we end up with an effective theory for the charge degrees of freedom without any contractions.

To present the results, we introduce the abbreviations $l = \ln(t_c/t_c^0)$, $\Delta_N = E_{N+1} - E_N$, $\bar{E}_N = E_N t_c$, and $\bar{\Delta}_N = \Delta_N t_c$. The RG equations, then, are

$$\frac{d\bar{E}_N}{dl} = \bar{E}_N + i\left(\alpha_{N-1}e^{i\bar{\Delta}_{N-1}} + \alpha_N e^{-i\bar{\Delta}_N}\right) \tag{6.13}$$

$$\frac{d\bar{\Delta}_N}{dl} = \bar{\Delta}_N + i\left(\alpha_N e^{i\bar{\Delta}_N} + \alpha_{N+1}e^{-i\bar{\Delta}_{N+1}} - \alpha_N e^{-i\bar{\Delta}_N} - \alpha_{N-1}e^{i\bar{\Delta}_{N-1}}\right) \tag{6.14}$$

$$\begin{aligned}\frac{d\alpha_N}{dl} = \alpha_N \Bigg\{ & 2\alpha_{N+1}\frac{e^{-i\bar{\Delta}_{N+1}} - e^{-i\bar{\Delta}_N}}{-i(\bar{\Delta}_{N+1} - \bar{\Delta}_N)} + 2\alpha_{N-1}\frac{e^{i\bar{\Delta}_N} - e^{i\bar{\Delta}_{N-1}}}{i(\bar{\Delta}_N - \bar{\Delta}_{N-1})} \\ & -\alpha_N e^{i\bar{\Delta}_N} - \alpha_{N+1}e^{-i\bar{\Delta}_{N+1}} - \alpha_N e^{-i\bar{\Delta}_N} - \alpha_{N-1}e^{i\bar{\Delta}_{N-1}}\Bigg\} .\end{aligned} \tag{6.15}$$

We solve these equations numerically.

6.4 Discussion of the RG Equations

We note the following:

(i) All energies become complex, which is related to the broadening of the levels.

(ii) The coupling strength α_N and the difference $\Delta_{N+1} - \Delta_N$, which are initially α and $2E_C$, respectively, evolve different for different charge states N.

(iii) The RG equations contain all terms from perturbation theory up to $\mathcal{O}(\alpha^2)$.

(iv) Eqs. (6.14) and (6.15) include also all terms of the poor man's scaling method. If one considers for $n_x \approx 1/2$ only two charge states $N = 0, 1$, and expands all exponentials $\exp(\pm i\bar{\Delta}_0) \approx 1 \pm i\bar{\Delta}_0$, Eqs. (6.14) and (6.15) reduce to the well-known formulas

$$\frac{d\bar{\Delta}_0}{dl} = \bar{\Delta}_0(1 - 2\alpha_0) \qquad \text{and} \qquad \frac{d\alpha_0}{dl} = -2\alpha_0^2 \tag{6.16}$$

with solutions

$$\frac{\Delta_0(l)}{\Delta_0(0)} = \frac{\alpha_0(l)}{\alpha_0(0)} = [1 + 2\alpha_0(0)l]^{-1} \tag{6.17}$$

and $\alpha_0(0) = \alpha$. Due to the restriction to a two charge state these results, unlike the solution of Eqs. (6.14) and (6.15), still depend on the initial cutoff t_c^0.

6.5 Results

In Figs. 6.1-6.3, we show E_0, $\langle N\rangle$, and E_C^* as function of n_x up to $\alpha = 0.5$ ($\mathcal{T} \sim 20$) and compare with QMC data from Refs. [113, 118]. (In the numerics we had to choose the initial cutoff t_c^0 much smaller than $0.1E_C^{-1}$. Here, we chose $0.01E_C^{-1}$.) As expected we find a gradual flattening of the ground-state energy with increasing coupling and a rounding of the average charge towards a linear function. The average charge $\langle N\rangle(n_x)$ agrees well with available QMC data for $\alpha \leq 0.3$, except for $n_x \gtrsim 0.4$. This deviation can be traced back to a finite temperature used in the QMC simulations.[2] From our results we conclude:

[2] C.P. Herrero, private communication.

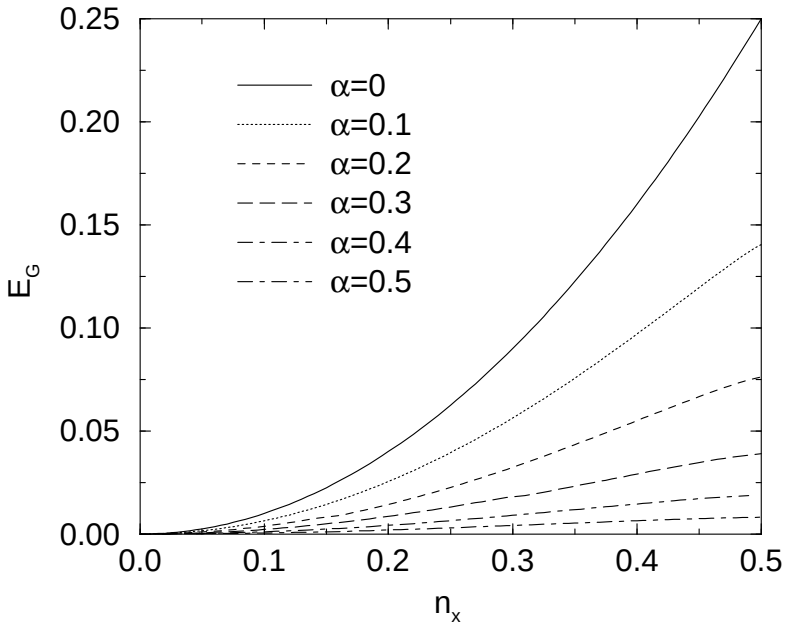

Figure 6.1: Ground-state energy as function of n_x.

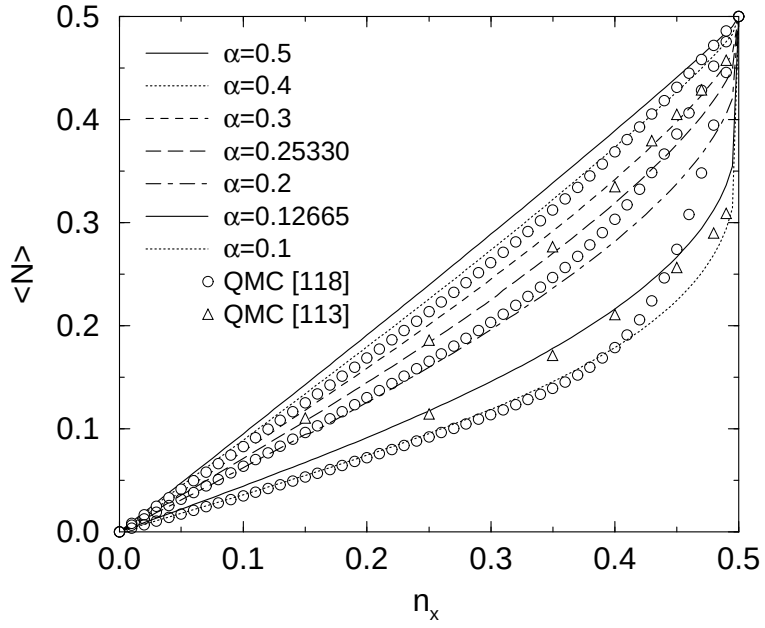

Figure 6.2: Average charge as function of n_x. The step at $n_x = 1/2$ is rounded for increasing α, approaching more and more a straight line. The circles are QMC data from Ref. [118] for $\alpha = 0.3, 0.2, 0.1$. The triangles are QMC data from Ref. [113] for $\alpha = 0.25330, 0.12665$.

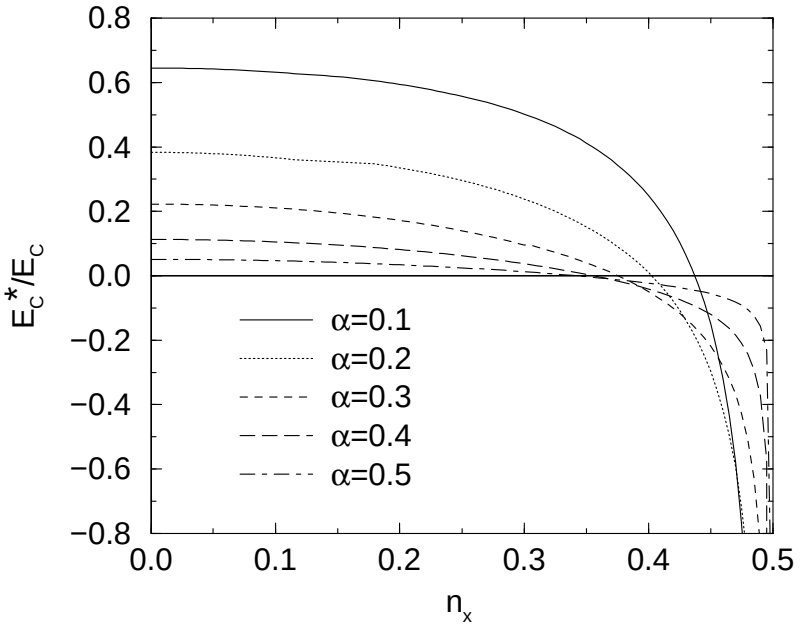

Figure 6.3: E_C^* as a function of n_x. For $n_x \to 1/2$ it diverges.

(i) For $\mathcal{T} \sim 27$, the shape of $\langle N \rangle(n_x)$ is nearly indistinguishable from a straight line within an error of 1%.

(ii) The slope of $\langle N \rangle$ at $n_x = 1/2$ is infinite, i.e., there is always a very small crossover region around the degeneracy point showing a deviation from a straight line. This is explicitly shown in Fig. 6.3 for the renormalized charging energy which diverges at $n_x = 1/2$. However, this region is so small that it can hardly be identified experimentally.

(iii) The renormalized charging energy at $n_x = 0$ decreases with increasing coupling. This reveals another indication for the washing out of charge quantization and is shown in more detail in Figs. 6.4 and 6.5 using a logarithmic scale for $E_C^*(0)$ as function of the coupling α. Here we find very good agreement of our results with perturbation theory [23, 113] up to $\alpha \sim 0.4$ ($\mathcal{T} \sim 15$) and the QMC data of Ref. [113]. Including error bars, our data are consistent with the QMC data of Ref. [116],[3] but are slightly lower than those of Ref. [117], and higher than those of Ref. [118]. For $\mathcal{T} > 25$ no QMC data are available yet but the numerical solution of the RG-equations (6.13)-(6.15) is stable until $\mathcal{T} \sim 50$. For $\mathcal{T} \gtrsim 20$ our data are consistent with the exponential behavior $E_C^*(0)/E_C \sim \mathcal{T}^\eta \exp(-\mathcal{T}/2)$ predicted by instanton techniques [114, 115] but with $\eta = 6.5$ rather than $\eta = 2$ or 3.

The method presented in this chapter can be easily generalized to nonequilibrium situations to calculate the current. Finite temperature effects are included by using the corresponding contractions Eq. (6.11). Furthermore, a similar approach can be developed for the quantum dot with discrete level spectrum. The results presented here are very

[3] The authors report that the saturation for the largest $\mathcal{T}$ is still unclear.

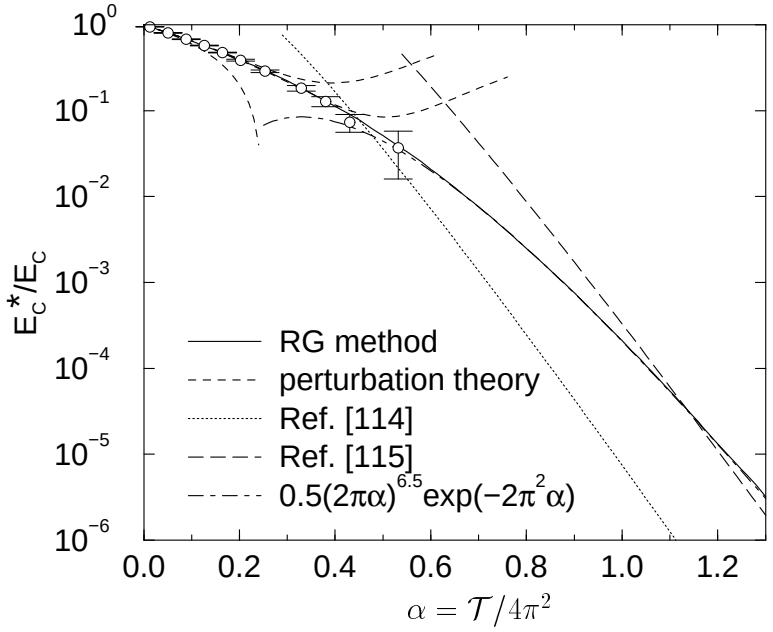

Figure 6.4: E_C^* as function of α for $n_x = 0$. Solid line: renormalization-group method described in this chapter. Dashed lines: perturbation theory of order α, α^2, and α^3 from Refs. [23, 113]. Dotted line and long-dashed line: large-α expansions from [114] and [115], respectively. Dot-dashed line: For $\alpha \gtrsim 0.5$ our data are consistent with $0.5(2\pi\alpha)^{6.5}\exp(-2\pi^2\alpha)$. Circles: QMC data from Ref. [113].

encouraging that this RG method provides a very powerful tool to describe quantum fluctuations.

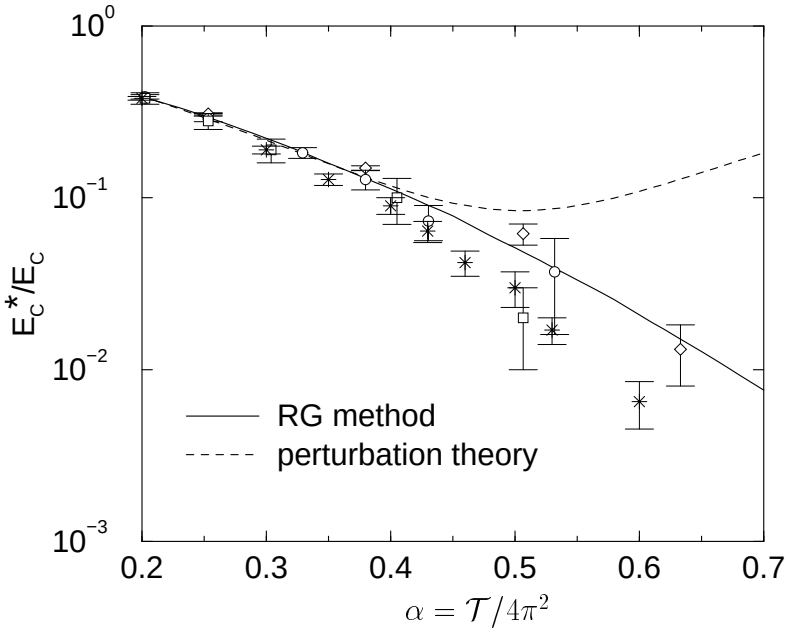

Figure 6.5: E_C^* as function of α for $n_x = 0$. Solid line: renormalization-group method described in this chapter. Dashed lines: perturbation theory of order α^3 [113]. The QMC data are from Ref. [117] ($\diamond$), [113] ($\circ$), [116] ($\Box$) and [118] ($*$).

Chapter 7

Level Statistics of Quantum Dots Coupled to Reservoirs

In the last chapter of this thesis we discuss the effect of quantum fluctuations on the statistical properties of the level distribution. They determine many physical properties of quantum dots, including thermodynamic properties, transport coefficients, the response to external a.c. fields, and statistical fluctuations [119–123]. For a model of non-interacting electrons confined within a moderately disordered quantum dot (diffusive disorder), the description of the single-particle levels for energies below the Thouless energy conforms to the Wigner-Dyson theory of random matrices (RMT) [121, 124–126]. As a result of the level repulsion, on energy scales smaller than the average single-particle spacing Δ, the statistics of the interlevel spacings for $s \ll 1$ is given by

$$P_o(s) = \frac{\pi}{2} s \qquad , \qquad P_u(s) = \frac{32}{\pi^2} s^2 \qquad , \qquad P_s(s) = \frac{2^{18}}{3^6 \pi^3} s^4 \tag{7.1}$$

for an orthogonal, unitary, and symplectic ensemble, respectively. Here s is measured in units of Δ. In the first case the random system possesses time-reversal and spin-rotation symmetry, in the second case time-reversal symmetry is broken, and in the third one spin-rotation symmetry is absent [127]. This level statistics manifests itself in the response to low-frequency fields. For instance, the a.c. dissipative conductance scales as the applied frequency ω_0, or as ω_0^2, for the two symmetry classes, respectively. This result, valid for the grandcanonical ensemble, is modified for the canonical ensemble[1] [119, 120, 123, 128].

We have seen in Chapter 4 that the discrete bare levels acquire a finite width Γ. While the broadening is known to depend on the coupling and on the energy measured from ϵ_F (see e.g. [129]) it is commonly assumed that the levels statistics is unchanged. This means, the standard Kubo-Greenwood formalism can be employed, provided that the δ-function describing energy conservation is replaced by a Lorentzian with finite width.

In this chapter we study the influence of a dot-reservoir coupling on the effective level statistics and the asymptotic ω_0-dependence of the absorbed power. We use a simple,

[1] This applies for $\Delta \gg \omega_0 > \Gamma$.

but generic, model, where the dot electrons are coupled to a reservoir of non-interacting electrons by tunnel barriers. The total spectrum is continuous, but the dot levels can still be defined by the spectral weights of the bare levels contributing to each eigenvector (the statistics of the dot levels differ from that of the total, dissipative system, see, e.g., Refs. [130, 131]). In most of our analysis we ignore interactions in the dot. Breaking the RMT invariance by the choice of a preferred basis may modify the level statistics as was demonstrated for disorder in metals in Ref. [132]. In our case, the system is not invariant under rotation between the dot and the lead states. We show that the coupling to the lead gives rise to a renormalization of both the low-frequency spectrum and the bare level broadening Γ. *We attribute the origin of the modified statistics and broadening to renormalized spectral weights rather than renormalized eigenvalues of the Hamiltonian.* Subsequently the frequency- and temperature-dependent absorption is calculated. Finally we comment briefly on the effect of Coulomb interactions.

7.1 Model

The dot is assumed to contain a large number of levels with a mean spacing Δ. The model Hamiltonian

$$H = \sum_k \epsilon_k a_k^\dagger a_k + \sum_{\sigma=1,2} \epsilon_\sigma c_\sigma^\dagger c_\sigma + \sum_{k\sigma} \left[T_{k\sigma} a_k^\dagger c_\sigma + h.c. \right] \tag{7.2}$$

describes two of them, $\sigma = 1, 2$, with $\Delta\epsilon = \epsilon_2 - \epsilon_1 \ll \Delta$. They are coupled to the *same* electron reservoir.[2] The tunnel matrix elements are assumed to be independent of the reservoir state, $T_{k\sigma} = T_\sigma$. If both dot levels are well separated, they acquire a finite width $\Gamma_\sigma = 2\pi \sum_k |T_{k\sigma}|^2 \delta(\omega - \epsilon_k)$. We focus on the limit $\Gamma \ll \Delta$. In this case other dot levels can be neglected.

If the levels are degenerate, $\epsilon_1 = \epsilon_2 = \epsilon$, a rotation within the dot subspace, $c'_{1/2} = (T_{1/2} c_1 \pm T_{2/1} c_2)/\sqrt{|T_1|^2 + |T_2|^2}$, yields

$$H' = \sum_k \epsilon_k a_k^\dagger a_k + \epsilon \sum_{\sigma=1,2} c'^\dagger_\sigma c'_\sigma + \sum_k \left[T_{k1} a_k^\dagger c'_1 + h.c. \right] \tag{7.3}$$

and shows that only the new level 1 is coupled to a reservoir of electrons (leading to a Lorentzian form of the spectral density) while the new level 2 is isolated (with a δ-peaked spectral density). Therefore, in the unrotated basis c_1, c_2, the spectral density of each level consists of a Lorentzian part but also contains a δ-function. The sharp peak persists if the degeneracy is slightly lifted.

[2] This describes either the situation in which the spin labeled by σ is not a conserved quantum number or in which σ labels some other non-conserved quantum number. In the latter case spin is ignored either due to strong Zeeman splitting or since for a non-interacting quantum dot the total Hamiltonian separates into two parts describing either spin. The corresponding levels do not influence each other.

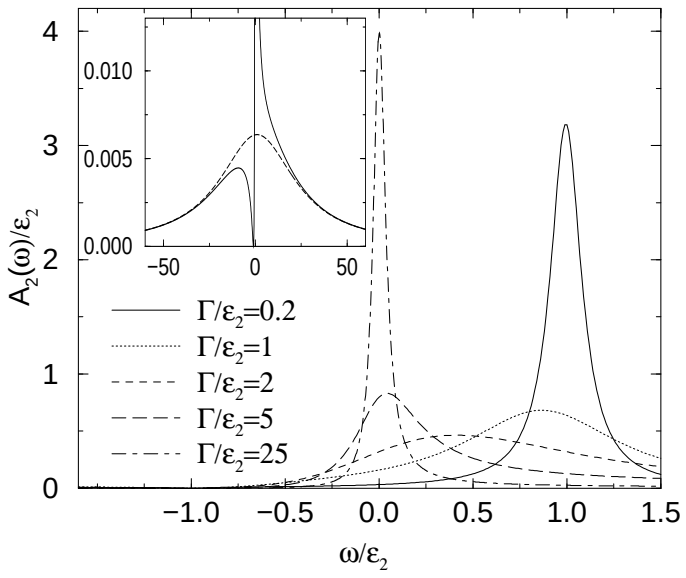

Figure 7.1: Spectral density for level 2 with $\Gamma_1 = \Gamma_2 = \Gamma$ and $\epsilon_1 = -\epsilon_2$. For $\Gamma \ll \epsilon$ a peak with width $\tilde{\Gamma} \ll \Gamma$ evolves near zero. The spectral density of level 1 is related to that of level 2 by $A_1(\omega) = A_2(-\omega)$. Inset: Spectral density for $\Gamma/\epsilon_2 = 25$ (solid line) showing a sharp peak sitting atop a Lorentzian with width 2Γ (dashed line).

7.2 Spectral Density

In order to capture the evolution of the sharp peak in the spectral density quantitatively, we employ the equations of motion for the Green's functions $C_{\sigma\sigma}(t) := -i\Theta(t)\langle\{c_\sigma(t), c_\sigma^\dagger(0)\}\rangle$. Since the Hamiltonian Eq. (7.2) is quadratic, we can find the exact solution

$$C_{\sigma\sigma}(\omega) = \left[\omega - \epsilon_\sigma - \Sigma_{\sigma\sigma} - \frac{\Sigma_{\sigma\bar{\sigma}}\Sigma_{\bar{\sigma}\sigma}}{\omega - \epsilon_{\bar{\sigma}} - \Sigma_{\bar{\sigma}\bar{\sigma}}}\right]^{-1} \tag{7.4}$$

with $\Sigma_{\sigma\sigma'} = \sum_k T_{k\sigma}T^*_{k\sigma'}/(\omega - \epsilon_k)$, i.e., $\Sigma_{\sigma\sigma}(\omega + i0^+) = -i\Gamma_\sigma/2$ and $\Sigma_{\sigma\bar{\sigma}}(\omega + i0^+)\Sigma_{\bar{\sigma}\sigma}(\omega + i0^+) = -\Gamma_\sigma\Gamma_{\bar{\sigma}}/4$. The spectral function follows from $A_\sigma(\omega) = -\mathrm{Im}\, C_{\sigma\sigma}(\omega + i0^+)/\pi$. For $\epsilon_1 \neq \epsilon_2$ it is

$$A_\sigma(\omega) = \frac{\Gamma_\sigma\left(\omega - \epsilon_{\bar{\sigma}}\right)^2/2\pi}{\left(\omega - \epsilon_\sigma\right)^2\left(\omega - \epsilon_{\bar{\sigma}}\right)^2 + \left[(\Gamma_1 + \Gamma_2)\omega/4 - \hat{\epsilon}\right]^2} \tag{7.5}$$

with $\hat{\epsilon} = (\Gamma_1\epsilon_2 + \Gamma_2\epsilon_1)/(\Gamma_1 + \Gamma_2)$. In Fig. 7.1 we plot the spectral density of level 2 for several ratios $\Gamma/\Delta\epsilon$. Here, and for the following we define $\Delta\epsilon = \epsilon_2 - \epsilon_1$. If the bare levels are well separated, i.e., $\Delta\epsilon \gg \Gamma$, the spectral density is approximately a Lorentzian with width Γ_σ,

$$A_\sigma(\omega) = \frac{1}{\pi}\frac{\Gamma_\sigma/2}{(\omega - \epsilon_\sigma)^2 + (\Gamma_\sigma/2)^2}, \tag{7.6}$$

and the maximum is at the bare value ϵ_σ, i.e., the level splitting remains unrenormalized $\Delta\tilde{\epsilon} = \Delta\epsilon$. We see, however, from Fig. 7.1 that things are different in the opposite limit

$\Delta\epsilon \ll \Gamma$. Then, the level position is renormalized which leads to a modified level statistics, and the width is much smaller than the bare broadening.

For the degenerate case $\epsilon_1 = \epsilon_2$ we find

$$A_\sigma(\omega) = \frac{\Gamma_\sigma/2\pi}{(\omega-\epsilon_\sigma)^2 + (\Gamma_1+\Gamma_2)^2/4} + \frac{\Gamma_{\bar\sigma}\delta(\omega-\epsilon_\sigma)}{\Gamma_1+\Gamma_2} \tag{7.7}$$

and recover the expected δ peak.

7.3 Modified Level Statistics

For $\Delta\epsilon \ll \Gamma$, Eq. (7.5) effectively reduces to the sum of two Lorentzians,

$$A_\sigma(\omega) = \frac{\Gamma_\sigma}{\Gamma_1+\Gamma_2}\frac{(\Gamma_1+\Gamma_2)/2\pi}{(\omega-\epsilon_\sigma)^2 + \left[(\Gamma_1+\Gamma_2)/2\right]^2} + \frac{\Gamma_{\bar\sigma}}{\Gamma_1+\Gamma_2}\frac{\tilde\Gamma/2\pi}{(\omega-\tilde\epsilon_\sigma)^2+(\tilde\Gamma/2)^2}. \tag{7.8}$$

It shows a broad peak with width $\Gamma_1+\Gamma_2$, and a sharper one with width $\tilde\Gamma$ (see inset of Fig. 7.1). For the latter peak the level splitting $\Delta\tilde\epsilon$ and the width $\tilde\Gamma$ are given by

$$\frac{\Delta\tilde\epsilon}{\Delta\epsilon} = \frac{\tilde\Gamma}{\Gamma_1+\Gamma_2} = \frac{4\Gamma_1\Gamma_2}{(\Gamma_1+\Gamma_2)^4}(\Delta\epsilon)^2\,. \tag{7.9}$$

This result implies a new statistics for the renormalized interlevel spacing $\tilde s = \Delta\tilde\epsilon/\Delta$ in the regime $\tilde s \ll \Gamma/\Delta \ll 1$,

$$\tilde P_o(\tilde s) = \frac{\pi}{6}\left[\frac{(\Gamma_1+\Gamma_2)^4}{4\Gamma_1\Gamma_2\Delta^2}\right]^{2/3}\tilde s^{-1/3} \tag{7.10}$$

$$\tilde P_u(\tilde s) = \frac{32}{3\pi^2}\frac{(\Gamma_1+\Gamma_2)^4}{4\Gamma_1\Gamma_2\Delta^2} \tag{7.11}$$

$$\tilde P_s(\tilde s) = \frac{2^{18}}{3^7\pi^3}\left[\frac{(\Gamma_1+\Gamma_2)^4}{4\Gamma_1\Gamma_2\Delta^2}\right]^{5/3}\tilde s^{2/3} \tag{7.12}$$

and a renormalized broadening $\tilde\Gamma = 4\Gamma_1\Gamma_2(\Delta\epsilon)^2/(\Gamma_1+\Gamma_2)^3$. In the orthogonal case the distribution even diverges for $\tilde s \to 0$ with integrable divergence.

Results for a wider range of energies are displayed in Figs. 7.2 and 7.3 for the renormalized level spacing as a function of the bare one and for the new level statistics, respectively, and compared to the low-energy asymptotic results Eqs. (7.9), (7.10) and (7.11).

What is the origin of the modified $\tilde P(\tilde s)$? If we omit the tunneling part of the Hamiltonian Eq. (7.2) then the eigenvalues, ϵ_k and ϵ_σ, have spectral weights totally within the corresponding states k and σ. It is tempting to assume that the coupling of the level σ to the reservoir states k leads to a renormalization of the eigenvalues ϵ_σ, thus explaining the modified level statistics. But this is not the case. The crucial point is rather the renormalization of the eigenvectors. Due to the tunneling each eigenvector acquires a finite overlap with the bare dot states. What we see in Fig. 7.1 is the envelope of the square of this overlap. The relevant physics is, therefore, a *spectral-weight renormalization* effect rather than energy renormalization.

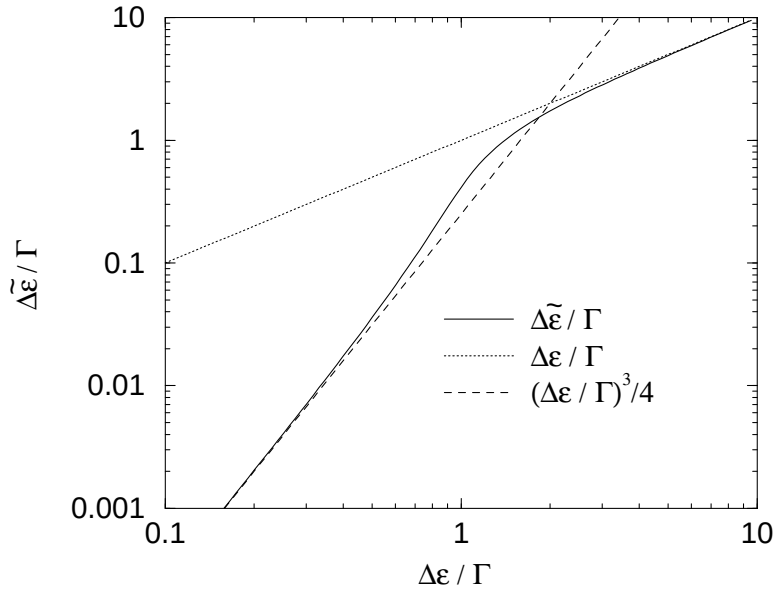

Figure 7.2: Renormalized level spacing as a function of the bare one for $\Gamma_1 = \Gamma_2 = \Gamma$. The dotted and the dashed curve are the high- and low-energy (see Eq. (7.9)) asymptotes.

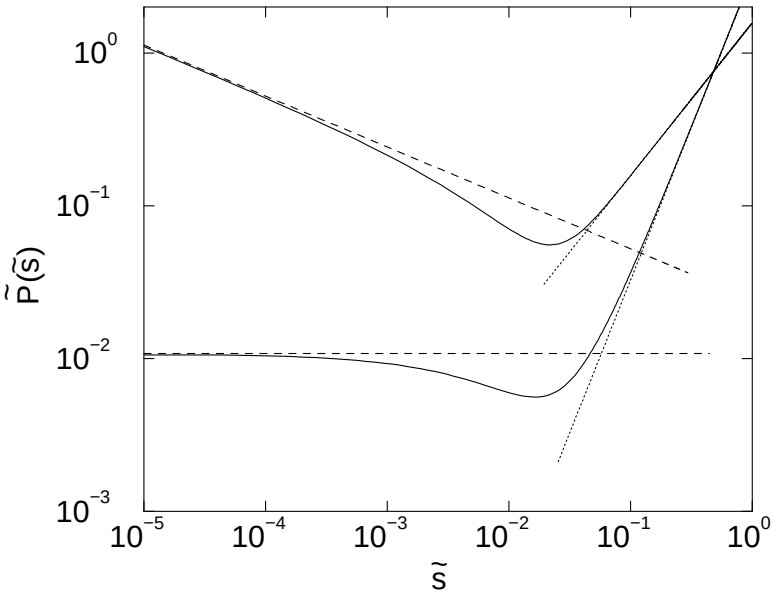

Figure 7.3: Solid lines: new level statistics $\tilde{P}(\tilde{s})$ in the orthogonal (upper curve) and unitary ensemble (lower curve) with $\Gamma_1 = \Gamma_2 = \Gamma = \Delta/20$. Dashed lines: low-energy asymptotes Eqs. (7.10) and (7.11). Dotted lines: high-energy asymptotes (Wigner-Dyson distribution).

7.4 Signatures in an Absorption Experiment

How can the evolution of the sharp peak be probed? In the following we discuss consequences for an absorption experiment. For a single quantum dot the absorption power of a photon with energy ω_0, accompanied with a transition from level σ to level σ', is given by

$$\int_{-\infty}^{\infty} d\,\omega\, A_\sigma\left(\omega-\frac{\omega_0}{2}\right) A_{\sigma'}\left(\omega+\frac{\omega_0}{2}\right) f\left(\omega-\frac{\omega_0}{2}-\mu\right)\left[1-f\left(\omega+\frac{\omega_0}{2}-\mu\right)\right]. \qquad (7.13)$$

Since in realistic experiments an ensemble of dots is probed, the total signal $I_{\sigma\sigma'}$ is determined by the average over all possible configurations, i.e., we have to average over the chemical potential $\Delta^{-1}\int_{\hat{\epsilon}-\Delta/2}^{\hat{\epsilon}+\Delta/2}\mu\ldots\approx\Delta^{-1}\int_{-\infty}^{\infty}d\mu\ldots$ as well as over the bare level separation $\int_0^1 ds\,P(s)\ldots$. After performing the integral over $d\mu$ we get

$$\begin{aligned} I_{\sigma\sigma'} &= \frac{\omega_0}{\Delta}\frac{e^{\beta\omega_0}}{e^{\beta\omega_0}-1}D_{\sigma\sigma'} && (7.14)\\ D_{\sigma\sigma'} &= \int_0^1 ds\,P(s)B_{\sigma\sigma'} && (7.15)\\ B_{\sigma\sigma'} &= \int_{-\infty}^{\infty} d\,\omega\, A_\sigma\left(\omega-\frac{\omega_0}{2}\right) A_{\sigma'}\left(\omega+\frac{\omega_0}{2}\right). && (7.16)\end{aligned}$$

The quantity $B_{\sigma\sigma'}$ probes the properties of the transition for a given level spacing. It accounts for the renormalization of the level spacing and width. The total signal, however, is determined by the average over all (bare) level spacings, $D_{\sigma\sigma'}$. For $\sigma=\sigma'$ the absorption is accompanied by a transition within one level and for $\sigma\neq\sigma'$ a transition between the two levels. In the following we are interested in the asymptotic behavior for $\omega_0\to 0$, i.e., $\omega_0\ll\Gamma\ll\Delta$.

In order to establish some reference frame we first approximate $A_\sigma(\omega)$ by (i) delta functions (which neglects the coupling of each level to the reservoir) and by (ii) Lorentzians with width Γ_σ (which neglects the indirect coupling of the levels) before (iii) we use the exact form Eq. (7.5).

(i) In the first case we find $D_{12}=P(\omega_0)$, i.e., $D_{12}^o=\pi^2\omega_0/2$, $D_{12}^u=32\omega_0^2/\pi^2$, and $D_{12}^s=2^{18}\omega_0^4/3^6\pi^3$ while $D_{11}=D_{22}=D_{21}=0$. This means that the absorption power vanishes for $\omega_0\to 0$.

(ii) In the second case

$$\begin{aligned} B_{12} &= \frac{1}{2\pi}\frac{\Gamma_1+\Gamma_2}{(\omega_0-\Delta\epsilon)^2+(\Gamma_1+\Gamma_2)^2/4} && (7.17)\\ B_{21} &= \frac{1}{2\pi}\frac{\Gamma_1+\Gamma_2}{(\omega_0+\Delta\epsilon)^2+(\Gamma_1+\Gamma_2)^2/4} && (7.18)\\ B_{\sigma\sigma} &= \frac{1}{2\pi}\frac{\Gamma_\sigma}{\omega_0^2+\Gamma_\sigma^2}, && (7.19)\end{aligned}$$

which yields for $\omega_0 = 0$

$$D^o_{12} = D^o_{21} = \frac{1}{4}\frac{\Gamma_1+\Gamma_2}{\Delta^2}\ln\frac{2\Delta}{\Gamma_1+\Gamma_2} \tag{7.20}$$

$$D^u_{12} = D^u_{21} = \frac{16}{\pi^3}\frac{\Gamma_1+\Gamma_2}{\Delta^2} \tag{7.21}$$

$$D^s_{12} = D^u_{21} = \frac{2^{17}}{3^7\pi^4}\frac{\Gamma_1+\Gamma_2}{\Delta^2} \tag{7.22}$$

and $D^o_{\sigma\sigma} = 1/4\Gamma_\sigma$, $D^u_{\sigma\sigma} = 32/3\pi^3\Gamma_\sigma$, and $D^s_{\sigma\sigma} = 2^{18}/(5\cdot 3^6\pi^4\Gamma_\sigma)$. Two points are remarkable. First, due to the broadening there is always an overlap of the shifted spectral functions, i.e., D_{12} remains finite even for $\omega_0 = 0$. Second, for systems with time reversal symmetry the $(\Delta\epsilon)^{-2}$ behavior of Eq. (7.17) leads to logarithmic behavior, which is cut off at low energies by the average level width $(\Gamma_1+\Gamma_2)/2$.

(iii) The renormalization of the level splitting and width due to indirect coupling of the levels to each other is fully included in the exact spectral function Eq. (7.5). The leading terms are

$$D^o_{12} = D^o_{21} = \frac{1}{8}\frac{\Gamma_1+\Gamma_2}{\Delta^2}\ln\frac{\Delta}{\sqrt{\omega_0\frac{(\Gamma_1+\Gamma_2)^3}{4\Gamma_1\Gamma_2}}} \tag{7.23}$$

$$D^u_{12} = D^u_{21} = \frac{8}{\pi^3}\frac{\Gamma_1+\Gamma_2}{\Delta^2} \tag{7.24}$$

$$D^s_{12} = D^s_{21} = \frac{2^{16}}{3^7\pi^4}\frac{\Gamma_1+\Gamma_2}{\Delta^2} \tag{7.25}$$

and

$$D^o_{\sigma\sigma} = \frac{1}{4\Gamma_\sigma} + \frac{1}{8}\frac{\Gamma_1+\Gamma_2}{\Delta^2}\frac{\Gamma_{\bar\sigma}}{\Gamma_\sigma}\ln\frac{\Delta}{\sqrt{\omega_0\frac{(\Gamma_1+\Gamma_2)^3}{4\Gamma_1\Gamma_2}}} \tag{7.26}$$

$$D^u_{\sigma\sigma} = \frac{32}{3\pi^3\Gamma_\sigma} + \frac{16}{\pi^3}\frac{\Gamma_1+\Gamma_2}{\Delta^2}\frac{\Gamma_{\bar\sigma}}{\Gamma_\sigma}\,. \tag{7.27}$$

$$D^s_{\sigma\sigma} = \frac{2^{18}}{5\cdot 3^6\pi^4\Gamma_\sigma} + \frac{2^{17}}{3^7\pi^4}\frac{\Gamma_1+\Gamma_2}{\Delta^2}\frac{\Gamma_{\bar\sigma}}{\Gamma_\sigma} \tag{7.28}$$

We note that the low-energy cutoff $\sqrt{\omega_0(\Gamma_1+\Gamma_2)^3/4\Gamma_1\Gamma_2}$ is frequency dependent and determines the asymptotic absorption power as can be seen in Fig. 7.4. In comparison to Eqs. (7.20) and (7.21) a factor 1/2 arises due to details in the spectral density.

7.5 Effects of Interaction

To get a qualitative understanding for the effect on interactions we include a finite charging energy in the Hamiltonian $H \to H + Un_1n_2$. As an example we consider the degenerate case $\Delta\epsilon = 0$. A rotation within the dot subspace, as discussed above, can still decouple one

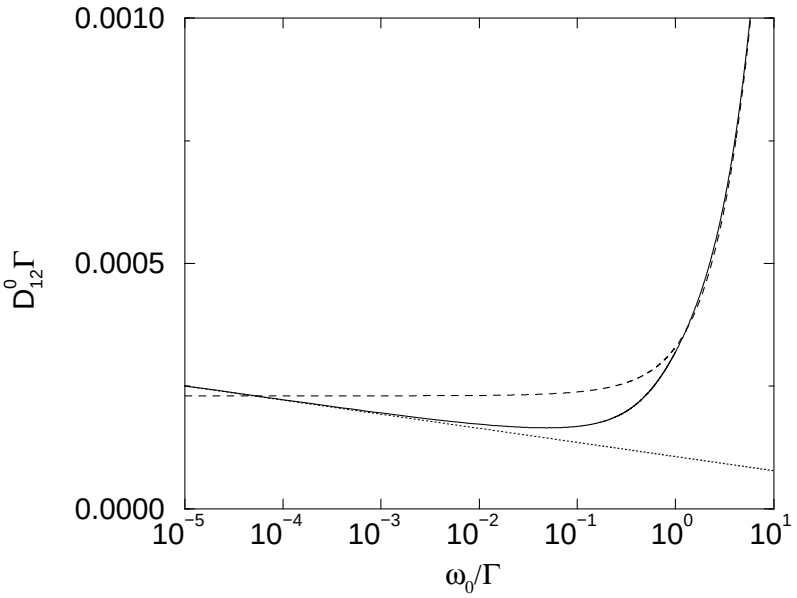

Figure 7.4: For the orthogonal ensemble the asymptotic absorption power is logarithmically divergent at small frequencies (solid line). In the simplified model where the indirect coupling between the levels is neglected, the low-energy behavior shows a saturation at Γ (dashed line). The dotted curve is the asymptote Eq. (7.23).

new level from the reservoir. But the levels still influence each other due to the charging energy term $Un_1'n_2'$ and the conclusion that there will be a delta-function peak in the spectral density is no longer valid. If we neglect all terms in the equations of motion which would correspond to correlations in the reservoirs we get a closed set of equations for the Green's functions. The resulting expression for $C_{\sigma\sigma}(\omega + i0^+)$ for arbitrary U is a lengthy but simplifies for $U \to \infty$ to

$$C_{\sigma\sigma}(\omega) = \frac{1}{2}\left(\frac{\langle(c_\sigma - c_{\bar\sigma})c_\sigma^\dagger\rangle}{\omega - \epsilon + i\Gamma} + \frac{\langle(c_\sigma - c_{\bar\sigma})c_\sigma^\dagger\rangle}{\omega - \epsilon - 2\hat\Sigma(\omega)}\right) \tag{7.29}$$

with

$$\mathrm{Re}\,\hat\Sigma(\omega + i0^+) = \frac{\Gamma}{2\pi}\left[\ln\left(\frac{\beta U}{2\pi}\right) - \mathrm{Re}\,\Psi\left(\frac{1}{2} + i\frac{\beta\omega}{2\pi}\right)\right] \tag{7.30}$$

$$\mathrm{Im}\,\hat\Sigma(\omega + i0^+) = -\frac{\Gamma}{2}f(\omega)\,. \tag{7.31}$$

Here, $\Psi(z)$ is the digamma function. If the levels are far (in units of Γ) from the Fermi level they only contribute to the absorption power in the case $|\omega - \epsilon| \lesssim T$ since otherwise the levels are totally empty or filled. Then, the second term acquires a width of the order of Γ and does not show a sharp peak. If the levels are close to the Fermi level also the low-temperature regime is important. But then the spectral density shows a richer structure

related to collective many-particle states. The analysis of the levels properties and their effect on the absorption power becomes more complicated and is out of the aim of this model calculation.

Chapter 8

Conclusions

Charging effects in single-electron devices are based on the fact that charge is quantized. At low temperatures, thermal fluctuations are small, and Coulomb-blockade phenomena arise and lead to pronounced signatures, e.g., in the linear and nonlinear conductance of the single-electron transistor. These signatures can be explained within the orthodox theory, a master-equation description of sequential tunneling with rates obtained in lowest-order perturbation theory.

However, if the coupling of the island electrons to the leads is increased, quantum fluctuations become important. They are caused by higher-order tunneling processes and wash out the pronounced signatures, reducing the accuracy of the devices in the desired applications. But this is only one reason to develop a theory of quantum fluctuations in single-electron devices. The other one is more fundamental: it turns out that the interplay of quantum fluctuations and charging effects gives rise to Kondo behavior. This cannot be explained within the orthodox theory.

The theory of quantum fluctuations developed in this thesis is based on a diagrammatic expansion of the time evolution of the reduced density matrix. We have established a general real-time transport theory which allows for an interpretation of each diagram as a specific tunneling process or a term describing renormalization of energies and coupling strengths. For a systematic and conserving approximation one has to sum up self-consistently a certain class of diagrams. The simplest approximation just includes sequential tunneling and, therefore, neglects quantum fluctuations. The corresponding irreducible self-energy diagrams consist of one tunneling line. The cotunneling approximation accounts for all diagrams with two lines. They describe processes in which two electrons tunnel coherently. This leads to a renormalization of the system parameters (cotunneling at resonance). A nonperturbative treatment is given by the resonant-tunneling approximation, in which diagrams with an arbitrary number of tunneling lines are included. The criterion is, then, to sum up all terms with at most two charge states and at most two tunneling lines at a given time.

For concrete calculations we have concentrated on the two limits of a single-level quantum dot and a metallic island with continuous level spectrum and large channel number. They are related to the single- and multi-channel Kondo model, respectively, and show

qualitatively different behavior. In quantum dots, Kondo resonances in the spectral functions of the dot electrons lead to zero-bias anomalies in the differential conductance. Our theory successfully explains magnetic-field dependent Kondo-assisted tunneling which has been observed in recent experiments. In metallic islands, too, Kondo physics has been detected experimentally. The height of the Coulomb oscillation peaks have a logarithmic temperature dependence. The quantitative coincidence of the experimental data with our theoretical results demonstrates the power of the theory presented in this thesis.

Furthermore, we have developed a new renormalization-group method for the equilibrium properties of the metallic single-electron transistor. The main idea has been to iterate the propagator renormalizations and vertex corrections, which describe the renormalization of the energy gap and the coupling strength, respectively. Thus, many more contributions than in the resonant-tunneling approximation are taken into account, and systems with substantially stronger coupling can be described. A challenge for future research is to extend this procedure to nonequilibrium situations as well as to quantum dots.

Finally, we have found that quantum fluctuations not only influence the transport properties but also the statistics of the level distribution in the quantum dot. For the case of negligible Coulomb interaction we have calculated the asymptotic level statistics and absorption power for a quantum dot. This model is exactly solvable. It is surprising that even in the absence of charging effects quantum fluctuations lead to new exponents in the low-energy level statistics and power absorption. An interesting challenge for the future is to discuss the influence of the combination of both quantum fluctuations and charging effects on the level spectrum.

Bibliography

[1] D.V. Averin and K.K. Likharev, in *Mesoscopic Phenomena in Solids*, ed. B.L. Altshuler et al. (Elsevier, 1991).

[2] Zeitschrift für Physik B **85**, special issue on *Single-Charge Tunneling* (1991).

[3] *Single Charge Tunneling*, NATO ASI Series **294**, H. Grabert and M.H. Devoret, eds., (Plenum Press, 1992).

[4] A. Korotkov, in *Molecular Electronics*, ed. J. Jortner and M.A. Ratner (Blackwell, 1997), 157.

[5] G. Schön, in *Quantum Transport and Dissipation*, ed. T. Dittrich, P. Hänggi, G.-L. Ingold, B. Kramer, G. Schön, and W. Zwerger (Wiley-VCH Verlag, 1998), Chap. 3.

[6] L.P. Kouwenhoven and P.L. McEuen, to be published in *Nano-Science and Technology*, G. Timp ed. (AIP Press, New York).

[7] D.V. Averin, A.N. Korotkov, and K.K. Likharev, Phys. Rev. B **44**, 6199 (1991).

[8] C.W.J. Beenakker, Phys. Rev. B **44**, 1646 (1991).

[9] L.I. Glazman and K.A. Matveev, Pis'ma Zh. Eksp. Teor. Fiz. **48**, 403 (1988), [JETP Lett. **48**, 445 (1988)].

[10] C. Bruder and H. Schoeller, Phys. Rev. Lett. **72**, 1076 (1994).

[11] J.P. Pekola, K.P. Hirvi, J.P. Kauppinen, and M.A. Paalanen, Phys. Rev. Lett. **73**, 2903 (1994).

[12] L.J. Geerligs, D.V. Averin, and J.E. Mooij, Phys. Rev. Lett. **65**, 3037 (1990).

[13] U. Meirav, M.A. Kastner, and S.J. Wind, Phys. Rev. Lett. **65**, 771 (1990).

[14] P. Lafarge, H. Pothier, E.R. Williams, D. Esteve, C. Urbina, and M.H. Devoret, Z. Phys. B **85**, 327 (1991).

[15] T.K. Ng and P.A. Lee, Phys. Rev. Lett. **61**, 1768 (1988).

[16] L.I. Glazman and M.E. Raikh, Pis'ma Zh. Eksp. Teor. Fiz. **47**, 378 (1988) [JETP Lett. **47**, 452 (1988)].

[17] S. Hershfield, J.H. Davies, and J.W. Wilkins, Phys. Rev. Lett. **67**, 3720 (1991).

[18] S. Hershfield, J.H. Davies, and J.W. Wilkins, Phys. Rev. B **46**, 7046 (1992).

[19] Y. Meir, N.S. Wingreen, and P.A. Lee, Phys. Rev. Lett. **70**, 2601 (1993).

[20] N.S. Wingreen and Y. Meir, Phys. Rev. B **49**, 11040 (1994).

[21] M.H. Hettler and H. Schoeller, Phys. Rev. Lett. **74**, 4907 (1995).

[22] D.S. Golubev and A.D. Zaikin, Phys. Rev. B **50**, 8736 (1994).

[23] H. Grabert, Phys. Rev. B **50**, 17364 (1994).

[24] G. Falci, G. Schön, and G.T. Zimanyi, Phys. Rev. Lett. **74**, 3257 (1995).

[25] H. Schoeller and G. Schön, Phys. Rev. B **50**, 18436 (1994).

[26] H. Schoeller and G. Schön, Physica B **203**, 423 (1994).

[27] J. König, *Diplomarbeit*, Karlsruhe 1995.

[28] J. König, H. Schoeller, and G. Schön, Philosophical Magazine B, Vol. **77**, No.5, 1219 (1998), Proceeding of the Minerva Workshop on *Mesoscopics, Fractals and Neural Networks*, Eilat March 1997.

[29] J. König, H. Schoeller, and G. Schön, Uspekhi Fiz. Nauk **168**, 170 (1998), Proceedings of the Conference *Mesoscopic and Strongly Correlated Electron Systems*, Chernogolovka, 1997.

[30] J. König, H. Schoeller, G. Schön, and R. Fazio in *Quantum Dynamics of Submicron Structures*, ed. H. A. Cerdeira, B. Kramer and G. Schön, NATO ASI Series **E 291** (Kluwer, Dordrecht, 1995), p. 221.

[31] J. König, H. Schoeller, and G. Schön, Europhys. Lett. **31**, 31 (1995).

[32] J. König, H. Schoeller, and G. Schön, in *Path Integrals: Dubna '96*, V.S. Yarunin and M.A. Smondyrev, eds., JINR E96-321, Dubna, (1996), p. 278.

[33] J. König, H. Schoeller, and G. Schön, Phys. Rev. Lett. **78**, 4482 (1997).

[34] D.S. Golubev, J. König, H. Schoeller, G. Schön, and A.D. Zaikin, Phys. Rev. B **56**, 15782 (1997).

[35] J. König, H. Schoeller, and G. Schön, Phys. Rev. B **58**, 7882 (1998).

[36] J. König, H. Schoeller, G. Schön, and A.D. Zaikin, in *Nanoscale Science and Technology*, NATO FORUM, Toledo, May 1997, NATO ASI Series E - 348, Kluwer, 107 (1998), eds. N. Garcia, M. Nieto-Vesperinas, and H. Rohrer.

[37] J. König, H. Schoeller, and G. Schön, to be published in the Proceedings of the conference *Path Integrals from peV to TeV* held in Firenze, August 1998.

[38] T. Pohjola, J. König, H. Schoeller, and G. Schön, cond-mat/9810245.

[39] J. König, H. Schoeller, and G. Schön, Phys. Rev. Lett. **76**, 1715 (1996).

[40] J. König, J. Schmid, H. Schoeller, and G. Schön, Phys. Rev. B **54**, 16820 (1996).

[41] J. König, H. Schoeller, and G. Schön, in *Festkörperprobleme / Advances in Solid State Physics*, Vol. 35, ed. by R. Helbig (Vieweg, Braunschweig/Wiesbaden), p. 215 (1996).

[42] J. König, J. Schmid, H. Schoeller, and G. Schön, Czech. J. Phys. 46 S 4, 2399 (1996).

[43] T. Pohjola, J. König, M. Salomaa, J. Schmid, H. Schoeller, and G. Schön, Europhys. Lett. **40**, 189 (1997).

[44] J. Schmid, J. König, H. Schoeller, and G. Schön, Physica E **1**, 241 (1997).

[45] J. König and H. Schoeller, Phys. Rev. Lett. **81**, 3511 (1998).

[46] J. König, Y. Gefen, and G. Schön, Phys. Rev. Lett. **81**, 4468 (1998).

[47] D.V. Averin and A.A. Odintsov, Phys. Lett. A **140**, 251 (1989).

[48] D.V. Averin and Yu.V. Nazarov, Phys. Rev. Lett. **65**, 2446 (1990).

[49] D.C. Ralph and R.A. Buhrman, Phys. Rev. Lett. **72**, 3401 (1994).

[50] D. Goldhaber-Gordon, H. Shtrikman, D. Mahalu, D. Abusch-Magder, U. Meirav, and M.A. Kastner, Nature **391**, 156 (1998).

[51] D. Goldhaber-Gordon, J. Göres, M.A. Kastner, H. Shtrikman, D. Mahalu, and U. Meirav, Phys. Rev. Lett. **81**, 5225 (1998).

[52] S.M. Cronenwett, T.H. Oosterkamp, and L.P. Kouwenhoven, Science 281, 540 (1998).

[53] P. Joyez, V. Bouchiat, D. Esteve, C. Urbina, and M.H. Devoret, Phys. Rev. Lett. **79**, 1349 (1997).

[54] B.Su.V.J. Goldman and J.E. Cunningham, Science **255**, 313 (1992).

[55] P. Gueret, N. Blank, R. Germann, and H. Rothuizen, Phys. Rev. Lett. **68**, 1896 (1992).

[56] A.T. Johnson, L.P. Kouwenhoven, W. de Jong, N.C. van der Vaart, C.J.P.M. Harmans, and C.T. Foxon, Phys. Rev. Lett. **69**, 1592 (1992).

[57] E.B. Foxman, P.L. McEuen, U. Meirav, N.S. Wingreen, Y. Meir, P.A. Belk, N.R. Belk, M.A. Kastner, and S.J. Wind, Phys. Rev. B **47**, 10020 (1993).

[58] J. Weis, R.J. Haug, K. v. Klitzing, and K. Ploog, Phys. Rev. B **46**, 12837 (1992).

[59] S. Tarucha, D.G. Austing, T. Honda, R.J. van der Hage, and L.P. Kouwenhoven, Phys. Rev. Lett. **77**, 3613 (1996).

[60] T. Schmidt, R.J. Haug, K. v. Klitzing, A. Förster, and H. Lüth, Phys. Rev. Lett. **78**, 1544 (1997).

[61] D.C. Ralph, C.T. Black, and M. Tinkham, Phys. Rev. Lett. **74**, 3241 (1995).

[62] D.C. Ralph, C.T. Black, and M. Tinkham, Phys. Rev. Lett. **76**, 688 (1996).

[63] D.C. Ralph, C.T. Black, and M. Tinkham, Phys. Rev. Lett. **78**, 4087 (1997).

[64] D.L. Klein, R. Roth, A.K.L. Lim, A.P. Alivisatos, and P.L. McEuen, Nature **389**, 699 (1997).

[65] C. Schönenberger, H. van Houten, H.C. Donkersloot, Europhys. Lett. **20**, 249 (1992).

[66] R.P. Feynman and F.L. Vernon, Ann. Phys. (N.Y.) **24**, 118 (1963).

[67] A.O. Caldeira and A.J. Leggett, Physica A **121**, 587 (1983).

[68] A.O. Caldeira and A.J. Leggett, Ann. Phys. (N.Y.) **149**, 374 (1983).

[69] A.O. Caldeira and A.J. Leggett, Ann. Phys. (N.Y.) **153**, 445(E) (1983).

[70] U. Weiss, *Quantum Dissipative Systems*, Series in Modern Condensed Matter Physics, Vol. 2 (World Scientific, 1993).

[71] U. Eckern, G. Schön, and V. Ambegaokar, Phys. Rev. B **30**, 6419 (1984).

[72] G. Schön and A.D. Zaikin, Phys. Rep. **198**, 237 (1990).

[73] M. Grifoni, M. Sassetti, and U. Weiss, Phys. Rev. E **53**, R2033 (1996).

[74] D. Weinmann, W. Häusler, W. Pfaff, B. Kramer, and U. Weiss, Europhys. Lett. **26**, 467 (1994).

[75] A. Groshev, T. Ivanov, and V. Valtchinov, Phys. Rev. Lett. **66**, 1082 (1991).

[76] A. Kawabata, J. Phys. Soc. Japan **60**, 3222 (1991).

[77] T.K. Ng, Phys. Rev. Lett. **70**, 3635 (1993).

[78] A.L. Yeyati, A. Martin-Rodero, and F. Flores, Phys. Rev. Lett. **71**, 2991 (1993).

[79] C. Bruder, R. Fazio, and H. Schoeller, Phys. Rev. Lett. **76**, 114 (1996).

[80] P. Fulde, *Electron Correlations in Molecules and Solids*, Springer series in solid-state Sciences, 2nd edition, (1993).

[81] A.C. Hewson, *The Kondo Problem to Heavy Fermions*, Cambridge studies in magnetism, (1993).

[82] D.C. Langreth, Phys. Rev. **150**, 516 (1966).

[83] N.E. Bickers, Rev. Mod. Phys. **59**, 845 (1987).

[84] F.D.M. Haldane, Phys. Rev. Lett. **40**, 416 (1978).

[85] N.S. Wingreen, K.W. Jacobsen, and J.W. Wilkins, Phys. Rev. Lett. **61**, 1396 (1988).

[86] N.S. Wingreen, K.W. Jacobsen, and J.W. Wilkins, Phys. Rev. B **40**, 11834 (1989).

[87] L.I. Glazman and R.I. Shekhter, Sov. Phys. JETP **67**, 163 (1988).

[88] M. Jonson, Phys. Rev. B **39**, 5924 (1989).

[89] M.H. Devoret, D. Esteve, H. Grabert, G.-L. Ingold, H. Pothier, and C. Urbina, Phys. Rev. Lett. **64**, 1824 (1990).

[90] A.A. Odintsov, G. Falci, and G. Schön, Phys. Rev. B **44**, 13089 (1991).

[91] K. Flensberg, S.M. Girvin, M. Jonson, D.R. Penn, and M.D. Stiles, Phys. Scripta **T42**, 189 (1992).

[92] H.T. Imam, V.V. Ponomarenko, and D.V. Averin, Phys. Rev. B **50**, 18288 (1994).

[93] G.D. Mahan, *Many-Particle Physics*, (Plenum, 1990).

[94] G. Ingold and Yu.V. Nazarov, in Ref. [3].

[95] D. Pfannkuche and S.E. Ulloa, Phys. Rev. Lett. **74**, 1194 (1995).

[96] K. Jauregui, W. Häusler, D. Weinmann, and B. Kramer, Phys. Rev. **53**, R1713 (1996).

[97] C. Caroli, R. Combescot, P. Nozières and D. Saint-James, J. Phys. C5, 21 (1972).

[98] F. Hekking, Y.V. Nazarov, and G. Schön, Europhys. Lett. **14**, 489 (1991).

[99] F. Hekking, Y.V. Nazarov, and G. Schön, Europhys. Lett. **20**, 255 (1992).

[100] A.G.M. Jansen, A.P. van Gelder, P. Wyder, and S. Strassler, J. Phys. **F11**, L15 (1981).

[101] D.C. Ralph and R.A. Buhrman, Phys. Rev. Lett. **69**, 2118 (1992).

[102] D.C. Ralph and R.A. Buhrman, Phys. Rev. B **51**, 3554 (1995).

[103] D.C. Ralph, A.W.W. Ludwig, J. von Delft and R.A. Buhrman, Phys. Rev. Lett. **72**, 1064 (1994).

[104] M.H. Hettler, J. Kroha, and S. Hershfield, Phys. Rev. Lett. **73**, 1967 (1994).

[105] Y.V. Nazarov, J. Low Temp. Phys. **90**, 77 (1993).

[106] D.V. Averin, Physica **194-196**, 979 (1994).

[107] P. Lafarge and D. Esteve, Phys. Rev. B **48**, 14309 (1993).

[108] G. Göppert and H. Grabert, Phys. Rev. B **58**, R10155 (1998).

[109] D.S. Golubev and A.D. Zaikin, JETP Lett. **63**, 1007 (1996), [Zh. Eksp. Teor. Fiz. Pis'ma Red. **63**, 953 (1996)].

[110] K.A. Matveev, Sov. Phys. JETP **72**, 892 (1991), [Zh. Eksp. Teor. Fiz. **99**, 1598 (1991)].

[111] D. Chouvaev, L.S. Kuzmin, D.S. Golubev, and A.D. Zaikin, cond-mat/9803015.

[112] M. Büttiker and T. Christen, in *Mesoscopic Electron Transport* NATO ASI Series **345**, L.L. Sohn et al., eds., (Kluwer, 1998).

[113] G. Göppert, H. Grabert, N. Prokof'ev, and B. Svistunov, Phys. Rev. Lett. **81**, 2324 (1998).

[114] S.V. Panyukov and A.D. Zaikin, Phys. Rev. Lett. **67**, 3168 (1991).

[115] X. Wang and H. Grabert, Phys. Rev. B **53**, 12621 (1996).

[116] W. Hofstetter and W. Zwerger, Phys. Rev. Lett. **78**, 3737 (1997).

[117] X. Wang, R. Egger, and H. Grabert, Europhys. Lett. **38**, 545 (1997).

[118] C.P. Herrero, G. Schön, and A.D. Zaikin, cond-mat/9807112.

[119] L.P. Gorkov and G.M. Eliashberg, Zh. Eksp. Teor. Fiz. **48**, 1407 (1965) Sov. Phys. JETP **21**, 940 (1965).

[120] B.I. Shklovskii, Pis'ma Zh. Eksp. Teor. Fiz. **36**, 287 (1982) JETP Lett. **36**, 352 (1982).

[121] K.B. Efetov, Adv. Phys. **32**, 53 (1983).

[122] Y. Imry, Europhys. Lett. **1**, 249 (1986).

[123] A. Kamenev, B. Reulet, H. Bouchiat, and Y. Gefen, Europhys. Lett. **28**, 391 (1994).

[124] K.B. Efetov, *Supersymmetry in Disorder and Chaos*, Cambridge University Press, New York (1997).

[125] C.W. Beenakker, Rev. Mod. Phys. **69**, 731 (1997).

[126] T. Guhr, A. Müller-Groeling, and H.A. Weidenmüller, Phys. Rep. **299**, 189 (1998).

[127] M.L. Mehta, *Random Matrices*, Academic Press, 2nd edition, (1991).

[128] A. Kamenev and Y. Gefen, Int. J. Mod. Phys. **B9**, 751 (1995).

[129] F. Zhou, B. Spivak, N. Taniguchi, and B.L. Altshuler, Phys. Rev. Lett. **77**, 1958 (1996).

[130] R. Grobe, F. Haake, and H.J. Sommers, Phys. Rev. Lett. **61**, 1899 (1988).

[131] R. Grobe and F. Haake, Phys. Rev. Lett. **62**, 2893 (1989).

[132] J.L. Pichard and B. Shapiro, J. Physique **4**, 623 (1994).

Lebenslauf

Name:	König
Vorname:	Jürgen
geboren:	am 03.02.1970 in Karlsruhe
Familienstand:	verheiratet mit Bärbel König geb. Nirk
Eltern:	Gerhart König und Marianne König geb. Domes
Schule:	Aug. 1976 – Juli 1980: Grundschule (Heynlinschule Stein) Sept. 1980 – April 1989: Gymnasium (Bildungszentrum Königsbach) April 1989: Abitur
Wehrdienst:	Juni 1989 – Aug. 1990
Studium:	Okt. 1990 – Nov. 1995: Physikstudium an der Universität Karlsruhe Okt. 1992: Vordiplom Nov. 1995: Diplom
Diplomarbeit:	"Resonanztunneln in mesoskopischen Systemen", angefertigt bei Prof. Dr. Gerd Schön am "Institut für Theoretische Festkörperphysik" der Universität Karlsruhe (TH)
Promotion:	Dez. 1995 – Dez. 1998: Doktorand bei Prof. Dr. Gerd Schön am "Institut für Theoretische Festkörperphysik" der Universität Karlsruhe (TH)
Auszeichnung:	Diplom "mit Auszeichnung" Promotion "mit Auszeichnung"
Preis:	"Preis der Stadt Karlsruhe 1997" für die wissenschaftliche Leistung während der Diplomarbeit